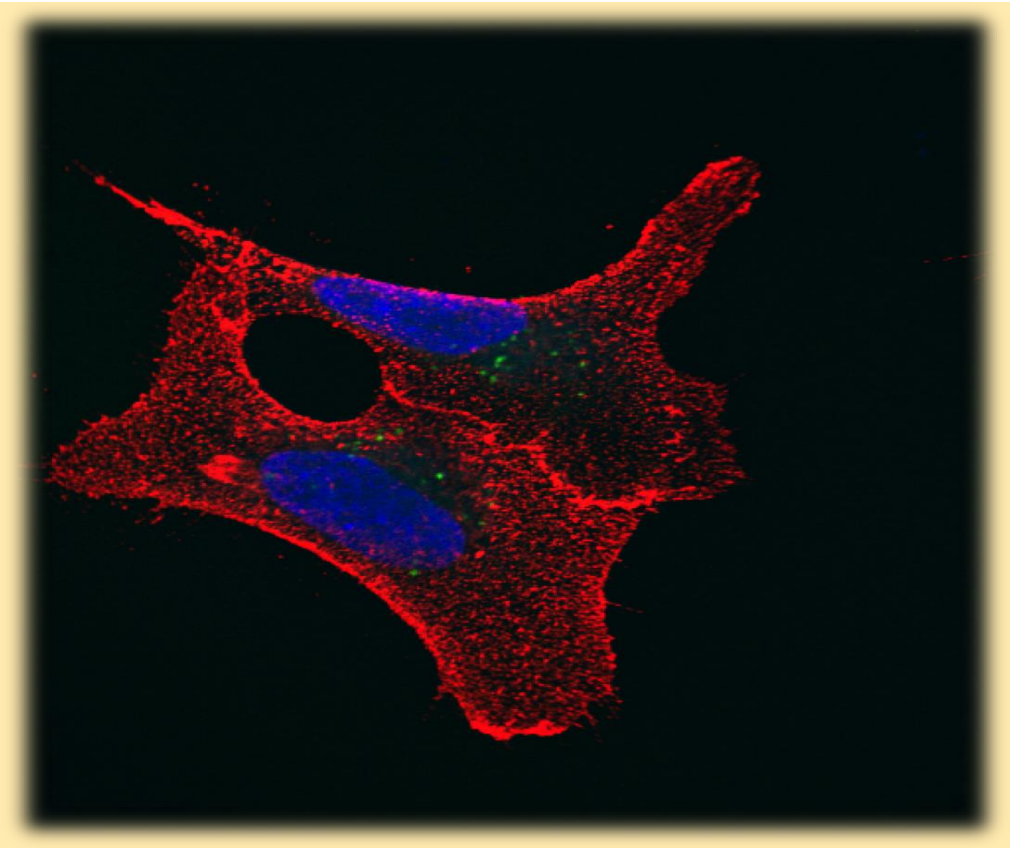

Renata Sofia Mota Gomes

"Nanomaterials for miRNA delivery and non-invasive imaging in cardiovascular regeneration"

Dissertação de Doutoramento na área científica de Bioquímica, especialidade Tecnologia Bioquímica, orientada pelo Professor Lino Ferreira e institucionalmente pelo Professor Rui de Carvalho, e apresentada ao Departamento de Ciências da Vida da Faculdade de Ciências e Tecnologia da Universidade de Coimbra.

Setembro de 2013

· U C ·

Universidade de Coimbra

“Nanomaterials for miRNA delivery and non-invasive imaging in cardiovascular regeneration”

Table of Contents

Thesis Abstract

The development of noninvasive platforms to assess cell fate after transplantation is of utmost importance in the context of Regenerative Medicine. Magnetic Resonance Imaging (MRI) is a powerful non-invasive imaging platform, heavily relying on the use of contrast agents, mostly nanoparticles (NPs). Gadolinium (Gd) and Superparamagnetic Iron Oxide (SPIO) NPs are contrast agents in clinical use, however these agents may cause liver toxicity, give rise to image artifacts in MRI, and typically have not been used as a drug delivery system. In this work, we developed a novel NP formulation containing fluorine to overcome the previous limitations. The NPs are based on poly(lactic-*co*-glycolic acid) (PLGA) which is a biocompatible and versatile polymer approved for human use . PLGA NPs containing fluorine were developed to label and track cells overtime and as vectors for microRNA (miR) delivery, which improves cell survival in hypoxic conditions. Herein we show that the fluorine-based NPs are a reliable approach to track non-invasively cells with clinical relevance (endothelial cells and cord-blood derived mononuclear cells) and simultaneously control the intracellular delivery of pro-survival and pro-angiogenic miRs. Also systems for *in vitro* and *in vivo* imaging via MRI of fluorine are developed and here explained. Furthermore *in vivo* studies are performed which show the therapeutic uses of such system. Additionally we also address the optimization of protocols for stem cell culture which may enhance proliferation and promote pluripotency in cardiac stem cells (CSCs) so as we can fully explore the potential of these cells in vivo using out novel theranostic NPs platform. We are the first authors developing and relating these novel developments.

Resumo de Tese

O desenvolvimento de plataformas não-invasivas para avaliar o destino das células após o transplante é de extrema importância no contexto da medicina regenerativa. Imagem por Ressonância Magnética (MRI) é uma plataforma de imagem não invasiva poderosa, baseando-se fortemente na utilização de agentes de contraste, principalmente nanopartículas (NP). Gadolínio (Gd) e NPs de óxido de ferro superparamagnéticas (SPIO) são os agentes de contraste em utilização clínica, no entanto, estes agentes podem provocar toxicidade hepática, dar origem a artefactos de imagem em MRI, e, tipicamente, não têm sido utilizados como um sistema de entrega de biomoleculas. Neste trabalho, foi desenvolvida uma nova formulação de NPs com contendo de flúor para superar as limitações anteriores. As NPs são baseados em poli (ácido láctico-co-glicólico) (PLGA), que é um polímero biocompatível e versátil aprovado para uso humano. PLGA NPs contendo flúor foram desenvolvidas a usadas para marcação de células e como vectores para entrega microRNA (miR), que melhora a sobrevivência das células em condições de hipóxia. Aqui, mostramos que os NP com flúor são uma abordagem fiável para rastrear as células de forma não invasiva com relevância clínica (células endoteliais e células mononucleares derivadas de sangue do cordão) e, simultaneamente, controlar a entrega intracelular de miRs de pró-sobrevivência e pró-angiogénicos. Para sistemas *in vitro* e *in vivo* de imagens por meio de ressonância magnética do flúor também foram também desenvolvidos sistemas aqui demonstrados. Além disso, em estudos *in vivo* realizados mostramos os usos terapêuticos de tal sistema. Além disso, também abordamos a optimização de protocolos de cultura de células estaminais que podem aumentar a proliferação e promover a pluripotência em células estaminais cardíacas (CSCs), de modo que possamos explorar plenamente o potencial dessas células *in vivo* utilizando a nova plataforma NP. Nós somos os primeiros autores a desenvolvimento e relatar estes novos desenvolvimentos.

Acknowledgments

Completing a PhD thesis is not an easy task and only possible with help, as a result I would like to thank many individuals and institutions that helped me through this journey.

I am very grateful to my principal supervisor Dr Lino Ferreira for the opportunity, patience and guidance over the past years. My co-supervisor Dr Rui Carvalho has been fantastic, taught me the real power of magnetic resonance and guided me, with great patience, through all the bureaucracy of the PhD paperworks. Although not officially a supervisor, Dr Ricardo Neves has been a true master, contributed deeply my development as a scientist, the daily discussions that we had, and taught me imaging and not to be afraid of providing critical thinking, values which have allowed me to continue to succeed in science. It would have been impossible to complete this thesis without the support and friendship from my foreign institution supervisors, Dr Carolyn Carr, Dr Lowri Cochlin, Professor Kieran Clarke, Professor John Martin and Professor Seppo Yla-Hertualla, whom made my constant travels and living between the UK and Finland a much easier and enjoyable task, even when temperatures reached -40^{0}C and no day light was to be seen for months.

To Professors Oliver Smithies, Nobuyo Maeda and Paul Greengard, I thank them for the scientific discussions, friendship and advice that kept me motivated over the last year, even in extreme and difficult conditions.

I am grateful to the "troops" for helping me, working with me many times until 4am and returning back to the lab with me, 4 hours later for another day of work, and even bringing me chicken soup home when I was sick – Ana Francisca Lima, Suat Cheng Tan, Filippo Perbellino, Jill Brown, Ricardo Neves, Petra Korpisalo and Galina Dragneva. Above all, thank you for the friendship and loyalty, without which science has no value.

My family has been fantastic, Maria Celia, Aurelio, Ju, Ema, Bella, Avo Joaquim e Avo Emilia, for tolerating all the Christmas, special occasions and family reunions, that I wasn't able to attend because I was either at the MRI suite finishing animal trials, doing more surgeries or even stuck at the airport when all flights were grounded. To my best friend Ana Ferraz, thank you for our latest inventions together, which keep me motivated. Far from least, to my fiancée I am forever in debt for believing in me and never even allowing me to consider failure, even in times of sickness, and stimulating me to have more ideas than ever and supporting me always.

I would like to dedicate my thesis to Professor Karin Schallreuter and in memory of Professor John Wood, both gave me the first chance at having a go at research and always been on the other side of the line for me.

Forever in debt to the BUPA International Cancer Care and NHS Oncology team for allowing me to complete this PhD in “one piece”, a heartfelt thank you to the surgeons and nurses in these amazing teams.

This thesis reflects some of the published works performed between 2008-2012 under the Biomedicine and Experimental Biology PhD Program managed by the Centre of Neurosciences and Cell Biology at the University of Coimbra, Portugal. My work was performed in collaboration with the University of Oxford, UK and the University of Kuopio, Finland. My deepest gratitude to the Portuguese Foundation for Science and Technology for a full PhD Scholarship between 2008-2012 (FRH/BD/33466/2008), to the British Heart Foundation for an excess of £50,000 allowance to develop all ^{19}F systems and cover all outstanding fees at the University of Oxford, UK (RG/07/004/22659). Also I would like to acknowledge the investment of €30,000 by the University of Kuopio and the Finnish Academy of Science on the rabbit and mice animal studies used in the final works for publication of the developed technology. I am also very thankful to the Max Plank Institute and the European Society of Radiology for sponsoring all of my advanced training. My thankfulness to British Airways and Lufthansa for all the free flights between Portugal, UK, Germany and Finland, that allowed to work and reduce extremely the financial expense on travel.

Chapter I

Overview and thesis aims

1.1. Brief overview

Magnetic resonance imaging (MRI) provides a long-term non-invasive, *in vivo* method for studying the fate of transplanted cells labelled with superparamagnetic iron oxide (SPIO) nanoparticles (diameter below 200 nm) [3]. In most cases, the internalization of these NPs by stem cells do not affect cell viability, growth, or differentiation [3]. These NPs are composed of an iron oxide core coated with dextran or carboxydextran, which ensures aqueous solubility and prevents nanoparticle aggregation [4, 5]. The NPs can induce strong field inhomogeneities in proximal water molecules during MRI. As such, when NPs are internalised by targeted cells they can create a significant dephasing of protons, which predominantly reduces the T2 and T2* relaxation times [6]. MRI offers several advantages over other techniques such as positron emission tomography, which include greater speed, higher spatial resolution, a direct anatomical correlation, and lower costs [7]. *In vivo* images with a spatial resolution of 50 x 50 x 500 micrometer can be acquired over 2-3 h [8]. Unfortunately, SPIOs are not detected directly, but indirectly through microscopic disturbances of the magnetic field that misalign the orientation of water protons from which the magnetic resonance signal is derived [9]. Therefore, it is difficult to correlate the magnetic resonance signal to the number of cells. Furthermore, anatomic (^{1}H) MRIs often are difficult to interpret because it is not always clear whether dark areas are caused by these NPs or by other inhomogeneities [10]. In addition, it is not possible to differentiate two or more groups of cells, which are labelled with iron oxide agents. Therefore, there is the need for the development of new NPs for MRI.

Fluorine-based NPs, can be detected directly by ^{19}F imaging, offer an alternative to SPIOs for accurate counting of local cells, to overcome MRI artifacts, and label two or more groups of cells [11]. Because the human body naturally lacks fluorine, ^{19}F signals originating from injected ^{19}F-containing compounds exhibit an excellent degree of specificity. Furthermore, ^{19}F MRI using fluorine-based NPs

can be used to report the pressure of O_2 in ischemic tissue environments such as the myocardium [12]. Finally, fluorine-based NPs provide an unequivocal and unique signature for stem/progenitor cells and permit quantification and detection of multiple fluorine signatures via ^{19}F MR spectroscopy [13].

The main goal of this project was to develop NPs containing fluorine to track stem cells by ^{19}F MR spectroscopy after being transplanted into models of vascular disease. The developed NPs should incorporate biomolecules to enhance for stem/progenitor while simultaneously tracking them.

1.2. Thesis outlines

The main objective of this project is to develop fluorine-based nanoparticles that can be used to track stem cells or their progenies by MRI and simultaneously deliver biomolecules. The following specific objectives will be addressed:

1. **Characterization of nanoparticles containing fluorine.**
2. **Development of efficient methodologies to introduce NPs within cells.**
3. **Study cell viability and proliferation of cells labeled with fluorine-based NPs.**
4. **Develop methodologies for miR attachment to the NPs.**
5. **Study the effect of the NPs complex with miR within cells.**
6. **NP delivery carrying miR in models of vascular disease and study its effects.**
7. ***In vivo* applications of this novel technology.**

Chapter II

General Introduction

2.1. Cardiac and ischemic disease

Cardiovascular disease (CVD) is responsible for 50% of deaths in developed nations; nowadays CVD equals the rate of morbidity as caused by viral and bacterial epidemics of previous centuries. According to the British Heart Foundation statistics, in the UK a person suffers a heart attack every 2 minutes. The burden on national healthcare systems is enormous and expected to worsen [14], current therapies are falling patients not only for myocardial infarction therapies but also for vascular regeneration and ischemic episodes. Life expectancy and quality are severely diminished despite modest improvement on the major therapies developed in the 1960's. The 5-year mortality rate remains between to 45-50% [1]. CVD is characterized by many conditions such as: coronary heart disease, ischemic heart disease, myocardial infarction, angina pectoris, cerebrovascular disease, hypertension heart disease, peripheral/ischemic vascular disease, heart failure, rheumatic heart disease, congenital heart disease, cardiomyopathies.

Any CVD episode prior de age of 64 is considered premature; at present most cases of CVD are premature and based on environmental factors related to inadequate and undisciplined nutritional diets [2]. Most CVD episodes are highly correlated with high cholesterol levels cumulating into atherosclerotic plaque formation responsible for cardiac and vascular ischemia as shown in **Figure 1**.

2.2. Common therapies

Commonly on the event of CVD the first line of prevention for further episodes and response rely on the use of pharmaceutical drugs and surgical procedures.

2.2.1. Pharmacological interventions

The first lines of combat traditionally target hypertension pharmacologically by the use of angiotensin-converting enzyme inhibitors (ACE), beta-bloquers and calcium channel blockers. Hypertension is responsible only not for elevated blood pressure but also remodeling of vessels and tissues. Angiotensin-Converting Enzyme Inhibitors (ACE) have been developed in the 1980's. This system is characterized by the interaction between renin, an enzyme released from the kidney, and angiotensinogen, a peptide circulating in the blood stream [15]. The rational for ACE use is that inhibit synthesis of angiotensin II in the bloodstream and in various tissues it decreases angiotensin II-mediated vasoconstriction and vascular structural changes. It can also promote proliferation of vascular smooth muscle cells essential for vessel remodeling [16]. Diuretics can also be referred to however they are a less sophisticated formulation to lower hypertension, which can lead to dehydration.

Another pharmacological intervention for hypertension is by the use of beta-bloquers. Beta-bloquers are used in case of hypertension that results from increased sympathetic stimulation of the heart. Developed in the 1960's, some beta-blockers bind to beta-1 adrenergic receptors located on the myocardium blocking the cardio acceleration effects of endogenous catecholamines (norepinephrine, epinephrine); whereas alpha-blockers bind to alpha- adrenergic receptors located on the smooth muscle of the peripheral vasculature helping to reduce catecholamine-induced vasoconstriction. Both types of drugs have been used extensively for treating hypertension, and both groups have additional properties that potentially can affect the long-term control of blood pressure [17, 18].

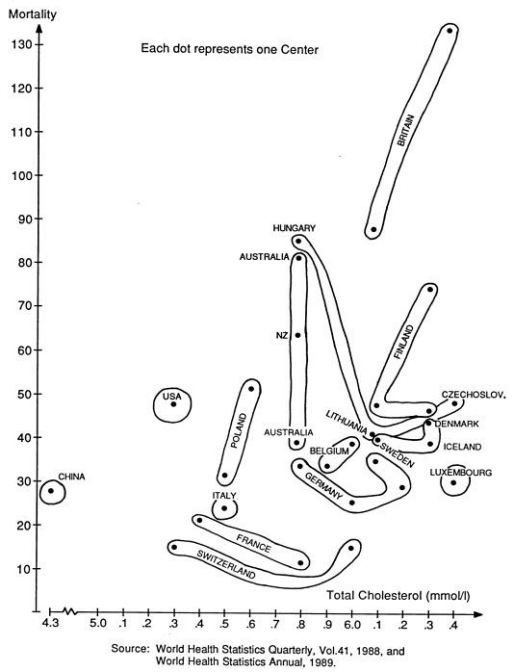

Figure 1. Correlation between cholesterol levels and CVD mortality. Total age-standardized cholesterol and ischemic heart disease mortality (per 100 000) in 30 MONICA centers: Men aged 35 to 64 years. Adapted from Circulation Research [2].

Calcium channel blockers, are also heavily used in hypertension which limit the entry of calcium into vascular tissues, thus limiting contraction of vascular smooth muscle [19]. Calcium channel blockers prevent some cardiovascular remodeling associated with hypertension. Long-term (6 months) administration of calcium channel blockers may help reduce structural changes in the left ventricle as well as small resistance vessels [20, 21]. These drugs seem to inhibit structural changes in the vasculature primarily through inhibition of vascular smooth-muscle cell proliferation and secondarily through inhibition of atherosclerotic plaque formation in the vascular cell wall [22].

In addition to drugs targeting hypertension, lipid-lowering drugs such as statins and stenols are included in the first line of combat to prevent further events as a result of arteriosclerosis [23]. Anticoagulants and aspirin are either initiated as a treatment therapy or preventive measure mostly for episodes of myocardial infarction and vessel occlusion.

2.2.2. Other Interventions

Surgical interventions are rather invasive but often needed in combination with pharmacological therapy. Stents in combination with angioplasty are common practice and the least invasive of procedures, an effective manner to unblock arteries and reinforce them as stents can also be left in situ in some situations [24]. However taking into consideration CVD epidemiology, heart bypass surgery has become more common as coronary arteries are often largely blocked [24]. Cardioversion and ablation are commonly used, as drugs alone by majority cannot convert arrhythmia to a normal heart rhythm after heart ischemic episodes. Pacemakers are a more extreme option, often used to target congestive heart failure and hypertrophic cardiomyopathy. In addition, left ventricular assist devices (LVAD) are commonly used nowadays as the "plastic hearts" as there is a scarce in human hearts for heart transplant. Although the combination between surgical and pharmacological procedures may delay the onset of disease development and in the short term improve life quality there is no evidence that traditional therapies improve life expectancy, as a consequence 45-50% of patients die within the first 5 years of disease manifestation [1]. Therefore new therapies are sought after. Great promise is seen within the use of cells, mostly stem cells as a tool for regeneration and homeostatic maintenance for CVD.

2.3. Cells as a therapeutic approach

Early studies in vascular regeneration either post myocardial infarction of for peripheral arterial disease as a result of limb ischemia have focused on the usage of angiogenic proteins such as vascular endothelial growth factor (VEGF) ad fibroblast growth factor (FGF). Pre-clinical and early phase trials were promising however did not achieve long lasting results, possibly due to single dosages or the proteins short half-life. However these proteins were followed up with viral vectors so as to over-express these proteins, however the gene transfer was not efficient in vivo [25-30]. Taking into

consideration that patients suffering from ischemic disease, for example, peripheral or ischemic arterial disease have been shown to have the same quality of life as a terminally ill cancer patients [31] it is very important to look into regeneration strategies.

The strategy is to focus on stimulation of angiogenesis *in vivo*, pro-angiogenesis. Angiogenesis is a multi-factorial process where endothelial cells are the leading players in angiogenesis; pericytes are part of the basement membrane coating endothelial cells as an angiogenic scaffold support system [32]. An angiogenic response will follow upon vascular degradation where migration of endothelial stalk cells occurs, recruitment of pericytes to the endothelial lumen follows and vascular stabilization might finally occur depending on the adhesion junctions at the basement membrane [33]. The angiogenic response is highly synchronized system where through specific receptors on vascular endothelial cells, VEGF, FGF, angiopoietins (ANGPT1 and ANGPT2), Notch ligands and transforming growth factor-β (TGF-β), angiogenesis is regulated, as shown in **Figure 2**. VEGF activates the eNOS, SRC, RAS-ERK and PI3K-AKT signalling cascades through VEGFR2 receptor on endothelial cells, inducing vascular permeability, endothelial migration, proliferation and survival, respectively [32, 34]. FGF2 promotes angiogenesis via the FGFR1 receptor on endothelial cells with signalling cascades similar to VEGF [35]. ANGPT1, secreted from pericytes, activates TEK/TIE2 receptor to maintain endothelial quiescence or stabilization, whereas ANGPT2, secreted from endothelial cells themselves by VEGF or hypoxia signalling, inhibits TEK to promote endothelial activation or sprouting [36]. JAG1-Notch signalling promotes angiogenic sprouting, whereas DLL4-Notch signalling inhibits angiogenic sprouting [37]. TGF-β signalling depending via which cascade can either inhibits endothelial cell activation or promote the migration and proliferation of endothelial cells [32]. The VEGF, FGF, Notch and TGF-β signalling cascades are directly involved in the angiogenic signalling of endothelial. The VEGF, FGF, Notch and

TGF-β signalling cascades cross-talk with WNT and Hedgehog signalling cascades to constitute the stem-cell signalling network [38]. FGF, Notch and canonical WNT signalling are involved in cell-fate determination based on mutual transcriptional regulation, whereas FGF, Notch, TGF-β, Hedgehog and non-canonical WNT signalling are involved in epithelial-to-mesenchymal transition (EMT) due to the up-regulation of SNAI1 (Snail), SNAI2 (Slug), ZEB1, ZEB2 and TWIST [39]. EMT is a cellular process similar to endothelial-to-mesenchymal transition (EndMT). Hypoxia induces angiogenesis as a result of VEGF up-regulation [40] and controls cancer stem cells and EMT transition through the stem-cell signalling network. In summary, angiogenesis is orchestrated by the VEGF, FGF, Notch, TGF-β, Hedgehog and WNT signalling cascades, which directly or indirectly regulate the quiescence, migration and proliferation of endothelial cells.

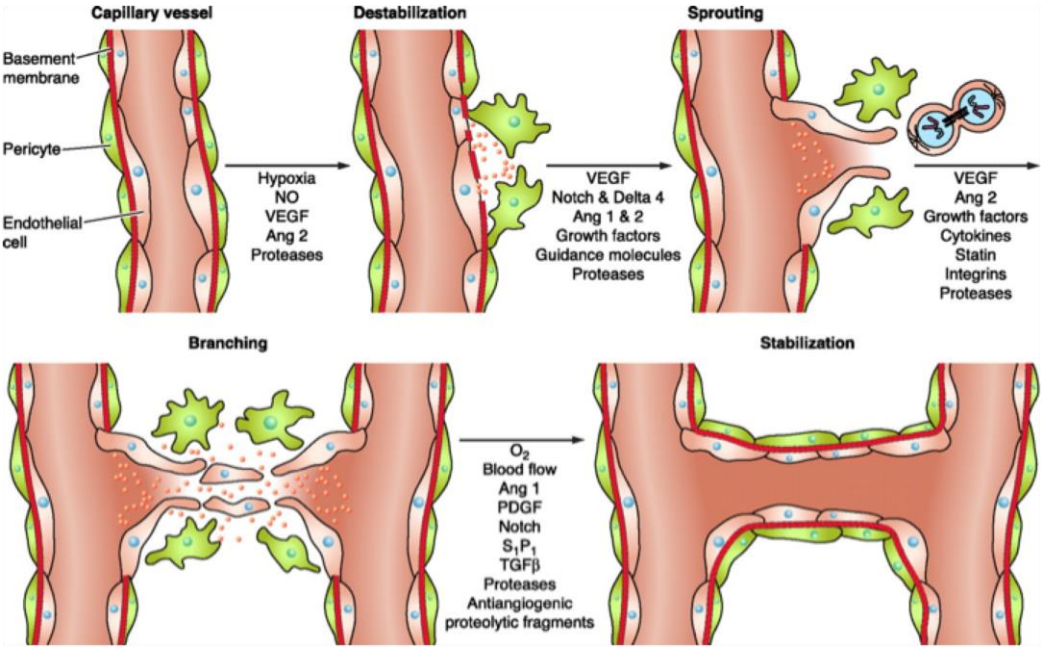

Figure 2 – **Illustration for the angiogenic process**. Extracted from Clapp et al [41]. The phases of angiogenesis as described in detail previously. In summary, hypoxia will trigger nitric oxide (NO), vascular endothelial growth factor (VEGF) and angiopoietin-1 and -2 (Ang 1 and Ang 2) expression. These molecules bind to the extracellular matrix and increase vessel permeability. Cells then migrate during the destabilization phase. New vessels are formed and maturated due to an increased expression of factors.

Stem cells have been widely used for many purposes namely vascular and cardiac regeneration. The ability of these cells to self-renew and differentiate into cardiovascular lineages render them as good candidates to aid where all therapies kept disappointing and are inconsistent among patient cohorts. Many stem cell types have been used for the regeneration such as Endothelial Progenitor Cells, Bone Marrow or Peripheral Blood mobilized Mononuclear Cells (MNCs), Mesenchymal Stem Cells (MSCs) and Cardiac Stem Cells (CSC) [41].

2.3.1. Endothelial Progenitor Cells (EPCs)

EPCs are defined as cells circulating in blood with the capability of producing endothelium lining. The exact identification of EPCs is difficult and are always referred to, or characterized by positive selection of several of its membrane receptors. EPCs are often obtained from bone marrow, peripheral blood, adipose tissue [42] and umbilical cord blood [43]. It is well established that CD34+ cells are known as EPCs due to their capacity of forming endothelial cells [44]. CD133+ are also EPCs and can be classified as "early"(CD34++,CD133++,KDR+), "mature" (CD133+, CD34low, KDR+, CD31+, VE-Cadherin+ and vWFR+) or "more mature" (CD133+, CD34+, KDR+) EPCs, as illustrated bellow (**Figure 3**). EPCs are either isolated from circulating blood, where they are present at very low numbers however after stimulation of the bone marrow with either granulocyte-colony stimulating factors (G-CSF) or granulocyte macrophage-colony stimulating factors (GM-CSF) larger numbers of EPCs can be collected.

Mobilized EPCs retain their ability to expand and form vascular structures *in vivo* [45]; however there have been many challenges in choosing the best delivery method and dosage. For peripheral arterial disease (PAD), many clinical trials have been performed where EPCs were mobilized using the colony

stimulating factors; most studies show improvements in pain symptoms in the ankle-brachial index (ABI) after 1-month treatment [46] or in pain free movement such as walking time [47, 48].

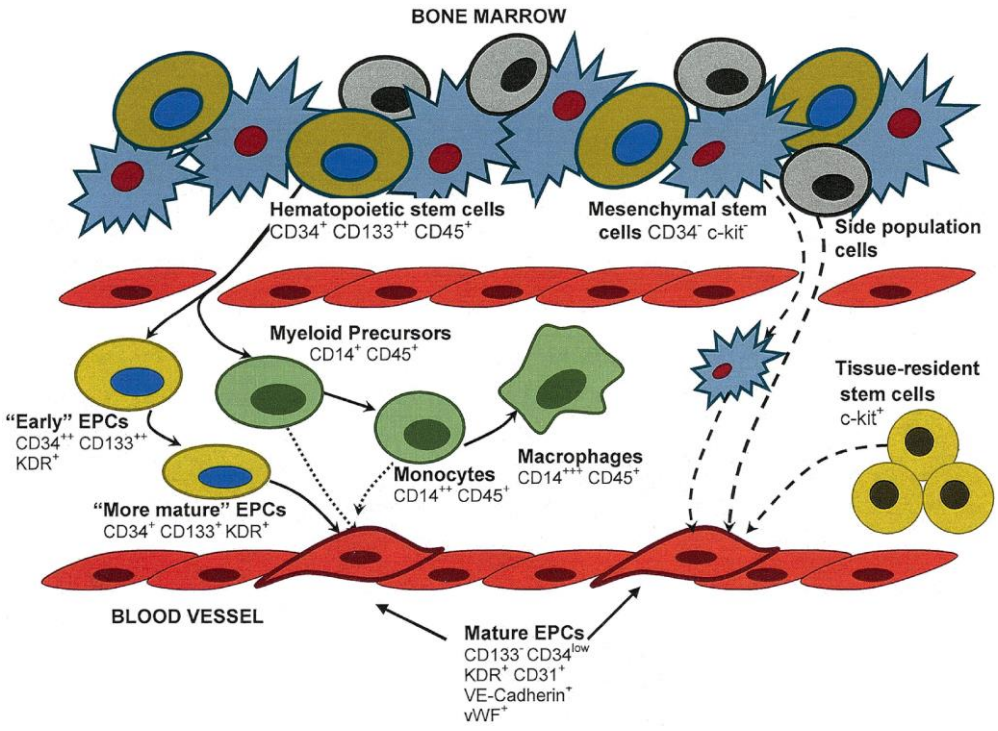

Figure 3 – **Illustration of Endothelial Progenitor Cells (EPCs) from the Bone Marrow** (illustration from Shantsila et al [49]). EPCs are released into the blood stream and can be sub-categorized into early EPCs (CD34++, CD133++, KDR+), more mature EPCs (CD34+, CD133+, KDR+), and matures EPCs (CD133+, CD34low, KDR+, CD31+, VE-Cadherin+ and vWFR+).

EPCs have also been isolated and then implanted into limb ischemic areas [50-57]. Higashi *et al* [51] delivered an enriched population of CD34+ cells (10^7 cells) intramuscularly and at a 4 week follow up there were significant improvements in transcutaneous oxygen pressure (TcPo2), a non-invasive method to quantify skin oxygenation, is particularly useful in advanced stages of arteriopathy of the lower limbs for evaluation of cutaneous ischemia. Furthermore there was a significant improvement in pain-free walking time, acetylcholine-mediated endothelium-dependent blood flow with cell therapy compared to baseline. Motokuru *et al* [53] also observed significant improvements in TcPo2 at 6 months

follow up (2 months further into treatment than Higashi *et al*). Patients reported significantly less ABI pain and significant ulcer healing was observed in comparison to controls, however all patients had stop smoking during the trial period and this by itself could have confounding implications as smoking and diabetes can influence PAD. Duong Van Huyen *et al* [50] performed a 1-year follow up on patients, which had received intramuscular delivery of an enriched cell population of CD34+ cells (10^6). These patients shown active angiogenesis distal to the injection site seen in histological samples with higher endothelial cells markers such as CD31+, CD34+ and vWF+ in comparison to age and sex matched controls. Ruiz-Salmeron *et al* [54] also performed a 1-year follow up however cells here were delivered intra-arterially (enriched cell population with 10^6 CD34+ cells), yet the improvements in ABI pain rating, wound healing and blow flow were also significantly improved. At an earlier time point follow up, at 6 months after intra-arterial delivery of again enriched cell population with 10^6 CD34+ cells in a single or double doe escalation therapy, Walter *et al* [56] reported significant improvement skin ulcer healing and rest pain however no improvements in ABI pain ratings or limb salvage. Another 1-year follow up study using again enriched cell populations with 10^6 CD34+ cells, yet Van Tongeren *et al* [55] wanted to see whether the combination of intramuscular and intra-arterial delivery would be of even higher benefit to the patients. Significant improvements were seen in both movement and ABI pain ratings. However the ultimate goal of limb salvage was not significant.

Angiogenesis is a multi-factorial process which can be affected by many factors, it is clear that diabetes and smoking can affect the treatment outcomes and in the above studies the possibility that statins which was taken by nearly all patients could be interfering with mechanisms that could render total limb salvage, however these mechanisms are yet still to be understood.

2.3.2. Mononuclear Cells (MNCs)

Total MNCs, are simply blood cells with a round nucleus and are a very homogenous population which have not only been widely used in PDA in similar methodologies and rational as mentioned above for EPCs but have been the focus for myocardial regeneration after infarction. For acute myocardial infarction, TOPCARE-AMI (Transplantation of Progenitor Cells and Regeneration Enhancement in Acute Myocardial Infarction) is the most well known trial where bone marrow derived MNCs (BM-MNCs) were expanded ex-vivo and enriched with EPCs from peripheral blood and transplanted via intracoronary infusion. The 5-year follow up demonstrates long-term safety and a small yet significant improvements of left ventricle ejection fraction (LVEF) comparing to the control group [58]. A further 2 trials (one concluded the other ongoing) (Transplantation in Myocardial Infarction Evaluation (TIME) study) is comparing the safety and efficacy of intracoronary delivery of BM-MNCs at 3 and 7 days post-MI in patients with ST-segment elevation [59]. The completed trial the LateTIME trial investigated whether delaying BM-MNC delivery for 2 to 3 weeks following MI and primary percutaneous coronary intervention improves global and regional left ventricle function [60]. No significant changes between baseline and 6-month measures were observed in LVEF and wall motion in the infarct and border zones, as measured by cardiac magnetic resonance imaging (MRI), in the BM-MNC group compared to placebo. Cell transplantation 2-3 week post-MI time point may exceed the therapeutic window of intracoronary BM-MNC therapy. A recent meta-analysis of 50 trials with over 2600 patients shown that there is a long-term clinical improvement in patients receiving BM-MNC therapy. BM-MNC therapy reduces death, recurrence of MI and thrombosis [61], and is a beneficial clinical practice even in sight of laborious methodologies for the *in vivo* transplantation.

Also for chronic cardiac ischemia or disease, many studies were performed using MNCs. FOCUS-CCTRN was the 1st trial in the USA injecting MNCs, a phase 2 trial in patients with chronic ischemic

cardiomyopathy that investigated the 6-month efficacy of transendocardial delivery of BM-MNCs on myocardial function and perfusion [62]. No significant effect on LV end-systolic volume, maximal oxygen consumption, or myocardial perfusion, exploratory analyses demonstrated significant improvement in stroke volume and LVEF, which correlated with higher bone marrow CD34+ and CD133+ progenitor cell counts. These findings support the notion that certain bone marrow-derived cell populations may provide a greater regenerative benefit and thereby determine clinical efficacy. As a consequence studies using only BM-MNC derived EPCs such as CD34+ were persuaded, in the ACT34-CMI trial (Adult Autologous CD34+ Stem Cells) the trial aimed to evaluate the safety and efficacy of intramyocardial injections of autologous CD34+ cells in patients with refractory chronic myocardial ischemia, which were not suitable candidates for conventional revascularization [63]. There was a significant improvement in exercise tolerance at both 6 and 12 months compared to placebo treatment, the trial preceded to larger scale studies. As many studies were also performed, looking into the meta-analysis of these is helpful. A meta-analysis of randomized controlled trials of BMSCT in patients with chronic ischemic cardiomyopathy was undertaken [64]. On the basis of a random-effects model, BM-MNCs improved the LVEF at 6 months by 4.48%. A greater improvement in the LVEF was seen with intramyocardial injection compared with intracoronary infusion. In summary BM-MNCs improve LVEF and favourably remodel the heart in patients with chronic ischemic cardiomyopathy. Intramyocardial injection may be superior to intracoronary infusion in patients with LV systolic dysfunction.

2.3.3. Mesenchymal Stem Cells (MSCs)

First described in 1974 [65], mesenchymal stem cells (MSCs) are another heterogeneous group of cells that can be isolated from many adult tissues, however these have limited cellular differentiation ability.

MSCs express on their surface mostly CD73, CD90 and CD105, while lacking the expression of CD11b, CD14, CD19, CD34, CD45, CD79a and HLA-DR surface markers under culture [66]. Data suggests that these cells are promising due their immunomodulatory and paracrine properties [67]. These cells have been shown to improve function in many disease models such as acute lung injury [68], sepsis [69] and acute myocardial infarction [70]. Manny clinical trials have followed mostly for acute myocardial treatments. In a small simple cohort Mohyeddin-Bonab et al [71] investigated the safety and effect of transplantation of MSCs in patients post MI at the time of coronary artery bypass grafting or percutaneous coronary intervention and compared with controls. On average $5.55x10^6$ MSCs were injected intramyocardial or intracoronary. Follow up was done by echocardiography plus single-photon emission computed tomography before and six months after the procedure. Serial clinical examination was performed every month through New York Heart Association class. It was reported that single-photon emission computed tomography scan results that infarct size decreased significantly in the test group after the procedure at six months follow-up. LVEF increased significantly. Therefore the transplantation of *ex vivo* expanded bone marrow derived mesenchymal stem cell in patients was a safe and feasible procedure and improved cardiac function without serious adverse effects.

In another study Yang et al [72] evaluated the safety and feasibility of autologous bone marrow MSC transplantation in patients with acute myocardial infarction (AMI) who had successfully undergone percutaneous coronary intervention (PCI). Cultured bone marrow MSCs were injected (average of $1.2x10^7$ cells per patient) into the myocardium via either the infarct-relative artery (left anterior descending branch artery, LAD) or a non-infarct relative artery (right coronary artery, RCA). A 6-month follow up was done using 2D echocardiography, technetium-99methoxyisobutylisonitrile (99mTc-MIBI) and ^{18}F-deoxyglucose single photon emission computed tomography to examine cardiac function, myocardial perfusion, and viable cardiomyocytes, respectively, at day 4 after PCI and

6 months after the cell infusion. There were no arrhythmia and any other side effects, including infections, allergic reactions or adverse clinical events, during, immediately after, or 6 months after cell transplantation. Cardiac function and myocardial perfusion had significantly improved; viable cardiomyocytes metabolism was detected in the infarcted areas in both groups after the cell infusion, shown by ^{18}F-deoxyglucose. Delivery via the non-infarct relative artery appears safe and feasible.

A meta-analysis for the use of MSCs was done by Lalu *et al* [73]. A total of 1012 participants with clinical conditions such as ischemic stroke, cardiomyopathy and MI were included in this analysis. Many parameters were assessed such as acute infusional toxicity, organ system complications, infection, death or malignancy. This study demonstrated that MSC therapy seems to be safe although there is a significant correlation between MSC infusion and transient fever. However from many other reports MSC transplant is causing improvements in cardiac prognosis and transient fever does not cause any worrying long term or side effects.

2.3.4. Cardiac Stem Cells (CSC)

Intrinsic cell mediated repair in the heart has been recently reported by the ability of forming new heart tissue *in vivo* [74-76], implying the existence of a stem cell-mediated tissue repair mechanism in the heart [77]. Cells expressing stem cell markers, including c-kit and Sca-1, can be isolated from adult tissue and expanded in culture [76]. *In vitro* clonal analysis has revealed that these cardiac stem cells (CSC) can give rise to immature cardiomyocytes, smooth muscle cells and endothelial cells [75, 76], and *in vivo* can generate cardiomyocytes and improve function after injection into the myocardium of infarcted rodents [78]. Quickly after its identification, CSCs were put into clinical trials. Phase I clinical trial Cardiac Stem Cell Infusion in Patients With Ischemic CardiOmyopathy (SCIPIO) [79] demonstrated that intracoronary

infusion of autologous C-Kit+ cardiac stem cells (CSCs) is safe and effective at improving LV systolic function and reducing infarct size in patients with chronic ischemic cardiomyopathy. The CArdiosphere-Derived aUtologous stem CElls to reverse ventricUlar dySfunction (CADUCEUS) [80] trial, a phase I randomized clinical trial of cardiospheres as a cell-based therapeutic, demonstrated a reduction in scar mass and an increase in viable heart mass, regional contractility, and regional systolic wall thickening at 6 months after cell therapy.

Great controversy over the CSCs over the recent months has raised many questions and a closer examination of the true identity of these CSC is under investigation [81, 82]. However some researchers have been using combinations of stem cell therapies, which seems promising. A preclinical study by Williams *et al* [83] shows that the combination of MSCs and C-Kit+ CSCs is more effective at reducing infarct size and restoring cardiac function than either cell type alone. In this study intramyocardial combination hCSCs/hMSCs ($1x10^6/200x10^6$), hCSCs alone ($1x10^6$), hMSCs alone ($200x10^6$), or placebo (phosphate-buffered saline) was injected into the infarct border zones at 14 days after MI. Cardiac function post transplantation was assessed via magnetic resonance imaging and micromanometer conductance catheterization hemodynamics. Each cell therapy by itself significantly reduced MI however the MI size reduction was 2-fold greater in combination versus either cell therapy alone, LVEF was also significantly improved in the combined therapy. Post-mortem histology showed 7-fold enhanced engraftment of stem cells in the combination therapy group versus either cell type alone.

A summary of the use and effect of all the above-mentioned stem cell types as therapeutic approach follows bellow on **Table 1**.

Table 1 – Summary of the various types of stem cells used on regeneration.

Stem Cell Type & Sub-population	Dosage, Delivery mode, Disease Model and end point	Results	Reference
EPCs with CD34+ enriched populations	Total cells count of $1.6\times10^{9}\pm0.3\times10^{9}$ containing $3.8\times10^{7}\pm1.6\times10^{7}$ CD34+, intramuscular delivery in human limb ischemia, end point 4 months	⇑ transcutaneous oxygen pressure (TcPo2) ⇓ pain during walking time ⇓ acetylcholine-mediated endothelium-dependent blood flow	Higashi *et al* [51]
EPCs with CD34+ enriched populations	Total cells count of $5.8\times10^{7}\pm4\times10^{7}$ containing $9.8\pm9.91\times10^{6}$ CD34+, in human limb ischemia, end point 6 months	⇑ transcutaneous oxygen pressure (TcPo2) ⇓ pain during walking time ⇑ ulcer healing ⇑ active angiogenesis	Motukuru *et al* [53]
EPCs with CD34+ enriched populations	Total cells count of $1.11–4.49\times10^{9}$ containing $0.39–1.93\times10^{6}$ CD34+, intramuscular delivery in human limb ischemia, end point 1 year	⇑ endothelial cells markers: CD31+, CD34+ and vWFR+ ⇔ amount of amputations ⇓ pain during walking time	Duong Van Huyen *et al* [50]
EPCs with CD34+ enriched populations	Total cells count of $1\text{-}4\times10^{8}$ containing 1×10^{6} CD34+, intra-arterially delivery in human limb ischemia, end point 1 year	⇑ wound healing ⇑ blood flow at 3 months under angiographic analysis	Ruiz-Salmeron *et al* [54]

Stem Cell Type & Sub-population	Dosage, Delivery mode, Disease Model and end point	Results	Reference
EPCs with CD34+ enriched populations	Total cells count of 1-2 × 10^8 containing 2-3 × 10^6 CD34+, intra-arterially delivery in human limb ischemia, end point 6 months	⇓ pain during walking time ⇑ ulcer healing ⇔ amount of amputations ⇑ mobility	Walter *et al* [56]
EPCs with CD34+ enriched populations	Total cells count of 1-5 × 10^8 containing 1-4 × 10^6 CD34+, intramuscular & intra-arterially delivery in human limb ischemia, end point 1 year	⇓ pain during walking time ⇔ amount of amputations	Van Tongeren et al [55]
BM-MNCs enriched with EPCs	Total cells count of 60-90 x 10^8 containing 10^6 CD34+, intramuscular delivery in human myocardial infarction, 5 year follow up but ongoing trial (TOPCARE-AMI)	⇑ Left Ventricle Ejection Fraction (LVEF) ⇓ MI reoccurrence ⇓ serum levels of N-terminal pro-hormone brain natriuretic peptide (NT-proBNP) ⊗ none of the patients showed any signs of intramyocardial calcification or tumours ⇓ functional infarct size	Leistner *et al* [58]

Stem Cell Type & Sub-population	Dosage, Delivery mode, Disease Model and end point	Results	Reference
BM-MNCs	Total cells count of 150×10^6, intra-coronary infusions, human acute myocardial infarction (AMI), 6 months (LateTIME)	◊ demonstrates timing of cell delivery following AMI is a critical factor in determining the efficacy of cell therapy ⊗ no improvement in global or regional function at 6 months ⇔ LV end-systolic volume	Traverse *et al* [59, 60]
BM-MNCs	Total cells count of 1×10^8 transendocardial delivery, chronic ischemic heart failure, 6 months (FOCUS-CCTRN)	⇔ maximal oxygen consumption & myocardial perfusion ⇑⇑ stroke volume ⇑⇑ LVEF	Perrin *et al* [62]
EPCs, CD34+ only	Total cells count of 1×10^5 or 5×10^5, intramyocardial, human refractory angina, 1 year (ACT34-CMI)	⇑⇑ in exercise tolerance (at 6 and 12 months)	Losordo *et al* [63]

Stem Cell Type & Sub-population	Dosage, Delivery mode, Disease Model and end point	Results	Reference
CSCs	Patient own expanded cells from endomyocardial biopsy suffering from human ischemic cardiomyopathy, ongoing clinical trial (CADUCEUS)	⇓ scar mass ⇑ viable heart mass ⇑ regional contractility ⇑ regional systolic wall thickening ⇓⇓ infarct size ⇑⇑cardiac function ⇑ LVEF ◊ Post-mortem histology showed 7-fold enhanced engraftment of stem cells	Makkar *et al* [80]
Combination of MSCs and C-Kit+ CSCs	Intramyocardial delivery, human myocardial infarction, ongoing clinical trial (CADUCEUS)		Williams *et al* [83]

Stem Cell Type & Sub-population	Dosage, Delivery mode, Disease Model and end point	Results	Reference
BM-MSCs	Total cells count of 5.55×10^6, at the time of coronary artery bypass grafting or percutaneous coronary intervention on human myocardial infarction, 6 months	⇓ infarct size ⇑ LVEF ◊ was a safe and feasible procedure	Mohyeddin-Bonab *et al* [71]
BM-MSCs	Total cells count of 1.2×10^7, delivered via infarct-relative artery (left anterior descending branch artery, LAD) or a non-infarct relative artery (right coronary artery, RCA) on human myocardial infarction, 6 months	◊ procedure was safe and feasibile ◊ no arrhythmia and any other side effects ⇑ cardiac function ⇑ myocardial perfusion ◊ viable cardiomyocytes detected in the infarcted areas	Yang *et al* [72]
CSCs , C-Kit+ enriched	Patient own expanded cells from aortic biopsy suffering from human ischemic cardiomyopathy, ongoing clinical trial (SCIPIO)	◊ procedure was safe ⇑ LV systolic function ⇓ infarct size	Chugh *et al* [79]

2.3.4.1. Expansion of CSCs

Beltrami *et al* were some of the pioneers in CSC isolation; they first reported the isolation and usage of CSCs [74]. They isolated CSCs by positive selection of Ckit marker also know as CD116 using magnetic beads and also FACS. These cells were expanded under normoxia for 5-7 days to attain enough numbers for transplantation. However proliferation was slow, doubling times were of 40 hours and not much more than 20,000 cells were available for each sort. At passage 2, after a starting with 20,000 cells only 100,000 cells were available and these were transplanted *in vivo*. Furthermore fibroblast contamination in these cultures was detected. Yet these protocols are widely used, including ourselves [78] and within the clinical trials cell preparations [79, 80]. Here as illustrated in **Figure 4**, cell are explanted from tissue removed from the atria, cells outgrow from the explanted tissue and are harvested to so as to form cardiospheres which later are made to adhere and create monolayers of cells cardiosphere derived cells (CDCs) [84]. From these protocols a total of 15 x 10^6 CDCs can be attained from one neonatal rat heart after 10 days of culture.

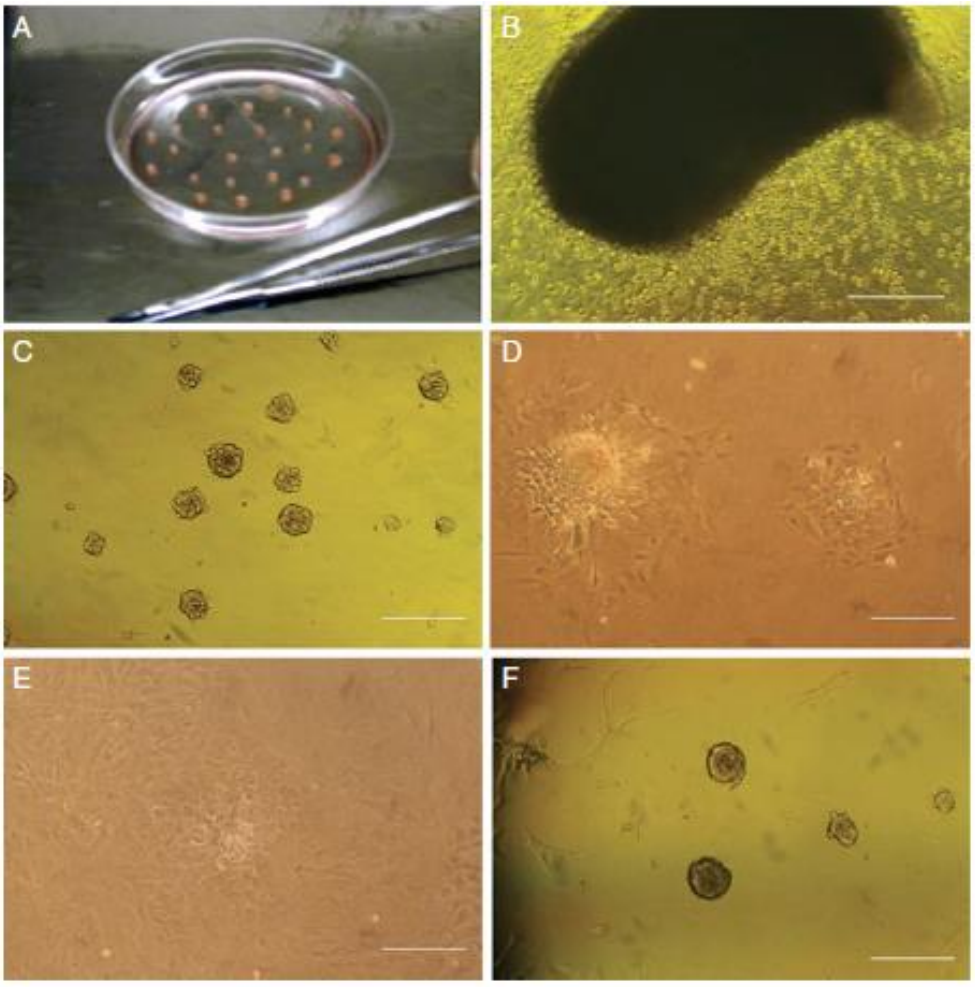

Figure 4. Isolation of CDCs. Extracted from Tan *et al* [84]; Cardiac stem cell isolation by explant culture. (**A**) Heart tissue is minced into pieces and explanted on a fibronectin-coated petri dish. (**B**) Phase-bright cells grow from the explant on top of a layer of stromal-like cells after 7 days. (**C**) Cardiospheres form after 4 days on poly-D-lysine. (**D**) Cardiospheres are expanded in a fibronectin-coated flask to become a monolayer. (**E**) Passage-0 cardiosphere-derived cells become confluent after 5 to 7 days. (**F**) Cardiosphere derived cells form second-generation cardiospheres at passage 5. Scale bar is 250 **μ**m.

Oh *et al* were set to determine the best isolation method for progenitor cells within the adult heart after digestion, so as to attain cultures as pure as possible. They used a double isolation method, first isolated cells via FACS and based on hematopoietic cell surface markers including Ckit and Sca-1. They found a side population based on Hoechst efflux. They concluded that 14-17% of the murine cells were Sca-1+ yet none positive for blood markers. Afterwards a second selection was done using magnetic enrichment for Sca-1+ cells, here there was above 90% purity of the cultures. This study was important

by the identification of markers for CSCs selection and that these cells could then be after isolation differentiated using 5-azacytidine (5-aza) and form "cardiomyocyte like cells". No cell numbers or doubling times were reported here [85]. Tang *et al* also followed a double isolation method [86], first, by expansion of endogenous cardiac stem cells through primary heart tissue explant, second, by isolation of stem cells from fibroblasts by cell sorting with stem cell markers, and cloning. The end product was a fibroblast-free culture system of Sca-1+ cells, which kept cellular self-renewal, and clonogenic character untouched, and also as shown by Oh *et al*, can differentiate into cardiomyocytes-like cells. Tang *et al* also show that these cells can double and from a starting point of 2×10^6 cells 10×10^6 cells can be attained 14 days later.

Nonetheless the antigens that are targeted for the isolation CSCs varies a lot between laboratories. These cells for lab or clinical trial usage have been produced under traditional cell culture setting, expansion has not been done any bioreactors, expansion is slow and extraction of tissue for culture is very invasive.

A summary of the isolation procedures above-mentioned follows bellow on **Table 2**.

Table 2 – Summary of the isolation procedure of the various sub-types of CSCs used on regeneration.

Cardiac Stem cell sub-type	Isolation technology	Source	Selection Marker	Characteristics	Reference
Cardiac c-kit +	Heart digestion + MACS/FACS	Rat heart	Lin-c-kit +	Self-renewing, clonogenic and multipotent	Beltrami *et al* [74]
Cardiac Sca-1+	Heart digestion + MACS	Mouse heart	Lin-, Sca-1 +, CD31 +, CD38 +, c-kit-, Flk-1-, CD45 −	Expression of cardiogenic transcription factors; differentiation after 5-aza induction	Oh *et al* [85]
	Two-step procedure: tissue explanting + MACS	Mouse heart	Sca-1 +, c-kit + and CD45 −	Self-renewing, clonogenic and multipotent	Tang *et al* [86]
Cardiosphere-derived cells (CDCs)	Sphere-forming cells from tissue explanting technology	Human atrial, ventricular biopsy; postnatal mouse hearts	KDR + CD31 +, CD34 +, c-kit +, Sca-1 +	Clonogenic	Messina *et al* [75]

2.3.4.2. CDCs and hypoxic pre-conditioning

Hypoxia might be beneficial for stem cell maintenance, as stem cells have been shown to live in niche of reduced oxygen levels. Recent studies show the importance of hypoxia in human MSCs and induced pluripotent stem cells (iPSCs), indicative that hypoxia promotes an undifferentiated state [87-90]. It is believed that the hypoxic environment maintains cell pluripotency by maintaining cells in a non-

dividing, or slow cycling stage and protected from detrimental accumulation of reactive oxygen species (ROS). It is reported that ROS would be reduced to secure the maintenance of stem cells in the case of hypoxia [91]. A study with adipose stem cells (ASC) demonstrates that these proliferate and migrate more significantly by increasing the intracellular levels of ROS [92, 93] yet the mechanisms are still unclear.

Hypoxia triggers a number of physiological and cellular mechanisms to adapt to reduced oxygen levels. Many processes involved in oxygen homeostasis are mediated by the hypoxia-inducible factor [94] transcriptional complex, which was discovered in 1992, and which comprises HIF-α and HIF-β subunits [95]. HIF-α protein is only detectable under hypoxic conditions while HIF-β protein is constitutively stable. Human HIF-α exists as three isoforms, the two best characterized of which (HIF-1α and HIF-2α) each contain two sites of prolyl hydroxylation and a single site of asparaginyl hydroxylation [96]. Prolyl hydroxylation occurs at residues Pro402 and Pro564 catalyzed by prolyl-4-hydroxylase (PHD) whereas asparaginyl hydroxylation at residues Asn803 catalyzed by factor-inhibiting HIF (FIH) enzymes [97]. Both hydroxylation inhibit HIF system, but yet in a slightly different mechanism. Prolyl hydroxylation marks the protein for degradation by the von Hippel Lindau protein (pVHL), leading to proteasomal degradation of total HIF-α protein, while asparaginyl hydroxylation within HIF-α C-terminal transactivation domain [98] inhibit the interaction of CAD with CBP/p300 (Creb-binding protein/protein 300), which is essential to link the HIF-α to the hypoxia response element (HRE) transcriptional factor, thus silencing the HIF system [99, 100]. Under hypoxia, HIF-α escapes both the prolyl and asparaginyl hydroxylation, translocates to the nucleus and dimerises with HIF-1β to form functional heterodimeric HIF.

No studies have been performed on effects on effects of hypoxia and CSCa, as a result we have in chapter V examined the effects on both proliferation and differentiation of CSCs.

2.4 Delivery of angiogenic growth factors

Limb ischemia often results from arterial occlusion and stenosis as a consequence of atherosclerosis. Endothelial dysfunction is an important factor in pathogenesis for plaque initiation and progression within limb ischemia [101, 102]. It is common clinical practice to tackle limb ischemia involves surgical revascularization either by stent implantation, laser revascularization or bypass surgery, however the success rates are still disappointing, leading to gangrene and amputation in a large majority of cases. It is speculated that successful treatment with the above therapies may eventually cause restenosis due to phenotypic redifferentiation of neovascular intimal smooth muscle cells [103].

Various forms of delivery of angiogenic growth factors have been approached using biomaterials [104-106]. When looking into growth factor delivery via biomaterials many factors are taken into account. Firstly, efficiency of factor entrapment and release is very important, taking into consideration the high cost of the growth factors. Furthermore, it is important that a sustained delivery is achieved rather than a burst effect for greater effect of biomolecules such as angiogenic factors [107]. Burst effects can be achieved with ease via traditional local injection, however these also introduce needle track injuries and responses to such.

In many cases, PLGA NPs, porous matrices and scaffolds, hydrogels, liquid-injectable hydrophobic polymers have been used for the delivery of growth factors [107-111]. In this chapter we focus on the use of PLGA NPs for delivery of biomolecules. NPs, namely PLGA NPs are capable of delivering sustained amounts of encapsulated factors and proteins over a relatively long-time in vivo [112-114]. NPs can deliver a range of biomolecules from interleukins to factors and proteins, used as vaccination systems too, for cancer or localized tumour regression.

PLGA renders these NPs biocompatible, have a reasonable shelf life and degrade completely *in vivo*. Yet polymer (PLGA) degradation can be an issue when delivering larger proteins, in terms of protein stability [115]. PLGA degradation can be responsible for creation of acidic environments, which in turn can induce the unfolding of the proteins. Furthermore, acidity might cause tissue inflammation where PLGA NPs degraded *in vivo* [116].

PLGA NPs can be used for growth factor delivery. Although burst release and creation of acidic environments *in vivo* can influence effectiveness of biomolecule delivery many authors have exploited the PLGA NPs for $VEGF_{165}$ delivery. Classical studies such as by Cleland *et al* [117], demonstrated that 9% (weight per volume) of the VEGF loaded into the NPs had a low affinity, overtime the VEGF aggregated and were not recognizable to ELISA assays, however the delivery was sustained over 28 days without a burst period. Nevertheless the VEGF release increased local angiogenesis without systemic side effects.

Several examples in the use of PLGA nano/microparticles for $VEGF_{165}$ delivery are documented in the literature. The first thorough report of VEGF degradation within PLGA NPs was by Kim *et al* [118]. The authors have used a system to release VEGF in order to develop a pharmacokinetic model for controlled VEGF release. However the *in vivo* release profiles of the proteins were slower than the *in vitro* release profiles but they followed similar trends. The PLGA microsphere degradation was the determinant step for VEGF release from the microspheres and its absorption at the subcutaneous site. It was found that 25% of VEGF activity was lost following release from PLGA NPs. This loss of activity may be due to degradation in acidic environments as a result of PLGA degradation [118]. The main problem for an efficient VEGF delivery was the acidic environments [119-122], therefore many have attempted to incorporate PEG and basic salts into the NP formulations. Inclusion of basic salts into formulations did not prevent acidity and the usage of PEG only kept the pH between 5-5.8.

2.5. Micro RNAs (miRs) for enhancing angiogenesis and cell survival

Taking into consideration the delivery of angiogenic proteins is rather problematic and somethimes inefficient; the delivery of oligonucleotide and smaller fragment such as miRs has been explored [123].

miRs are small 20-24 nucleotide long RNAs which regulate gene expression by binding to mRNAs. MiRs can regulate 30-50% of protein coding genes [124]. miRs are transcribed as a primary miR (pri-miRNA) transcript by RNA polymerase II. The miR transcripts are cleaved by a heterodimer of double strand RNA binding proteins, Drosha and DiGeorge Syndrome Critical Region 8 (DGCR8), releasing a 55-70 nucleotide small RNA hairpin, the pre-miR. This RNA hairpin is then exported out of the nucleus by Exportin-5 and Ran-GTP. In the cytoplasm, another RNAse III enzyme, Dicer cleaves the pre-miRs to generate 22nt duplex RNAs. These are by now mature miRs that get included into RNA induced silencing complex, the RISC complex, consisting of two major classes of proteins Argonaute and GW182. Translational repression or deadenylation will follow as shown in **Figure 5**. This is the accepted pathway of miR biogenesis, however recent research has shown several alternative pathways depending on cell type, organism and biological contexts [125, 126].

Initially it was proposed that miRs bind to target mRNAs using a seed sequence consisting of 6-8 continuous bases and a few more complementary bases along the miR sequence. In mammalia, the miRs rarely have a perfect complementarity with their targets. Therefore, it has been hypothesized that mammalian miRs suppressed translation of target mRNAs leading to a decrease in target proteins [127]. It has been proposed that miRs maintain robustness of gene expression by insulating biological systems against noise [128]. miRs offer a unique advantage by regulating gene expression in the cytoplasm this because of regulatory mechanisms that control gene expression programs such as transcriptional regulators, epigenetic modifications. Also there are miRs that could be up-regulated quickly in cells achieving greater potency than possible via other mechanisms. There have been simulations that

demonstrate that miR mediated feed forward loops are more effective than transcriptional repressors in buffering gene expression against external perturbations [129]. The beauty of miRs is that they can regulate multiple targets, often several of them in a single pathway, making it an effective tool to modulate gene expression in response to specific stimuli.

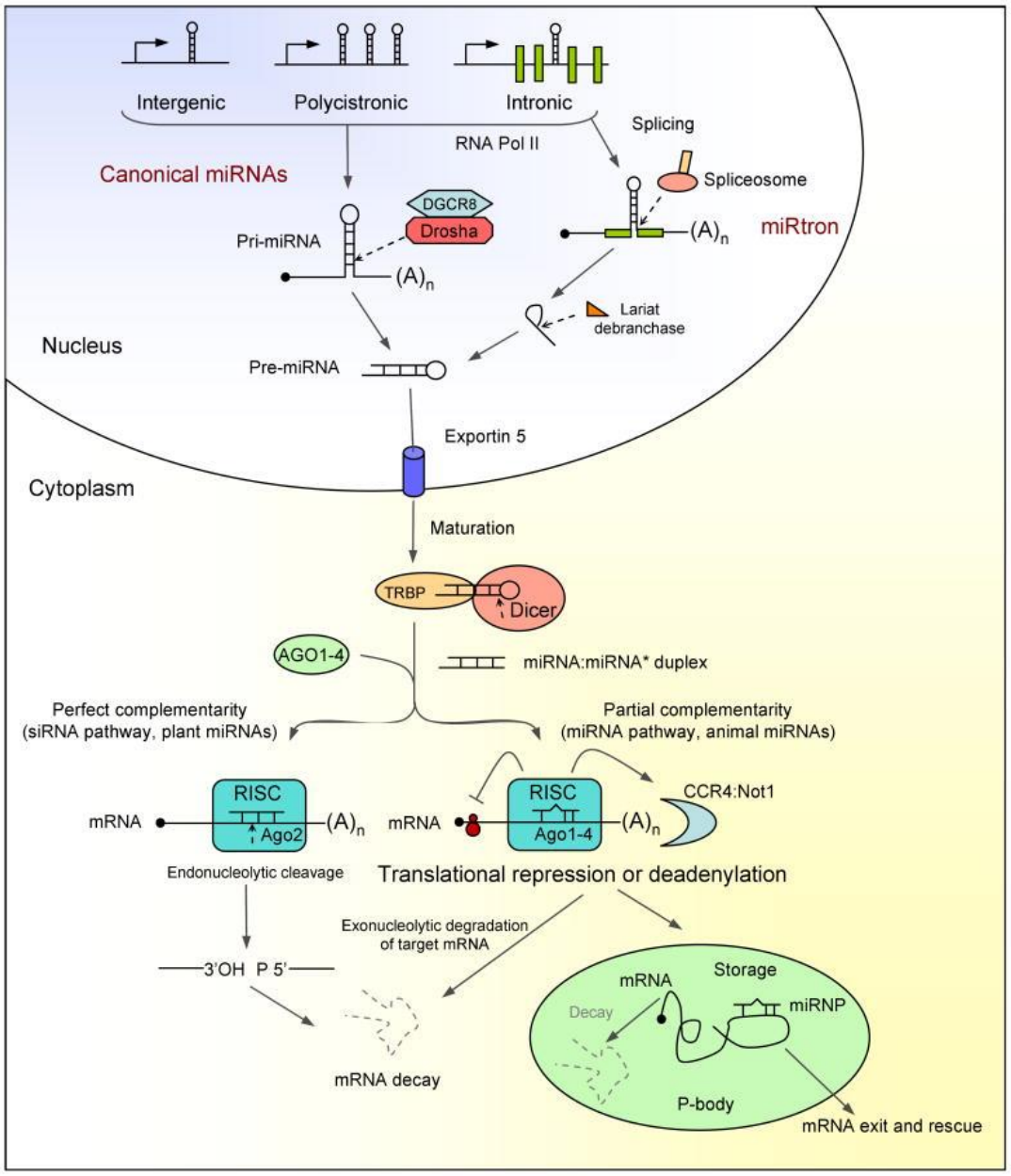

Figure 5 – Illustration of miR biogenesis and function. Extracted from Suarez and Sessa [130]. Nuclear miRs originate in the nucleus as RNA polymerase II primary transcripts (pri-miRs), transcribed from miR genes, from polycistronic transcripts, or from introns of protein-coding genes. Pri-miRNAs are then processed and catalyzed by RNase III type endonuclease Drosha and Dicer. These function in complexes with double-stranded RNA–

binding domain proteins, DGCR8 and TRBP for Drosha and Dicer, respectively. Drosha-DGCR8 processes pri-miRs to premiRs. A subset of miRs, miRtrons, also derived from introns, is processed into pre-miRNAs by the spliceosome and the debranching enzyme. Both miRs and miRtrons are exported to the cytoplasm via Exportin5, where they are further processed by Dicer-TRBP to yield 20-bp miRNA duplexes. One strand is selected to function as mature miR and loaded into the RISC, whereas the partner miR* strand is degraded. The mature miR leads to translational repression or mRNA degradation. The key components of the RISC are components of the Argonaute family. Fraction of miR* species can also access Ago complex and regulate targets. Perfect complementarity between miR and mRNA leads to an endonucleolytic cleavage, catalyzed by the human Ago2 in the RISC. Animal miRs usually show only partial complementarity to the target mRNA promoting translational repression or deadenylation coupled to exonucleolytic degradation of target mRNA. mRNAs repressed by deadenylation or at the translation–initiation step are moved to P-bodies for either degradation or storage [130].

2.5.2. miRs with pro-survival and pro-angiogenic activity

From the STRING database it can be seen that many miRs interact affecting receptors, ligand and transcription factors related to cell survival and angiogenesis. Some miRs when down-regulated such as miRs 21, 27, 34a, 34ac, 124, 130, 148, 221, 222 and 503, have been predicted to target NOTCH and VEGF signaling [131], a few miRs can amplify a pro-angiogenic signalling network. In contrast, up-regulation of miR-132 and 126 induce angiogenesis by negative regulators of VEGF signalling, like p120RasGAP and SPRED1, respectively. Poliseno *et al* performed the first study implying that miRs were involved in endothelial cell regulation [132]. Once the most abundant miRs were arrayed from HUVECs many miRs were predicted to target angiogenic growth factor receptors such as miR221/222 as negative regulators of angiogenesis [132]. miR126 is the most abundant miR in endothelial cells and in 2008 two studies reported the first evidence for *in vivo* function of miR126 [133, 134]. It was shown that miR126 was important for developmental and pathological angiogenesis and implicated Sprouty Related EVH Domain containing protein 1(SPRED1), a negative regulator of VEGF. It has also been reported that miR126 regulates endothelial cell recruitment to metastatic breast cancer cells, *in vitro* and *in vivo by* down-regulating a complex network of targets (suppressed metastatic endothelial recruitment, metastatic angiogenesis and metastatic colonization) [135]. miR92a was shown to have an

anti-angiogenic effect partly through targeting the integrin subunit α5 [136, 137]. Loss of miR92a improved functional recovery after myocardial infarction and limb ischemia by enhancing blood vessel growth [136, 137].

Angiogenesis is highly dependent on stimuli; during developmental and pathological angiogenesis many stimuli can trigger distinct miR expression profiles. miR210 and miR424 are up-regulated in response to hypoxia [138-141]. Some specific miRs are up-regulated in response to angiogenic growth factors VEGF and bFGF [142]; while others are regulated by Notch pathway signalling [143] and cytokines such as IL-3 [144]. All the above have been demonstrated to trigger miR expression via classic signal transduction pathways and transcription factors.

2.5.3. Nanomaterials for the delivery of miRs.

The success of a gene therapy application depends on three factors, a) the choice of an appropriate therapeutic gene, b) the delivery of this gene to a sufficient number of cells, c) the achievement of appropriate levels of gene expression [145]. The lack of an ideal vector, capable of fulfilling the above requirements is a constant hurdle. The highly effective vectors render worries about safety for human usage and others considered safe are not efficient enough. Importantly, a theranostic approach for the delivery of miR was not described before the performance of the current PhD thesis.

miR delivery *in vitro* is often done using cholesterol conjugated 2'-O-methyl antisense oligonucleotides, locked nucleic acid based antisense oligos (LNAs), oligos with multiple miR binding sites to act as competitive inhibitors (miR sponges) or oligos with gene specific sequences complementary to miR binding sites (miR masks) [146].

The effectiveness of these delivery methods depends on the miR to deliver and where within the cells.

It has been postulated that it is desirable to deliver exogenously prepared miRs because naked miRs are often unstable and destroyed [147], therefore delivery of miRs using NPs makes a lot of sense.

In vivo miR delivery has traditionally been done using naked injections which results in delivery of miRs to the liver however for specific tissue targeting, our practical experience is that to deliver miR within ischemic injury or tumour vasculature the naked injections are disappointing and challenging.

From the literature there is over 50 reports published for the delivery of miRs using NPs, bellow are described some of the most interesting. **Table 3** shows as reviewed by Kanwar *et al* [148], various types of nanomaterials can be used for miR delivery, however our focus shall be on NPs.

Table 3 – Summary of namomaterials for miR delivery, extracted and adapted from Kanwar *et al* [148].

Name	Composition	Features and uses	Reference
Carbon nanotubule	Composed of fullerenes (C60 compounds) and/or carbon-based hollow cage-like structures	Increased internal volume and ease of functional modification of internal and external surfaces. Single-walled nanotubes are used for drug and gene delivery. Double-walled nanoparticles have better implications for transfection	Foley *et al* [149] Martin *et al* [150]
Liposome	Amphipathic lipids	SUVs composed of single lipid bilayer, where as LUVs consist of multiple layers. They alter the pharmacokinetic profile of loaded drug molecules	Rawat *et al* [151]
Solid lipid nanoparticle	Amphipathic lipids	Comprise a hydrophobic core (50-100 nm in diameter); they can be used as an effective adjuvant for vaccines and as non-viral transfection agents	Cevc *et al* [152]
Polymeric nanoparticle	Biodegradable and biocompatible polymers	Nanocapsules entrap the drug and nanospheres can be used for coating the drug on their surfaces. They enable greater control of the pharmacokinetic behavior of the loaded drug, leading to more appropriate steady levels of the drug	Rawat *et al* [153]
Polymeric micelles	Amphipathic lipids	They are formed in hydrophobic environments and are suitable for the delivery of water-insoluble drugs because of their core shell structure	Torchilin *et al* [153]
Functionalized nanoparticle	Inorganic metal such as Pt, Pd, Au and Ag	Fluorescent properties can be incorporated to be used as biosensors. They can also be used as markers for research in molecular biology, targeted drug delivery and biosensing	Sechneider *et al* [154]

The delivery of miRs by NPs is recent and mostly used for *in vitro* applications. For example, most recently, Sohn *et al* [155], used polyketal polymer PK3-miR loaded NPs to deliver miR to somatic cells for 6 days. Resulted in the formation of colonies which when assayed for various pluripotency markers, there was a substantial induction Oct4, Sox2, and Nanog expression. These colonies were also SSEA-1 positive. Sohn *et al*, demonstrated that using NPs and miRs activation of pluripotency associated genes in mouse BM-mononuclear cells using embryonic stem cell (ESC)-specific miRs encapsulated in the acid sensitive polyketal PK3 is possible. Magnetic NPs have also been used for successful transfection and miR delivery [156].

Schade *et al*, developed a technique to deliver miR335 into hMSCs with using magnetic non-viral vector based on cationic polymer polyethylenimine (PEI) bound to iron oxide magnetic NPs. The toxicity of various constructs was tested; the release, processing and functionality of delivered miR335 were assessed. They found that these NPs were able deliver functional miR335 however at maximal NP internalization (~75%) there was a moderate cytotoxicity in hMSCs. Another interesting study shows introduction of short seed-directed LNA oligonucleotides (12- or 14-mer antiseeds) with a phosphodiester backbone (PO) for efficient miR inhibition, which lead to the formation of polymeric NPs [157]. The authors show the successful functional delivery of LNA (PO) 14-mer anti-seeds into cells. The LNA (PO) 14-mer antiseeds are attractive miR inhibitors, and their PEI-based delivery may represent a promising new strategy for therapeutic applications.

NPs have been also used as miR delivery vectors *in vivo*. Chen *et al*, developed a LPH (liposome-polycation-hyaluronic acid) NP formulation modified with tumor targeting single-chain antibody fragment (scFv) for systemic delivery of small interfering RNA (siRNA) and miR34a into experimental lung metastasis of murine B16F10 melanoma [158]. The two daily intravenous injections of the combined NPs significantly reduced the tumour in the lung. In this study it was shown that the simultaneously

delivery of miR34a and siRNAs within the NPs enhanced the anticancer effect. In a different model, Zhou *et al* used PLGA NPs to form NP/TGF-β1 miR plasmid (NP/plasmid) to silence the expression of TGF-β1 gene associated with scar and adhesion formation in the flexor tendons. Both *in vitro* and *in vivo* transfection against tenocytes revealed that the NP/plasmid complexes have significantly superior transfection efficiency over the lipofectamine/plasmid complexes [159].

In another study PLGA NPs were used to deliver antisense oligonucleotides to inhibits miR155 mouse model of lymphoma. It was shown that systemic delivery of antisense peptide nucleic acids encapsulated in the NPs inhibits miR155 and slows the growth of these "addicted" pre-B-cell tumours *in vivo*, suggesting a promising therapeutic option for lymphoma/leukemia [160].

Table 4 shows some other types of miRs that have been delivered using NPs, its characteristics and effects.

Table 4 – Summary of miR delivery by NPs.

NP type, size, charge	Loading efficiency, location of delivery, miR stability	Effect, theranostic system?	Reference
Iron oxide NPs, size range 50-220 nm, final charge of 41.54 ± 1.61 mV.	5pmol of miR335 per 1μg NP, delivered into mesenchymal stem cells, miR rendered functional, 74% of cells labelled and formulation delivered within the cytoplasm.	Target genes of miR335 were down regulates, is a possible theranostic modality however this study dies not show *in vivo* testing or MRI imaging of labelled cells.	Schade *et al* [156]
Silica NPs, 74 nm, charge not mentioned.	6.8×10^{9} particles/mL (40 μg/mL) delivered into NB1691, SK-N-AS and HEK293 cells carrying miR34a. Delivered into solid tumors after in vitro testing. The miR carried was stable and functional.	NPs were able to deliver miR to the tumor, which over-express miR-34a from 4 to 25 fold in NB1691 tumours, and 2 to 7 fold in SK-N-AS tumours. Imaging done using in vivo fluorescence system (IVIS).	Tivnan *et al* [161]
Silencing nanoparticles made of poly-L-lysine (iNOP-7)	2 mg kg^{-1} of iNOP-7 were systemically delivered into mice to determine the rolemiR-122 silencing on cholesterol metabolism.	iNOP-7 efficiently delivered anti-miR122 into cells, specifically silenced miR122 in a dose-dependent manner. Endogenous miR-122 was slightly reduced by 10 pM, ~90% of miR-122 was silenced at 1 nM. *In vivo* it was seen that miR122 participates in regulation of the cholesterol biosynthetic pathway and that silencing was achieved without apparent toxicities.	Su *et al* [162]

2.6. Cell tracking

One of the main issues related to the cell-based therapies for heart regeneration is to understand the ultimate fate of the transplanted cells, their location, survival and function. Multiple clinical trials are examining the therapeutic effect of different stem cells and it is necessary to develop approaches to monitor their mechanism and safety. Monitoring the fate of stem cells in clinical trials requires the use of non-invasive imaging techniques. Ideally, these imaging techniques would have single-cell sensitivity and would permit quantification of exact cell number at any anatomic location [163]. In addition, it is desirable to have a technique to track the injected cells for months to years for long-term follow-up of cell function and survival.

Several imaging techniques are available for in vivo tracking of stem cells, including X-ray-based methods (e.g. computed tomography), optical imaging (bioluminescence and fluorescence), ultrasound (e.g. echocardiography), single-photon emission computed tomography, positron emission tomography, and magnetic resonance imaging (MRI) [163, 164]. Echo is widely used of easy access and low cost, used in urgent bedside cases and useful to access vascular function and valve functions as well as other abnormalities [165], remains heavily used, especially given the benefits recently achieved by contrast and strain imaging. However echocardiography results are heavily dependent on the user and deviations are relatively high mostly due to user interface and might not be so comparable to more robust less prone to bias methodologies [166]. Three-dimensional Echo could overcome some of the above issues however it is not widely available [167]. SPECT is well established for the detection of myocardial ischemia in heart failure and other ischemic episodes [165]. Radionuclides are heavily used and present significant kidney and radiation risks. They are widely available and highly reproducible but limited spatial resolution and artifacts are common [168]. PET and MRI are widely used but of limited availability (due to expense) and safety concerns regarding the contrast agents used. MRI is the most comprehensive cardiac and vascular imaging tool,

offering high-quality information on cardiac structure, function, blood flow, and tissue characterization. SPECT provides high diagnostic accuracy and offers high hopes for incrementally offering perfusion and myocardial scar imaging but ionizing radiation exposure becomes an increasing concern with combined CT-based evaluations, and efforts to limit such exposure are of high priority for both CT and nuclear imaging-based technology development.

MRI combines the chemical sensitivity of nuclear magnetic resonance with high spatial and temporal resolution, therefore provides optimal technical characteristics to track stem cells at the myocardium. Beyond anatomical imaging, MRI has the ability to examine organ functionality and perfusion [169]. MRI can detect a wide range of biologic information, including flow, motion, morphology and tissue composition. The ability to label stem cells with NPs, such as superparamagnetic iron oxide (SPIO) NPs, gadolinium, fluorine, iodine and manganese-based NPs, can provide a method to initially localize the stem cells and monitor their migration. Some of these formulations are commercially available [3]. SPIO NPs are negative contrast MRI agents composed of an iron oxide core, responsible for the imaging contrast, and a dextran, carboxydextran or starch coat, which inhibits NP aggregation [170, 171]. Gadolinium-containing NPs are positive contrast MRI agents, which have gadolinium oxide, Gd2O3, at its core, providing high-contrast enhancement in MRI [172]. These NPs are mainly used as cardiovascular system contrast agents rather than a specific organ or cell markers; nevertheless they may be used for specific cell marking. Fluorine containing NPs are also emerging as an alternative formulation to label stem cells. In contrast to SPIO NPs, fluorine NPs allows the selective visualization of the labelled cells by ^{19}F MRI, while anatomical information is attained by ^{1}H MRI [3, 171] an example of use of $^{19}F/^{1}H$ MRI is shown on **Figure 6,** however here a fluorinated compound is used not fluorinated NPs.

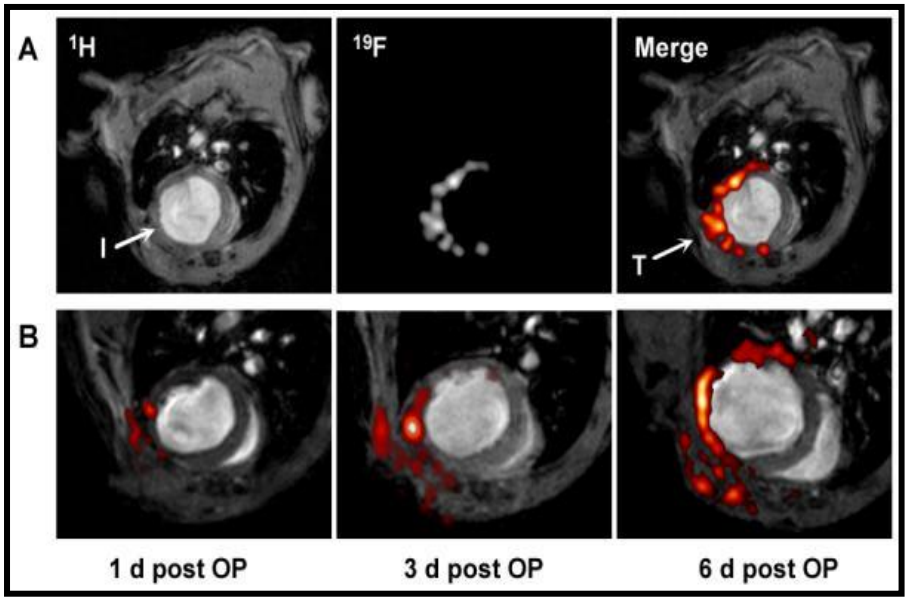

Figure 6 - ^{19}F/^{1}H imaging. Images extracted from Flögel *et al* [10] of he mouse thorax after ligation of the left anterior descending coronary artery (LAD) showing an accumulation of ^{19}F signal near the infarcted region (I) and also at the location of surgery, where the thorax was opened (T). Fluorinated compounds were injected at day 0 *via* the tail vein. (**B**) Sections of ^{1}H images superimposed with the matching ^{19}F images (red) acquired 1, 3, and 6 days after surgery indicate a time-dependent infiltration of PFCs into injured areas of the heart and the adjacent region of the chest affected by thoracotomy.

The detection threshold for NP-labelled cells is affected by a number of factors, including field strength, signal-to-noise ratio, pulse sequence and acquisition parameters [173, 174]. The minimum detectable dose of cells has been reported to be $1x10^5$ for a MRI with 1.5 T of field strength [175], but this number can be affected by differences in hardware, resolution of acquired images, cell type, and uptake of NPs by cells [174] . Cell labelling is initiated by the incubation of cells with the NPs. In most cases, the cellular uptake of the NPs requires the use of transfection agents, including protamine sulphate, poly-L-lysine or other polycationic polymers. Alternatively, cell labelling can be performed by electroporation using electrical pulses of approximately 130 volts to induce temporal permeability changes in cell membranes, thereby facilitating the diffusion of MRI contrast agents [176]. Of note, several studies indicate that the cellular uptake of NPs has minimal impact on stem cell viability and their differentiation program [3].

There are already examples of the clinical translation of SPIO labelled cells in the context of other cell-based therapies. The first study reported SPIO labelling of dendritic cells in human patients as cancer vaccines [177]. This approach allowed the assessment of the accuracy of dendritic cell delivery

and of inter- and intra- nodal cell migration patterns. The second example reported the use of SPIO-labelled neural stem cells for human brain regeneration [178]. Both studies seem to indicate the feasibility of using NP- labelled stem cells in humans. The use of MRI allows one to accurately deliver the NP- labelled stem cells to the infarcted area. This has been demonstrated for the catheter delivery of skeletal muscle-derived mesenchymal progenitor cells (1×10^8) labelled with iron oxide NPs to the anterior left ventricle myocardium in pigs [179]. The cells and the heart were imaged under a 1.5T MRI. A similar strategy has been adopted for the delivery of bone marrow aspirate (1 to 2×10^6 cells) at the periphery of the infarcted myocardium of a porcine model [180]. The use of MRI, labelled stem cells and catheters allow efficient and safe cell delivery into myocardial segments under direct and live imaging.

The use of NP-labelled stem cells and MRI makes it possible to monitor cell survival after transplantation. Rat bone marrow mesenchymal stem cells labelled with iron NPs (1.25×10^5) can successfully be tracked for at least 16 weeks once injected into the myocardium under a 11.7 Tesla MRI [181]. Results showed that the hypointense signal attained from labelled cells on the myocardium decreased every time the animals were imaged (up to week 16), suggesting that the cells were lost or died over time. The loss of exogenous stem cells transplanted at the myocardium has been observed in other studies. The 1.5 T MRI signals of labelled swine mesenchymal stem cells with iron oxide NPs (2.8×10^7 to 1.6×10^8 cells), delivered intra-myocardially into a swine myocardial infarction model, decreased over time [182]. The results suggest that the decrease was due to mesenchymal stem cell death. The use of labelled cells allows examining the efficiency of stem cell delivery. For example, bone marrow-derived mesenchymal stem cells (6×10^7) labelled with iridium NPs and delivered intracoronary, intravenously or endocardially at the infarcted heart of pigs show that the intracoronary route was the most efficient. The labelled cells were retained within the myocardium for at least 14 days [183].

CHAPTER III:

Efficient Pro-Survival/Angiogenic miRNA Delivery by a MRI-Detectable Nanomaterial

Efficient Pro-Survival/Angiogenic miRNA Delivery by a MRI Detectable Nanomaterial

Renata S.M. Gomes[1,2,3,4,5], Ricardo Neves[1,2], Lowri Cochlin[4$], Ana Lima[1,2$], Rui Carvalho[2], Petra Korpisalo[5], Galina Dragneva[5], Mikko Turunen[5], Timmo Liimatainen[5], Kieran Clarke[4], Seppo Ylä-Herttuala[5], Carolyn Carr[4], Lino Ferreira[1,2]*

1, CNC - Center for Neuroscience and Cell Biology, University of Coimbra, 3004-517 Coimbra, Portugal; 2, Biocant - Center of Innovation in Biotechnology, 3060-197 Cantanhede, Portugal; 3, Cardiovascular Biology & Medicine, Rayne institute, University College, London, UK; 4, Cardiac Metabolism Research Group, Department of Physiology, Anatomy & Genetics, University of Oxford, UK; 5, A.I. Virtanen institute, Department of Biotechnology and Molecular Medicine, University of Eastern Finland, Finland.

Published in ACS Nano, 2013, 7 [184], pp 3362–3372

3.1. Abstract

Herein, we report the use of biodegradable nanoparticles [185] containing perfluoro-1,5-crown ether [186], a fluorine-based compound (NP170-PFCE), with the capacity to track cells in vivo by Magnetic Ressonance Imaging (MRI) and efficiently release miRNA. NP170-PFCE complexed with miRNAs accumulate whitin the cell's endolysosomal compartment and interact with higher frequency with Argonaute 2 (Ago2) and GW182 proteins, which are involved in the biological action of miRNAs, than commercial complexes formed by commercial reagents and miRNA, which in turn accumulate in the cell cytoplasm. The release of miRNA132 (miR132) from the NPs increased 3-fold the survival of endothelial cells (ECs) transplanted in vivo and 3.5-fold the blood perfusion in ischemic limbs relatively to control.

3.2. Introduction

Several pro-angiogenic strategies have been proposed in the past years for the treatment of ischemic diseases, including growth factor delivery, cell-based therapies and gene therapies. Cell-based therapies, specifically the ones based on the use of vascular cells, hold high promisse as they can contribute simultaneously for the formation of neovessels and secrete angiogenic factors. Unfortunately, most transplanted cells die a few days after delivery [187, 188]. Cell modulation by miRNAs has been recently tested as a strategy to enhance cell survival and pro-angiogenic activity [189-191]. MiRNAs are non-conding single-strand RNAs that post-transcriptionally regulate gene expression [192]. In comparison to classical drugs, individual miRNAs can regulate many target genes and influence a whole gene network. Strategies have been reported for the in vivo delivery of miRNAs, including (i) chemical modification, (ii) liposomes, (iii) adeno-associated virus or lentivirus and (iv) biodegradable NPs [147, 193-195]. Unfortunately, there is no formulation for the delivery of miRNA that simultaneously offers control for intracellular location and the possibility to track the transfected cells. The technology would offer high efficiency in the regulatory mechanism of miRNAs and the possibility of monitoring cells transplanted into ischemic tissues by the use of non-invasive imaging techniques such as magnetic resonance imaging (MRI) [196].

Studies for miRNA delivery have explored NPs which accumulate in the cytoplasm and not in the endolysosomal compartment [197, 198] as it was believed RNA regulation occurred largely within the cytoplasmic, membrane-free cellular regions [199]. In the cytoplasm, Ago proteins bind to Dicer, which are able to interact with the miRNA duplex and induce the removal of one of the miRNA strands. The complex Ago-miRNA is then ready to bind target mRNA [199]. However, recent data indicates that RNA regulation occurs in the endolysosomal compartments [199, 200]. Many RNA processes may be spatially restricted in the endolysosomal compartments to promote specificity and kinetic efficiency [201]. Thus far, no NP formulation has been shown to accumulate in the endolysosomal compartment and efficiently release the miRNA.

Here we report a novel NP formulation that can be used simultaneously for cell tracking and miRNA delivery. The NP core was formed of poly(lactic acid-co-glycolic acid) (PLGA) and PFCE [11, 202], a fluorine compound which can be tracked non-invasively by ^{19}F-MRI (Figs. 1 and 4a). PFCE contains 20 equivalent ^{19}F spins that generate a single resonance in NMR imaging and it is relatively non-cytotoxic [202]. ^{19}F MRI can selectively image transplanted cells labelled with NP170-PFCE formulation since no fluorine exists endogenously within the human body. The NPs were further coated with protamine sulphate (PS), a polycationic peptide that has been shown to efficiently condense plasmid DNA [203]. All NP components are FDA-approved for biomedical applications [3]. We show that endothelial and mononuclear cells can rapidly internalize the NPs, which largely remained within the endolysosomal compartment. Most importantly, the NPs mediated the intracellular delivery of miR132, which subsequently exerted a pro-survival effect in cells exposed to hypoxia, both in *in vitro* and *in vivo* models. Finally, we demonstrated the possibility of tracking the transplanted cells with ^{19}F-MRI.

3.3. Results and Discussion

3.3.1. NP Engineering for cell labelling.

PLGA NPs without PFCE had an average diameter of 170 nm and a negative (~ -9 mV) zeta potential (**Table 1**). The PFCE encapsulation within the NPs increased their average diameter from 170 to 213 nm. ^{19}F NMR analysis, demonstrated the encapsulation efficiency was between 4.9 and 13.8% (**Table 2**). The NP170-PFCE formulation contained between 111.0 and 176.5 mg of PFCE per mg of PLGA. To facilitate the NP170-PFCE intracellular delivery and the loading of miRNA, the NPs were coated with PS, a small cationic agent (**Table 3**) [204]. The NPs were relatively stable at intracellular pHs and, at concentrations up to 1 mg/mL, did not exert substantial cytotoxicity to human umbilical vein endothelial cells (HUVECs) or mononuclear cells (MNCs) (**Figs. 1 and 2**).

Table 1- Properties of blank and PFCE-loaded PLGA NPs (average ± S.D., n=3).

NPs	Diameter (nm)[b]	Poly dispersity index (PDI)	Zeta potential (mV)[c]	Recovery yield (%)[d]
NP170 [a]	169.8 ± 7.1	0.680	-9.3 ± 2.8	80.5 ± 8.7
NP170-PFCE [a]	212.9 ± 14.3	0.244	-9.7 ± 0.7	75.3 ± 8.6
NP170-PFCE-PS [a]	218.0 ± 9.3	0.381	+7.0 ± 1.7	83.9 ± 3.1

[a] NP formulations were fluorescently labeled with fluoresceinimine (see Materials and Methods for details). [b] Diameter measurements were performed in 10 mM KCl, pH 5.5. [c] Zeta potential measurements were performed in 10 mM KCl, pH 5.5. [d] Recovery yield of NPs after production was calculated according to the following equation: recovery yield= (NP weight × 100) / (initial PLGA weight + mass of PFCE used).

Table 2- PFCE concentration and encapsulation efficiency in PLGA NPs.

NP formulation	PFCE (mg per mg of PLGA) [a]	Encapsulation efficiency (%, w/w) [b]	Fluorine concentration (mg of fluorine per mg of NP)
NP170-PFCE (3.6 mg PFCE: 1 mg PLGA)	176.5	4.9%	98.0
NP170-PFCE (0.8 mg PFCE: 1 mg PLGA)	111.0	13.8%	65.3

[a] The concentration of PFCE in the NPs was determined by dissolving 3 mg of NPs in dichloromethane (300 mL) in a 5 mm NMR tube. A sealed 3 mm tube containing trifluoroacetic acid with 1H-dichloromethane was inserted in the 5 mm and used as internal reference. A total of 50 scans were run with pulses at 90^{o} after a relaxation time of 15 sec. [b] Encapsulation efficiency (% w/w) = (experimental amount of PFCE in NPs × 100) / initial amount of PFCE.

Table 3- Titration of PS to coat NP170-PFCE. For the ratio of NP:PS of 1:1 (i.e. 1000 mg of NPs and 1000 mg of PS) the coated NPs do not significantly aggregate. For this ratio, approximately 13 mg of PS was adsorbed per mg of NPs as assessed by a ninhydrin assay.

PS (mg/mL in PBS) [a]	Zeta (mV±SD) [b]	PDI	Size (nm±SD) [c]
0	-10.56 ± 2.91	0.083	139.53 ± 2.74
1	-9.67 ± 3.62	0.692	-
10	-10.02 ± 2.46	0.143	-
100	-8.92 ± 1.83	0.262	-
1000	+9.83 ± 1.67	0.174	-
2000	+7.65 ± 2.59	0.215	148.95 ± 1.94

[a] NP170-PFCE (1 mg/mL of PBS) and PS (at variable concentration according to the table) were incubated for 10 min under agitation, at room temperature. After the incubation period, the NPs were centrifuged (4,200 rpm; 15 min) and resuspended in distilled water. This cycle was repeated 2 times and at the end the NP suspension was freeze-dried. The above measurements were done after washing before freeze-dry. [b] All measurements were done in KCl pH 5.5 10 mM. Results are average ± SD, n=3. All data were recorded with at least 6 runs with a relative residual value (measure of data fit quality) of 0.03. [c] All measurements were done in KCl pH 5.5 10 mM. Results are average ± SD, n=3.

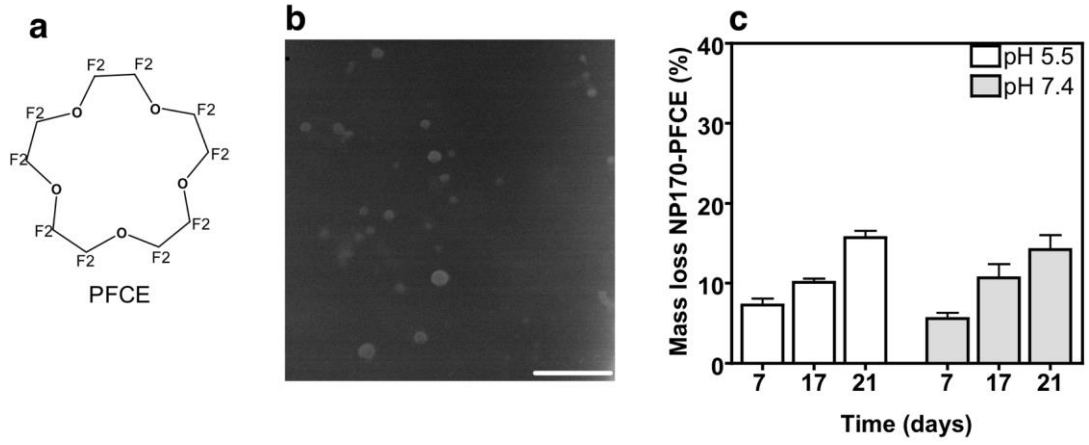

Figure 1- Properties of NP170-PFCE. (a) Chemical structure of PFCE. (b) NP size was evaluated by TEM (JEOL JEM-100 SX microscope at 80 kV). NPs were stained with osmium tetroxide before imaging. A NP

suspension (5 µL, 5 mg/mL in water) and osmium tetroxide solution (5 µL, 5% w/v) were placed on a 400 mesh copper grid with a carbon-coated Formvar membrane. The sample was then dried overnight before examination by TEM. Bar corresponds to 1 µm. (c) Mass loss of NP170-PFCE suspended in buffered solutions at pH 5.5 and 7.4 for several days, at 37ºC. NPs (20 mg/mL) were resuspended in PBS (pH 7.4) or KCl (pH 5.5) buffers and dialyzed against the corresponding buffers at 37ºC. At specific time points the NP suspension was lyophilized and percentage of mass loss was calculated by subtracting the final mass from the initial mass. Results are shown as mean ± SD, n=3.

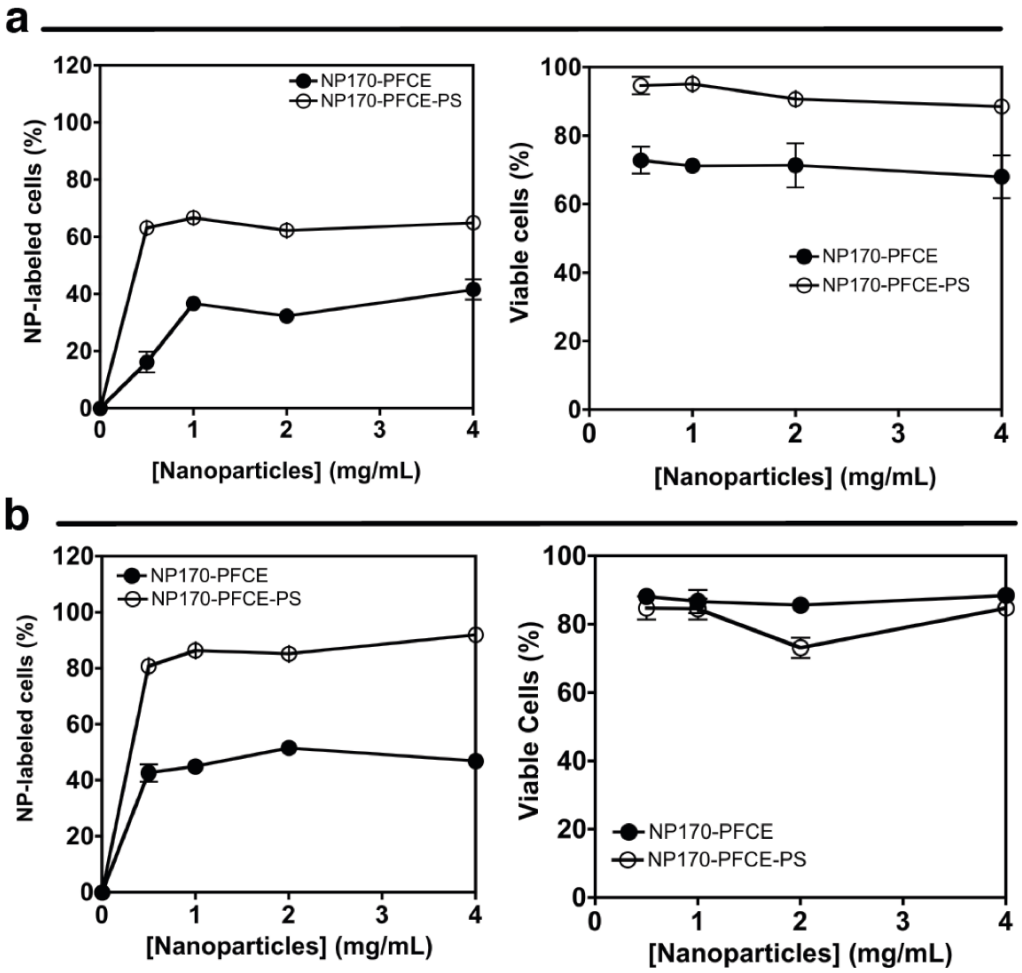

Figure 2- Quantitative assessment of NP uptake and viability by FACS on HUVECs (a) and MNCs (b). Cells were incubated with fluorescently-labelled NP formulations in serum-free EGM2 (HUVECs) or M199 (MNCs) media for 4 h. At the end of incubation, cells were washed and characterized by FACS. Cells labeled with non-fluorescent NPs were used to define the gates during FACS acquisition. Cell survival was quantified by the Mitrotracker CMX-ROS assay, during FACS. Cells positive for Mitrotracker CMX-ROS have mitochondrial activity and thus were considered as live cells. In all plots, results are average ± SD, n=3.

To characterize the intracellular delivery of NP170-PFCE into the cytoplasm of HUVECs or MNCs, we performed confocal microscopy analyses. The NPs were labelled with fluoresceinimine as a reporter to follow NP delivery in cells. Both cell types were incubated with 500 mg/mL of NPs

for 4 h in serum free media. NPs were internalised by HUVECs and accumulated in the endolysosomal compartment (**Fig. 3**). Endosomal sequestration persisted up to 144 h following incubation, indicating little self-mediated escape or disruption of endosomal membranes by the NPs themselves. Similar results were obtained for MNCs (**Fig. 3**).

To quantify cell-labelling efficiency under the different conditions, we performed Fluorescence Activated Cell Sorting (FACS) and ^{19}F-NMR. Cells were incubated with NPs at concentrations between 0.5 and 4 mg/mL for 4 h, washed to remove loosely bound particles, and then characterized by FACS. When 500 mg/mL of NP170-PFCE-PS was incubated with cells, 65% (HUVECs) and 80% (MNCs) of the cells were labelled after 4 h (**Fig. 2**). ^{19}F-NMR measurements indicated that this labelling corresponded to the internalization of 0.27 (HUVECs) and 0.15 ng (MNCs) of PFCE per cell, which was sufficient for cells to be detected on a ^{19}F 7T MRI volume coil (**Fig. 4b**). As expected, PS-coated NP170-PFCE formulation was internalised at higher levels by cells (approximately 2 times) than when given PS uncoated NP170 (**Fig. 2**).

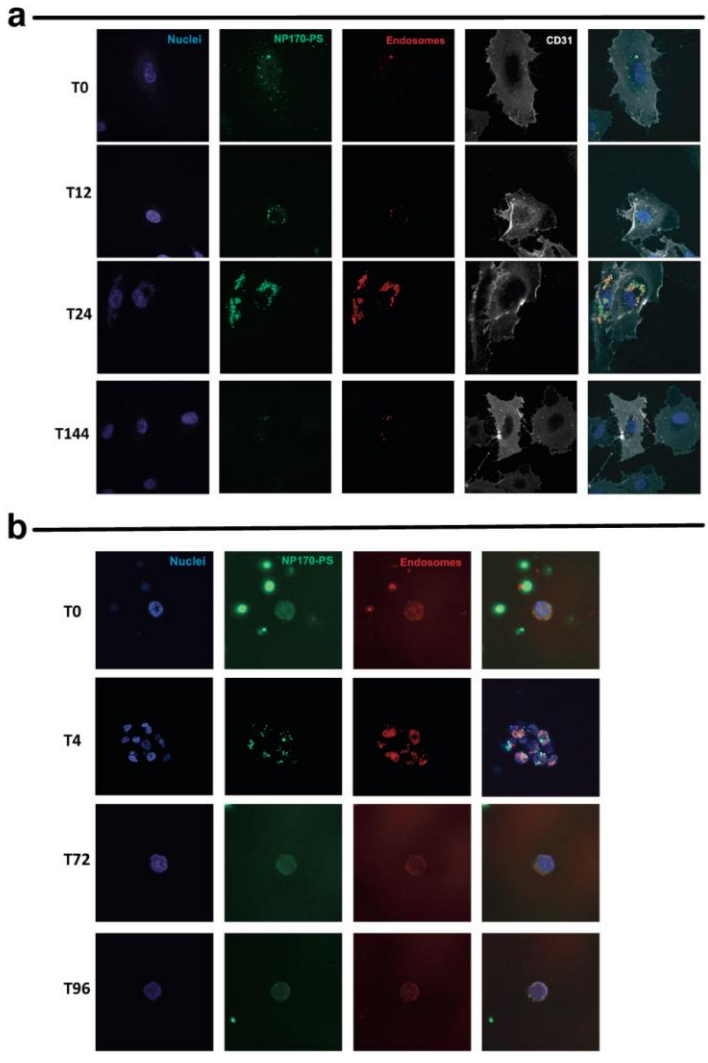

Figure 3- Confocal images showing the internalization of NPs by HUVECs (a) and human umbilical cord blood-derived MNCs (b). The NPs (500 μg/mL) were incubated with the cells for 4 h, after which the cells were washed with PBS, centrifuged, and cultured in EGM2 media (HUVECs) or EGM-2 supplemented with 18% serum (MNCs). T means time, and the numbers after T means hours. At different times, the cells were fixed and co-stained with DAPI (blue, cell nuclei), lysotracker (endosomes, red) and CD31 (cell membrane, grey; just in case of HUVECs).

Long-term observation of NP170-PFCE-labeled cells could be limited by of dilution of NPs following cell division. Therefore, we quantified cell NP labelling overtime using MRI (**Fig. 4b**). HUVECs were labelled with NPs for 4 h, and the labelled cell population isolated by cell sorting and cultured for 7 days in EGM-2 medium. During this time, cells proliferated and the percentage of NP170-PFCE labelled cells decreased overtime and was not detected by ^{19}F MRI at day 7 (approximately 4 cell doublings). When cell cycle was inhibited by Mitomycin C, the intracellular levels of NPs remained fairly constant over 7 days, confirming the decrease in the proportion of NP-labelled cells was due to cell division (**Fig. 4b**).

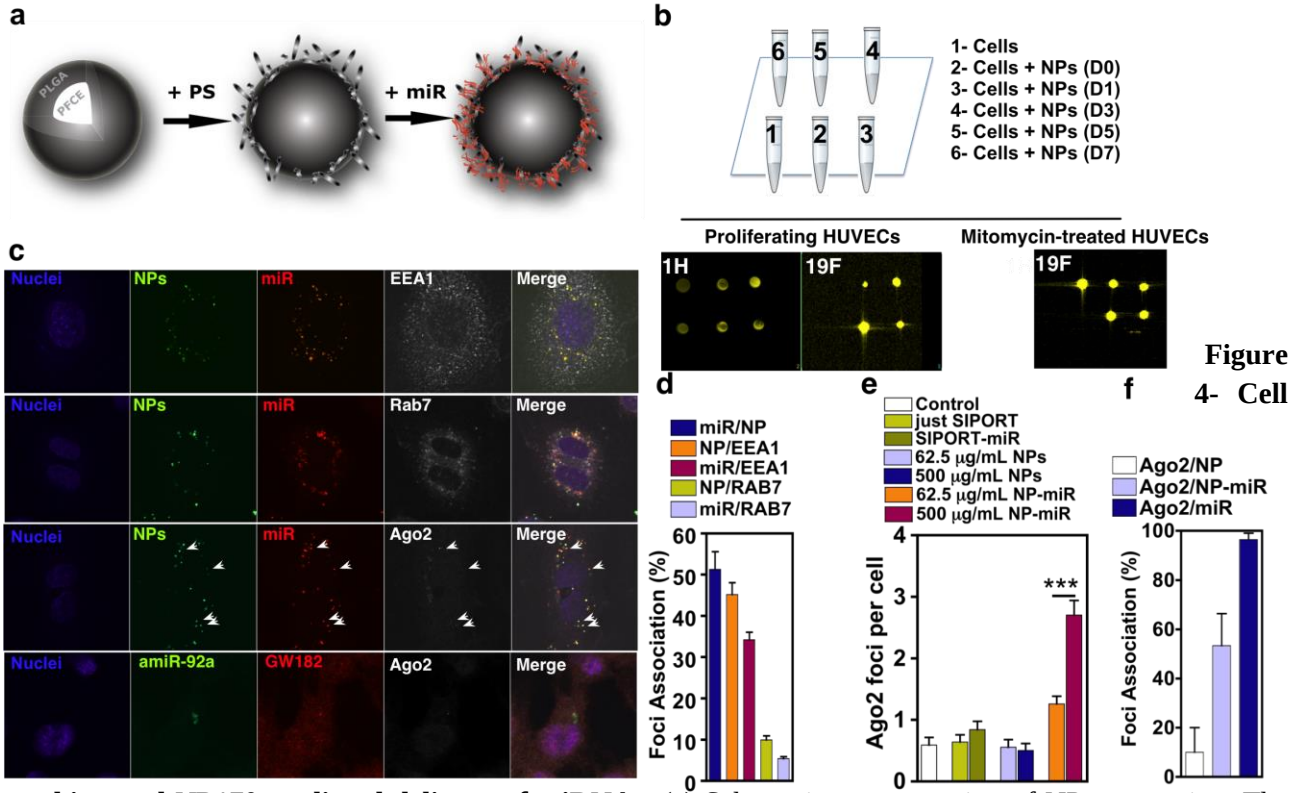

Figure 4- Cell tracking and NP170 mediated delivery of miRNAs. (a) Schematic representation of NP preparation. The NPs are formed by PLGA encapsulating PFCE. The NP is then coated with PS, which has a dual role: (i) to facilitate cell internalization and (ii) to mediate the complexation of miRNAs. (b) 19F signal during cell proliferation. MR images of eppendorfs containing unlabelled cells in PBS or cells transfected with NP170-PFCE (in both 10 × 106 cells) at day 0 (D0), 1 (D1), 3 (D3), 5 (D5) and 7 (D7) after labelling, with or without treatment with mitomycin. Eppendorfs were positioned in a support inside a $^{19}F/^{1}H$ MRI volume coil in a 7T magnet. The acquisition time was 10 min (5 averages) for 10×10cm, matrix 256×256, TR = 500 ms, Flip angle 500. (c) Representative images of the intracellular distribution of NP-PFCE-FITC (NPs) and miR-DY547 [205] in relation to the early endosome (EEA1) and late endosome/ lysosome (Rab7) vesicles (top panels) and the association between NP and miR-Dy547 foci with Ago2 (bottom panels). The amiR-92a associates with both GW182 and Ago2 proteins. (d) Intracellular localization of NP and miR-Dy547 foci in

relation to the endomembrane system. It is presented as the number of foci inside the cell (% from the total), which are interacting with the species in the denominator. (e) Quantification of the number of Ago2 foci present inside the cell under different transfection conditions showing that the number of Ago2 foci present in the cell increases with increased concentrations of NPs carrying miR-Dy547. ***P<0.001. (f) Analysis of Ago2 association profile in NP170-PFCE: miR-Dy547-transfected cells. Quantification of the degree of association of Ago2 foci and NP-only foci (Ago2/NP), NP foci and miR foci (Ago2/NP-miR), and foci containing only miR (Ago2/miR). In c, d, e and f, the analyses were performed at 24 h after cell transfection.

3.3.2. Intracellular release of miRNA. Next, we tested whether NP170-PFCE-PS could be used to deliver pro-survival miRNAs such as miR132, miR424 and antagomir-92a (amiR92a) within cells. MiR132 has been reported to induce EC proliferation and tube formation in a three-dimensional collagen matrix [194]. miR424 stabilizes hypoxia-inducible factor 1a and plays an important physiological role in post-ischemic vascular remodelling and angiogenesis [206]. AmiR92a induces angiogenesis in vitro and in vivo by regulating the expression of the integrin subunit a5 [190].

To investigate the internalization of miRNAs by the cells, Dy547-labeled miRNA was complexed with FITC-labeled NP170-PFCE for 1 h (under these conditions, 12 μg of miRNA were complexed per mg of NPs), washed, and then incubated with HUVECs for 4 h. Dy547-labeled miRNA is a mimic microRNA without any human targets (no fluorescent miR132 and miR424 could be obtained commercially). Cells were washed with PBS to remove NPs that were not internalized, and characterized by confocal microscopy. To evaluate the potential of our approach, we performed the same experiment using a commercial transfection agent - SIPORT NeoFX. The complex Dy547-miRNA: FITC-NP170-PFCE was highly internalized by cells, with over 90% of the cells transfected using NP170-PFCE: Dy547-miRNA, while only 50% of the cells were transfected using SIPORT: Dy547-miRNA (**Fig. 5**). However, cells transfected using SIPORT had more Dy547-miRNA within the cell cytoplasm than those transfected using NP170-PFCE: Dy547-miRNA.

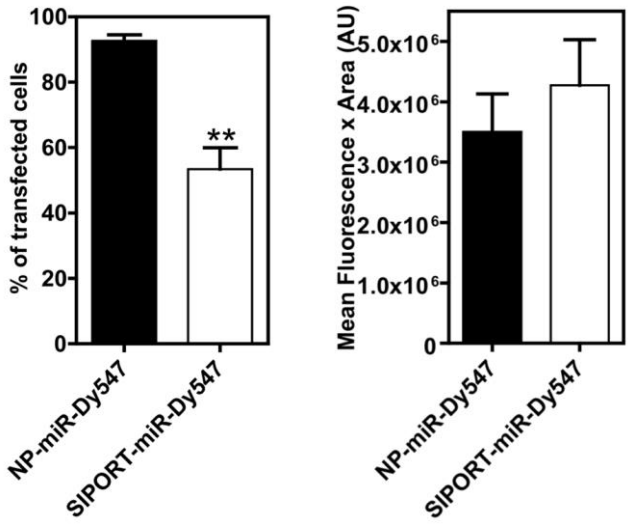

Figure 5- Comparison of miR-Dy547 transfection efficiency between NP170 and SIPORT delivery. Graph on the left shows that the percentage of cells transfected with the fluorescent miRNA is significantly higher ($P<0.01$) than using SIPORT delivery. Representative microscopic fields were used for quantification spanning a total area of 4.3 mm2. Graph on the right shows the total loading (integrated density = mean fluorescence x area) of miR-Dy547 in transfected cells (area of 0.250 mm2; approximately 200 cells were analysed).

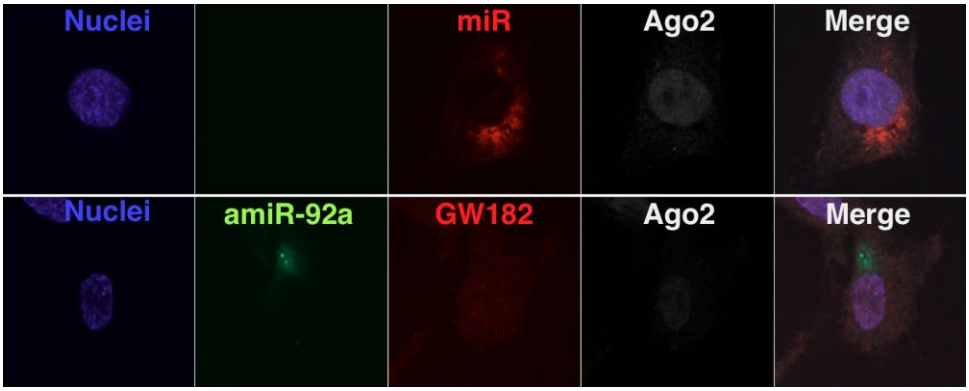

Figure 6- Representative photographs of SIPORT delivery of miR-Dy547 (miR, top panel) and amiR-92a (bottom panel). Both oligonucleotides fail to interact with Ago2. In addition, amiR-92a shows no association with GW182 using the SIPORT delivery system.

FITC-labelled NP170-PFCE formulation internalized by HUVECs was localized in restricted cell areas (**Fig. 4c**). At 24 h post-transfection, ~50% of the miRNA co-localized with the NPs, showing that half of the miRNA had already been released by the NPs (**Fig. 4d**). Approximately 35% of the miR-Dy547 foci were associated with early endosome vesicles (EEA1+ vesicles) while only 5% were located in late endosome and lysosome vesicles (Rab7+ vesicles). Overall, there was a low

degree of association of both NP and miR with late endosome and lysosome vesicles. In contrast, the Dy547-miRNA released by SIPORT NeoFX was distributed across the cell cytoplasm and not within confined intracellular areas (**Fig. 6**). Importantly, the NP170-PFCE formulation was able to present miRs to the RISC protein Ago2 more efficiently than SIPORT. NP delivery induced more Ago2 foci than SIPORT delivery (**Figs. 4e and 4f**). The same was observed in cells transfected with fluorescent amiR-92a (**Fig. 4c**). Amir-92a foci showed association with both Ago2 and GW182 proteins, indicating that this anti-miR oligonucleotide may be capable of microRNA-RISC strand invasion. Interestingly, the number of foci was higher in cells cultured under hypoxia than in normoxia, indicating higher efficiency for the biological effect of miRNA under these conditions (**Fig. 7**).

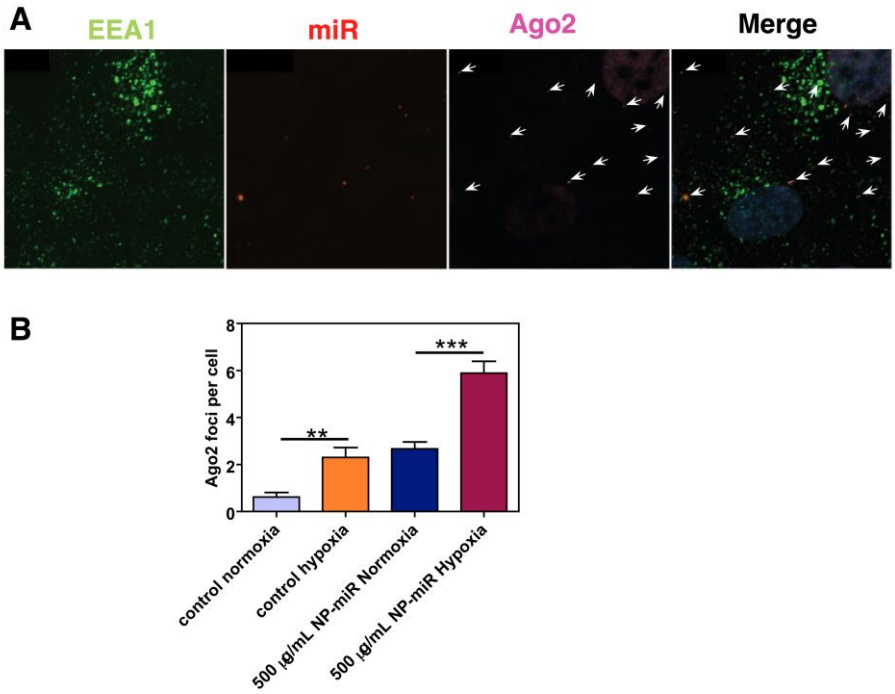

Figure 7- Effect of hypoxia in co-localization of miR with Ago2 and EEA1. HUVECs were transfected with NP170-PFCE: miR-Dy547 for 4 h, washed to remove NPs that were not internalized and incubated for 24 h in hypoxia and serum- deprived conditions. (A) Confocal microscopy results showing the association of miR-Dy547 with Ago2 and the early endosome protein EEA1. (B) Quantification of Ago2 foci per cell. Representative microscopic fields were used for quantification spanning a total area of 3.8 mm2 (approximately 120 cells were analyzed). Results are mean ± SEM (n=8-18). $P \leq 0.01$ (**) and $P \leq 0.001$ (***).

3.3.3. Pro-survival and pro-angiogenic activity of the miRNA-containing NPs. To demonstrate the pro-survival activity of different miRNAs, HUVECs were incubated for 4 h with miRNA-complexed NPs, washed, and finally cultured in ischemic conditions (pO_2 of 0.1%; media without serum) for 48 h. miR132, miR424 and amiR92a: NP170-PFCE formulations each significantly ($P<0.05$, n=3) increased cell survival, and this effect was dependent on the miRNA concentration (**Fig. 8a**). No significant differences were seen between the different miRNAs tested ($P>0.05$, n=3). miRNAs delivered by the SIPORT transfection agent mediated cell survival only at concentrations higher than those which gave increased survival using NP170-PFCE.

To demonstrate the pro-angiogenic effects of the miRNA-containing NP formulations, HUVECs were incubated for 4 h with miRNA-complexed NPs, washed, and finally cultured on top of Matrigel® to assess their capacity to form vascular networks. The transfection of the cells with miR132- and miR424-containing NP170-PFCE yielded vascular networks with greater tube length and more branching points than cells transfected with SIPORT for the same miRNAs (**Figs. 8b and 8c**).

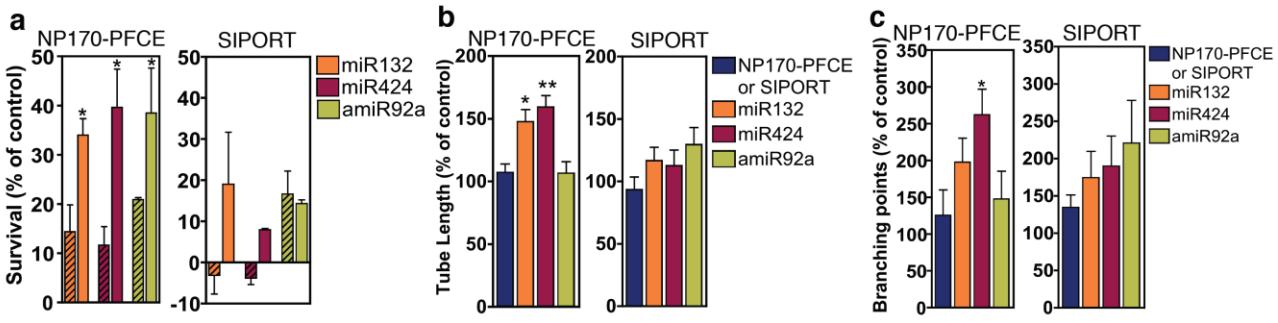

Figure 8- Pro-survival and pro-angiogenic effects of NP170-PFCE:miR complexes on ECs. (a) HUVECs survival under hypoxia and serum-deprived for 48 h as assessed by an ATP-based assay. NPs were complexed with 100 nM (stripe pattern) or 200 nM (no pattern) of miR. (b, c) HUVECs treated with different formulations in normoxia were cultured in a Matrigel assay for 24 h, after which the tube length (b) or branching points (c) were measured. In all graphs, results are average ± SEM (n=3). $P \leq 0.05$ (*) and $P \leq 0.01$ (**).

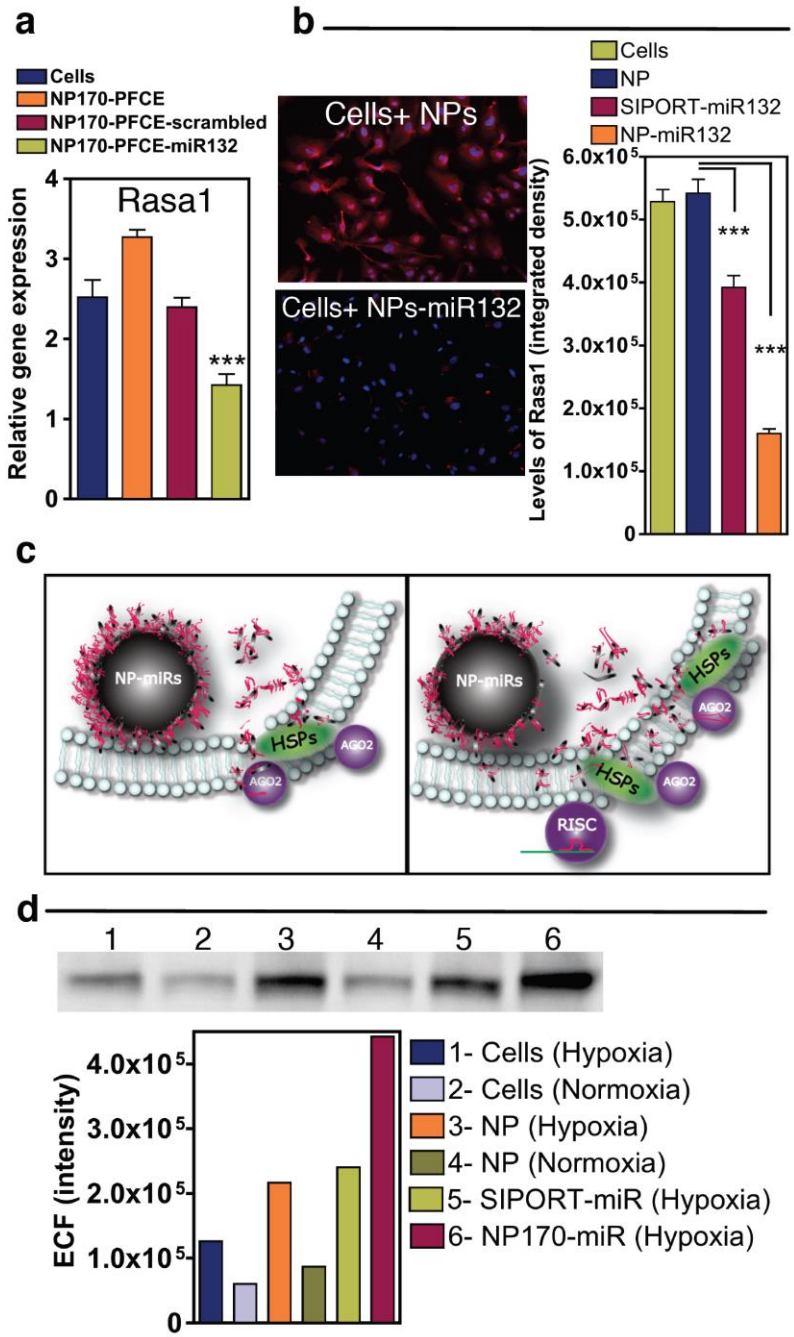

Figure 9- NP170-PFCE:miR-132 complexes target Rasa1. (a) Rasa1 gene expression in HUVECs treated with NP170-PFCE:scrambled miR or NP170-PFCE:miR132. Gene expression was normalized to GAPDH as a housekeeping gene. In all graphs, results show average ± SEM (n=4). $P \leq 0.001$ (***). (b) Rasa1 protein expression in HUVECs treated with different formulations. Levels of Rasa1 (integrated density: average ± SEM) were measured with ImageJ after immunofluorescence and imaging of 10 representative fields (20× Objective; ± 300 cells). (c) Schematic representation of the translocation of miRNAs involving HSPs. (d) Immunoprecipitation of HSP90 and detection of Ago2 under different conditions by Western blot.

From all the miRNAs tested, we selected miR132 for subsequent analysis. miR132 is expressed by ECs after 3-6 h of exposure to vascular endothelial growth factor or basic fibroblast growth factor

[194]. In addition, the constitutive expression of miR132 in HUVECs considerably increases cell proliferation and tube formation. One of the identified targets of miR132 is Rasa1, which encodes p120RasGAP. HUVECs transfected with miR132 have a decreased endogenous p120RasGAP expression, which increased Ras activity and mitogen-activated protein kinase extracellular related protein kinase-1 (MEK-1). To demonstrate that Rasa1 was indeed down-regulated in HUVECs transfected with NP170-PFCE: miR132, we performed quantitative real time polymerase chain reaction (qRT-PCR) (**Fig. 9a**) and protein quantification by immunofluorescence analysis (**Fig. 9b**). HUVECs were incubated for 4 h with NP170-PFCE: miR132 or NP170-PFCE: scrambled miR or only NP170-PFCE, followed by washing and evaluation of mRNA levels after 24 h and protein expression after 48 h. HUVECs transfected with NP170-PFCE: miR132 had a down-regulation in the expression of Rasa1 mRNA, while no effect was observed in control groups. Moreover, the NP-miR132 delivery was more effective in down-regulating p120RasGAP protein levels than SIPORT.

Overall, our results obtained on pro-survival, pro-angiogenic and molecular assays show that NP170-PFCE formulation is able to present miRNAs very effectively to the RISC complex machinery, outperforming the commercial transfection system (SIPORT) in terms of Ago2 assembly, evidenced by an increased number of Ago2 foci with increasing NP-miR concentrations. We hypothesize the better efficiency is related to the close association between the NP with the endomembrane system [199] (**Fig. 9c**). The close relationship between the RISC machinery and the endomembrane system may promote frequent encounters with the exogenous oligonucleotides and NPs, while these encounters are reduced with SIPORT delivery, due to the diffusion and dilution of the oligonucleotides in the cytoplasm. Since Ago proteins are located in the membrane of the endolysosomal compartment [199], and the miRNA binding site is located in the cytosolic part of the protein, the miRNA released from the NP has to cross the membrane of the endolysosomal compartment. This process may be mediated by the cationic NPs. Previous studies have shown that cationic NPs have the capacity to penetrate the endolysosomal membrane by generating transient

holes and to rupture the endosomal vesicles by the well known "proton sponge effect" [207]. Alternatively, the miRNA release from the endolysosomal compartment may be mediated by Ago-chaperones heat shock proteins (HSPs), such as HSP90 and Hsc70 [208], which have been reported to interact with acidic phospholipid membranes to create functionally stable ATP-dependent cationic pathways [209]. We decided to investigate the interaction between Ago2 and the chaperone HSP90. Immunoprecipitation studies show that when the NP170-PFCE is used to deliver miR, the pull-down of HSP90 binds more Ago2, indicating a closer interaction with its chaperone (**Fig. 9d**). Also, the interaction of Ago2-HSP90 was higher in cells cultured under hypoxia than in normoxia, corroborating the observed increase in the number of Ago2 foci (**Fig 9d and Fig. 10**). These results suggest that the NP170-PFCE are able to serve as a scaffold or to bridge the assembly of more Ago2-HSP90 complexes.

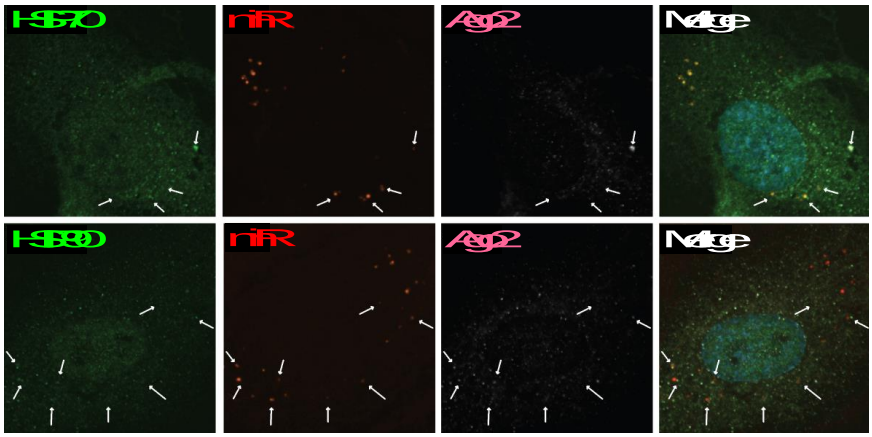

Figure 10- Association between HSPs (HSP70 and HSP90), Ago2 and NP170-PFCE: miR-Dy547. HUVECs were transfected with NP170-PFCE: miR-Dy547 for 4 h, washed to remove NPs that were not internalized and incubated for 48 h in hypoxia and serum- deprived conditions. Confocal microscopy results show the association of miR-Dy547 with both HSPs and Ago2 protein (arrows).

3.3.4. In vivo monitoring and activity of NP170-PFCE-miR132-transfected ECs in a hind limb ischemia animal model. Next, the potential for NP170-PFCE: miR132 to enhance EC survival and promote neovascularization in an *in vivo* model of hind limb ischemia was investigated. Mouse ECs labelled with a 1,1´-dioctadecyl-3,3,3´,3´-tetramethylindotricarbocyanine iodide (DiR) fluorescent probe were transfected with NP170-PFCE: miR132 for 4 h, washed and injected in mice legs

following ligation of the right femoral artery. Survival of the transplanted cells was assessed using a bioluminescence imaging system (IVIS), allowing evaluation of the spatiotemporal kinetics of EC survival. ECs transfected with NP170-PFCE-miR132 or SIPORT-miR132 proliferated by day 3, as confirmed by an increase in the radiant efficiency. At day 7, the number of cells transfected with NP170-PFCE-miR132 was 3-fold higher ($P<0.001$, $n=5$) than with NP170-PFCE without miR132 or cells alone (Fig. 11a).

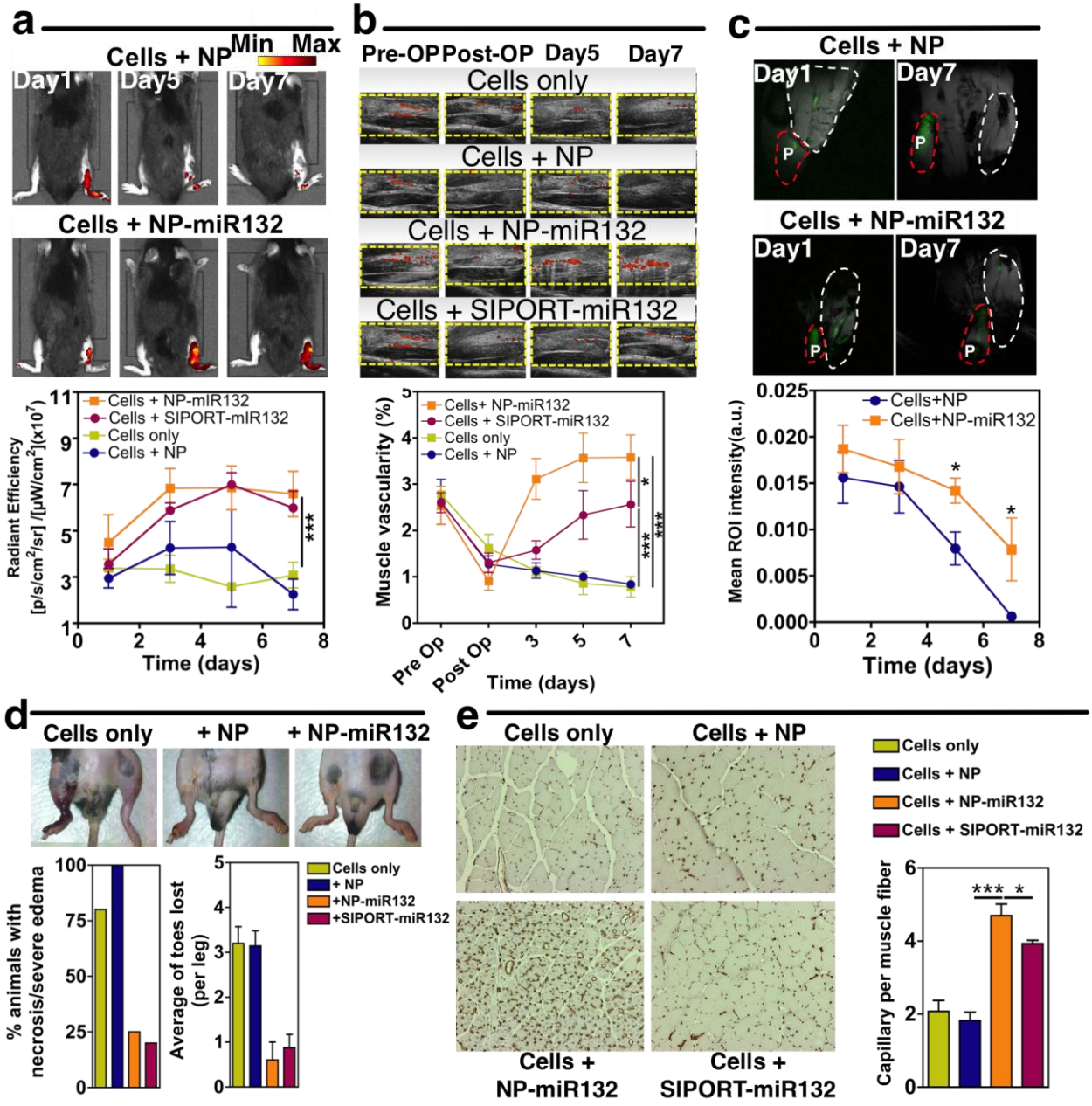

Figure 11- EC survival and angiogenic properties after transfection with NP170-PFCE:miR132 complexes, in a ischemic hindlimb animal model. (a) Representative bioluminescence images and quantified bioluminescence intensity of mice following ligation of the femoral artery and injection of

endothelial cells. (b) Representative images and quantification of blood perfusion analyses by VeVo. (c) Representative images and quantification of ^{19}F-MRI analysis. The intensity of the region of interest (ROI, in white) of the ^{19}F signal was measured and calibrated against an internal standard (phantom, P, in red). (d) Representative images of ischemic hindlimbs treated with ECs alone or ECs transfected with NP170-PFCE or NP170-PFCE: miR132 and quantification of limb necrosis and lost of toes. Images and quantifications were obtained at day 7. Limbs treated with ECs alone or transfected with NP170-PFCE show high sign of necrosis. Limbs treated with ECs transfected with NP170-PFCE: miR132 or SIPORT: miR132 have low signs of necrosis. (e) Immunohistochemical staining for CD31 and quantification of capillaries per muscle fiber at 7 days after ligation, for the various experimental groups. In all graphs, values are average ± SEM (n=4-8). $P \leq 0.05$ (*), $P \leq 0.01$ (**) and $P \leq 0.001$ (***).

The bioluminescence results were confirmed by evaluation of blood perfusion using a VeVo system (**Fig. 11b**), which was also able to ensure an effective surgical procedure, as shown by a reduction of the blood perfusion in the injured limb. Over time, blood flow increased 2- to 3-fold ($P<0.001$, n=4-8) in animals treated with cells transfected with NP170-PFCE: miR132 or SIPORT: miR132 compared with animals treated with cells alone or cells labelled with NP170-PFCE without miR132. This increase correlated with cell survival data attained from IVIS measurements. Importantly, animals treated with NP170-PFCE: miR132 had higher blood perfusion ($P<0.05$, n=4-8) than animals treated with SIPORT: miR132.

To monitor cell administration and survival we also used ^{19}F-MRI. The intensity of the region of interest in ^{19}F MRI images was measured (see Methods) (**Fig. 11c**). For both experimental groups tested, (animals treated with ECs transfected with NP170-PFCE or NP170-PFCE: miR132), there was a decrease in the ^{19}F signal over time. However, after 5 days, animals treated with ECs transfected with NP170-PFCE: miR132 had a higher ^{19}F signal, and thus higher cell number, than animals treated with cells transfected with NP170-PFCE without miR132 ($P<0.05$, n=5-6) (**Fig. 11c**).

To further characterize cell engraftment and neovascularization, gross anatomy recordings and histology were performed. Animals treated with ECs alone or cells transfected with NP170-PFCE showed necrotic limbs and auto-amputation of toes, while animals treated with NP170-PFCE:

miR132 or SIPORT: miR132 showed lower levels of necrosis (**Fig. 11d**). The muscles of the injured limbs were further characterized by immunohistochemical staining for CD31 as a marker of ECs and neovascularization. Higher levels of CD31 were observed in animals treated with ECs transfected with NP170-PFCE: miR132 as compared to cells transfected with NPs without miR ($P<0.001$, n=5) or with SIPORT: miR132 ($P<0.05$, n=5) (**Fig. 11e**)

Overall, our results show that ECs treated with NP170-PFCE: miR132 have a 3-fold higher survival and pro-angiogenic activity than cells without miRNA, in an ischemic hindlimb animal model. To the best of our knowledge this is the first study demonstrating the therapeutic effect of a NP formulation with miR132. Recently the therapeutic activity of miR132 has been shown after the transplantation of saphenous vein-derived pericyte progenitor cells in the infarcted mouse heart, where miR132 released from pericyte progenitor cells, stimulated endothelial tube formation by a Ras-dependent induction mechanism which in turn activated the PI3K/Akt pathway [210]. In our study, animals treated with cells transfected with NP170-PFCE: miR132 had an increase in blood perfusion, correlating with an increase in the near-infrared signal using IVIS and a decrease of signal in ^{19}F-MRI. Furthermore, immunohistochemistry results show a 2.5-fold increase in the number of cells expressing the endothelial marker CD31 indicative of neo-angiogenesis. Importantly, ECs transfected with NP170-PFCE: miR132 decreased limb necrosis (4-fold relatively to control) and number of toes per leg (6-fold relatively to control). The reduction in necrosis is similar to the one reported for mouse ischemic limbs treated with genetically modified human mesenchymal stem cells (hMSCs) transfected with vascular endothelial growth factor [211]. Furthermore, the percentage of animals without necrotic toes (60%) using cells transfected with NP170-PFCE:miR132 is superior to the ones treated with endothelial progenitor cells and outgrowth ECs in an alginate scaffold (below 20%) [212].

3.4. Conclusion

In conclusion, we have developed a NP formulation with potential clinical relevance for *in vivo* cell tracking and miRNA delivery. The theranostic aspect of our formulation makes it very promising for cardiovascular applications. We demonstrate the release of miR132 from the NPs increased by 3-fold the survival of ECs transplanted *in vivo* and 3.5-fold the blood perfusion in ischemic limbs relatively to control (cells transfected with empty NPs). Although some strategies are being investigated for the intracellular delivery of miRNA in cells, such as liposomes, adeno-associated virus and lentivirus [147], some of these strategies (viruses) raise several issues in terms of clinical translation while others (liposomes) have limitations in stability, versatility and traceability for miRNA delivery. The formulation reported in this work uses FDA-approved components, which should facilitate its biomedical translation. The formulation can be prepared with controlled size, incorporate multiple ligands, and monitored by ^{19}F-MRI. ^{19}F-MRI is the ideal tool for non-invasive assessment of cell fate after transplantation providing positive, quantitative and background free contrast. Our formulation is an alternative to superparamagnetic iron oxide NPs currently used in the clinic for MRI applications. Our work further highlights the importance of the targeted intracellular delivery to enhance the efficacy of miRNAs. We show several experimental evidences that the miRNA delivery within the endolysosomal compartment offers an excellent opportunity to enhance the biological effect of miRNAs. This creates new opportunities for the development of more effective synthetic formulations for miRNA delivery.

3.5. Materials and Methods

Preparation of PLGA NPs containing PFCE. Where required, PLGA (Resomers 502 H; 50:50 lactic acid: glycolic acid) (Boehringer Ingelheim) was covalently conjugated to fluoresceinamine (Sigma-Aldrich) according to a protocol reported elsewhere [213]. NPs were prepared by dissolving PLGA (100 mg, optionally labelled with fluoresceinamine) in a solution of dichloromethane: trifluoroethanol (1:8, 6.3 mL) containing perfluoro-1,5-crown ether (PFCE) (100 mg) (Fluorochem, UK). This solution was then added dropwise to a PVA solution (40 mL, 5% w/v in water) and stirred for 3 h. The NPs were centrifuged and washed with distilled water before freeze-drying. Where NPs were coated with PS, NPs (1 mg/mL) and PS (1 mg/mL) were incubated for 10 min under agitation, at room temperature. After the incubation period, the NPs were dialysed (MWCO of 50 kDa) against distilled water and freeze-dried. Measurement of the average diameter, and amount of fluorine in the NPs, was performed as described bellow.

NP characterization. Particle size was determined using light scattering via Zeta PALS Zeta Potential Analyzer and ZetaPlus Particle Sizing Software, v. 2.27 (Brookhaven Instruments Corporation). The NPs were suspended in 1 mM potassium chloride buffer pH 5.5 (500 mg/mL) and sonicated for short times (<1 min) before characterization. Size measurements were performed at 25°C, and data was recorded at 90° angle, with an equilibration time of 5 min and individual run times of 120 s (5 runs per measurement). The average diameters described in this work are number-weighted average diameters. The zeta potential of NPs was determined in a 1 mM KCl pH 6 solution, at 25ºC. All data was recorded with at least 6 runs with a relative residual value (measure of data fit quality) of 0.03.

Quantification of fluorine in NPs and NP-labelled cells by ^{19}F-NMR. ^{19}F NMR analyses were performed in a 600 MHz NMR Varian Instrument. NPs (5 mg) were dissolved in dichloromethane (300 µL) and transferred to a 5 mm NMR tube containing a sealed 3 mm tube with trifluoroacetic acid and ^{1}H-dichloromethane as an internal reference. A total of 50 averages were run, with pulses at 90^{o} angle after a relaxation time of 15 seconds. Batches of 2×10^{6} cells/condition, were labelled with NPs (between 0.5 mg/mL and 8 mg/mL) for 4 h in serum free EGM-2 (HUVECs) or serum free M199 (MNCs). After incubation, HUVECs were washed 3 times with PBS and trypsinized (0.2% trypsin), while MNCs were washed 3 times with PBS and then passed through a MACS column (Miltenyi Biotec) to further separate the cells from the non-internalized NPs. At the end, all cells were counted with trypan blue, resuspended in PBS, frozen at 80ºC and freeze-dried. The lyophilized cells were then dissolved in 1H- dichloromethane (300 µL), transferred to a 5 mm NMR tube and characterized by ^{19}F NMR according to the parameters described previously.

Development of ^{19}F MRI coil and NP imaging via MRI. Taking into consideration that radio frequency (RF) coils are extremely expensive and detuning imaging coils is difficult it was decided to build a coil, which would allow simultaneous ^{19}F and ^{1}H imaging. As the Lamour frequency of ^{19}F (25.16 107rad/s/T) is close to ^{1}H frequency (26.75 107rad/s/T) it was believed that the coil could be "home made". The coil built was based on a low pass birdcage design. **Figure 12** shows the schematic drawing of the initial prototype and the built coil used for the experiments. In this design RF shields were used to reduce the interaction between hardware within the MRI system and the RF coil built, reducing noise, thereby increasing signal noise ratio (SNR). The shielding decreased the effective inductance of a circuit, causing the resonant frequency to increase.

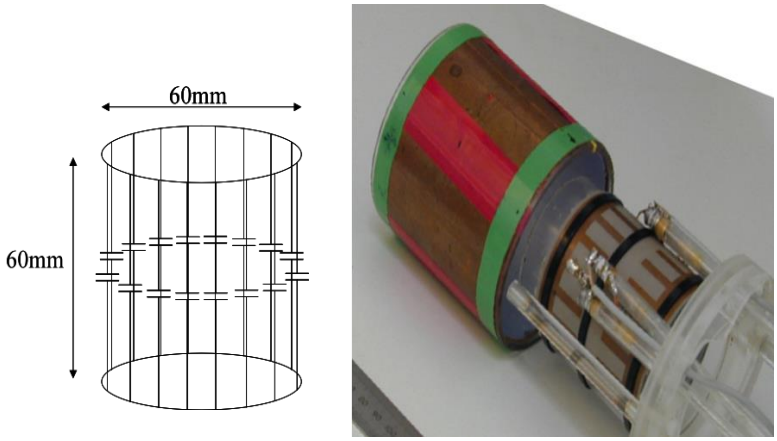

Figure 12. $^{19}F/^{1}H$ purpose built coil. Schematic drawing of the birdcage and the build coil.

A removable inner RF inductive shield for ^{1}H resonance (sliding adjustment) was added so the ^{1}H resoning frequency could be precisely attained when positioned inside de outer RF inductive coil for ^{19}F. Once the inner RF inductive shield for ^{1}H was removed the resonance precisely matched ^{19}F frequency as shown in the diagram of **Figure 13**.

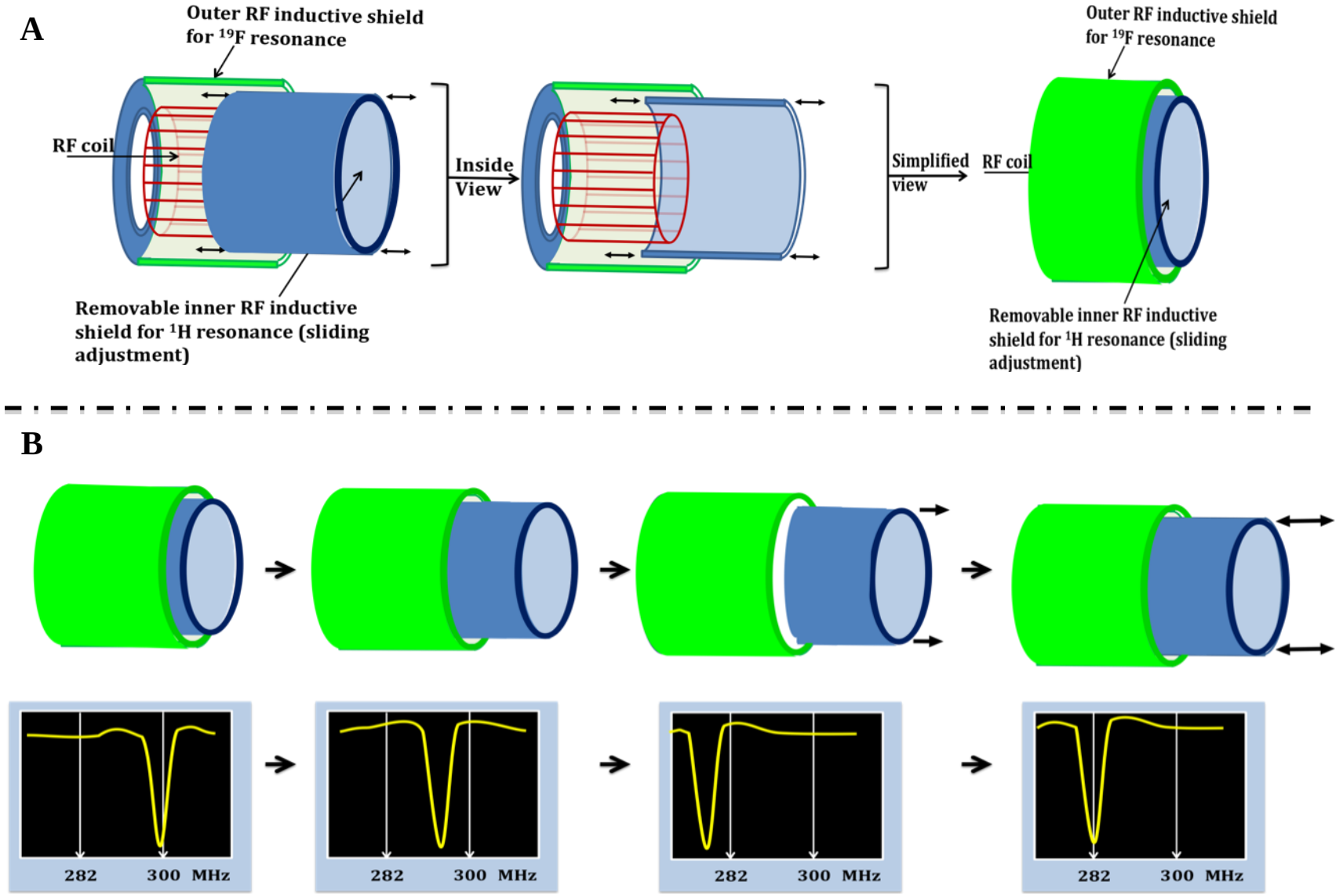

Figure 13. Schematics of the Purpose Built $^{19}F/^{1}H$ coil. A) Detailed drawing of the coil with internal view, showing positioning of the outer RF inductive shield for ^{19}F resonance and the removable ^{1}H RF shield to allow adjustment of resonances. **B)** Effect of sliding the removable inner RF inductive shield for ^{1}H resonance, it is seen that with this shield it is possible to image both at ^{19}F and ^{1}H resonance simply by sliding the removable shield changes the tune and match as shown in the frequency measurement graphs.

Next, it was important to determine whether it was possible to detect a signal from the NPs using MRI as this technique shows lower sensitivity than liquid state NMR. Using a 7T horizontal bore it was determined that the ^{19}F T1 was 1393 ± 5ms in solution and was easily located permitting acquisition of high-resolution fluorine images (**Fig. 14**). **Figure 14** shows that NPs, in this case NP170-PFCE can be visualized via MRI and using the purpose built coil.

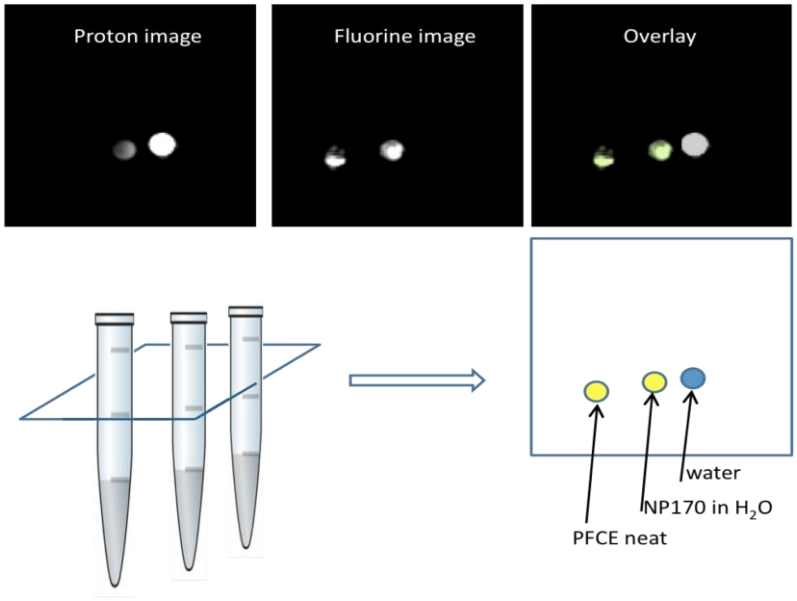

Figure 14- Magnetic Resonance Imaging (MRI) of NPs. Image acquisition on 7T horizontal bore MRI, coronal slices in relation to the magnet, axial cross sections of the eppendorphs, 10 minute acquisition (5 averages) on volume coil. Image acquired on 8mgs of NP170-FCE and 750µg of PFCE.

Isolation of mononuclear cells (MNCs) from umbilical cord blood (UCB). All human UCB samples were collected from donors, who signed an informed consent form, in compliance with Portuguese legislation. The collection was approved by the ethical committee at Hospital Infante D.

Pedro. The samples were stored in sterile bags containing 35 mL of citrate-phosphate-dextrose anticoagulant solution. MNCs were obtained from UCB samples after Ficoll (Histopaque-1077 Hybri Max; Sigma-Aldrich, St. Louis, USA) density gradient separation. MNCs were immediately used for experiments without further treatment.

Complexing of NPs with miRNAs and cell transfection. NP170-PFCE were weighed, sterilized under ultraviolet light (UV) light for 30 min, and resuspended in EGM-2 serum free medium to a final concentration of 500 mg/mL. The NP suspension was dispersed by ultrasound (2 × 10s, BRANSON 2510), and miRs added (100 or 200 nM, as specified in the text) and allowed to complex to the NPs for 1 h at 37ºC, with intermittent agitation. Cells were washed 2 times with pre-warmed PBS and the NP170-miR suspension was added to the cells for incubation at 37ºC for 4 h. Cells were transfected at a ratio of 1.25 mg of NP170-miRNA per million HUVEC cells.

For SIPORT (Ambion) transfection, SIPORT transfection agent and miRs were diluted in EGM-2 serum free medium and incubated at room temperature separately. After 10 min, the solutions were combined and incubated for another 10 min to allow the complexing of both components. The suspension was then dispensed on top of PBS-pre-washed cells and incubated for 4 h at 37ºC, as in the NP170 procedure. For visualization of transfection using fluorescence microscopy, NP170-PFCE with fluorescein and miR-Dy547 (Dharmacon) was used. Commercial oligos used in these studies were: miR132 (Ambion), miR424 (Ambion) and amiR92a (Exiqon).

FACS analysis. MNCs (1×10^6 cells) or HUVECs (0.2×10^6 cells) were incubated for 4 h in serum free M199 or serum free EGM-2, respectively, containing variable concentrations of NPs in a 24

well plate. After 4 h, HUVECs were washed with PBS on the plate 3 times. The cells were then re-suspended in serum free EGM-2, with or without mitotracker red CMX-ROS at 50 nM for 15 min at 370C in a CO2 incubator. The cells were later trypsinized with 0.2% (w/v) trypsin solution, centrifuged at 1000 rpm for 5 min, and fixed with 4% paraformaldehyde for 10 min at room temperature. After fixation they were re-washed and then re-suspended in PBS (500 µL), ready for FACS analysis. MNCs were transferred to a 2 mL eppendorf and centrifuged for 15 min at 20^0C, 1300 rcfs, then cells were further washed by using anti-CD45 human microbeads via Miltenyi Biotec Mini MACS system and protocol (Miltenyi Biotec, UK) to ensure that only MNCs were present in the final solution and no free NPs, the cells were then incubated with mitotracker (50 nM) for 15 min at 37^0C, washed once with PBS and fixed with 4% paraformaldehyde for 10 min at room temperature. After fixation, the cells were washed and resuspended in 500 mL of PBS before FACS analysis. A total of 80,000 events were recorded per measurement.

Confocal microscopy analyses. Cells were seeded onto circular 20 mm glass coverslips, coated with 0.2% gelatine, inside a 24 well plate and left to adhere. The cells were then incubated with NPs (500 µg/mL) for 4 h. Once the incubations were terminated, the coverslips were washed gently. In some conditions live cells were stained for lysosomes (using LysoTracker red DND-99 at 50 nM, 20 min incubation) or mitochondrial activity (using MitoTracker Red CM-Ros, 50 nM, 5 min incubation). Cells were fixed with 4% (w/v, in water) paraformaldehyde (EMS, Hatfield, USA) for 10 min at room temperature and then washed with PBS. For certain conditions, the slides were mounted straight away with mounting medium-4',6-diamidino-2-phenylindole (DAPI; Sigma-Aldrich) on a glass slide. Cell membrane staining was also performed. In this case, mouse antibodies against human CD31 (Dako, Glostrup, Denmark) or CD45 (BD Biosciences, Spain) were used to stain the

membrane of HUVECs or cord blood mononuclear cells (MNCs). Cells were washed 3 times after fixation (MNCs were washed by centrifugation), the cells were then blocked with 2% bovine serum albumin (BSA) (Sigma-Aldrich) in PBS for 30 min at room temperature. The CD31/CD45 (both at 1:50 dilution) primary antibody was added in PBS for 1 h at room temperature followed by 3 washes in PBS. The binding of primary antibodies was detected with anti-mouse DyLight 649 conjugate (at a dilution of 1:200) (Jackson ImmunoResearch, USA).

Transfection efficiency was evaluated by incubating cells grown on glass coverslips (4 h at 37ºC) with fluorescent miR-Dy547 (control mimic Dharmacon, red) carried by fluorescent NPs (NP-fluorescein, green) or using SiPORT transfection agent. Low magnification (20× objective, Zeiss Laser Scanning Microscope Meta 510) photographs were taken, observing the need for total signal capture (maximally opening the pinhole) and background normalization. Quantification of the percentage of transfected cells was done by counting the number of miR-DY547 positive cells and compared with the levels of fluorescence in non-transfected cells using ImageJ. Representative microscopic fields were used for quantification spanning a total area of 4.3 mm^2. The total loading per cell was calculated with ImageJ as the "integrated density" that is given by the product between the mean fluorescence intensity and the area of the cell; 200 cells were analyzed in each condition giving a total area of 0.250 mm^2.

For the intracellular distribution studies, NPs (fluorescein-labelled or unlabelled) or SiPORT complexed with fluorescent oligonucleotides (mimic miRNA transfection control miR-Dy547 (Dharmacon); antagomir-92a fluorescein labelled (Dharmacon)) were incubated with cells for 4 h at 37ºC. Cells were fixed as described above, permeabilized with 0.5% tritonX-100/ PBS, and blocked with PBB (2% BSA plus 2% FCS in PBS). Cells were incubated with primary antibodies diluted in PBB according to manufacturer's instructions and incubated overnight at 4ºC with anti-human

argonaute2 (Ago2, 1B1-E2H5 clone active motif, 1:500), Rasa1 (1:100) and anti-human GW182 (H70, Santa Cruz Biotechnology sc-66915, 1:100). Other antibodies were incubated for 1 hour at room temperature; namely, the early endosomal marker EEA1 (Cell Signaling C45B10, 1:200 dilution) and the late endosome/lysosome marker protein RAB7 (Cell Signaling D95F2, 1:100 dilution). Secondary antibodies were anti-mouse Cy3 (Sigma C2181), anti-rabbit Cy3 and anti-mouse DyLight 649 (Jackson ImmunoResearch). The nucleus of cells was stained with DAPI. After the indirect labelling, high magnification confocal images (60x objective) were taken, using the optimal pinhole for better discrimination between foci and assuring no over-exposure or bleed-through between channels. Usually images were composed of 4 channels (blue, green, red and far-red) where different interactions were analysed. NPs were green or non-fluorescent depending on how many co-interactions were analysed, e.g. when assessing the association between miR-Dy547/ AGO2/ GW182 or antagomir-92a/ AGO2/ GW182 non-fluorescent NPs were used. Images were exported to imajeJ and analysis was performed with stacks containing the different channels. The interaction of NPs and/ or miRs with the different proteins was assessed, considering positive associations to be within 500 nm distance between centres of foci using ImageJ. All the discrete foci (fluorescence levels higher than background) present inside the cell were analysed by overlaying a ruler of 500 nm length in all directions from the centre of each of the foci and scoring the number of foci in the other channels that were contained inside this area; at least 100 cells were analysed in each condition. Due to the highly variable number of foci present inside the cell (e.g. Ago2 low, EEA1 high, miRs high) we found automated co-localization tools available in ImageJ to be inadequate for this type of analysis.

Immunoprecipitation studies. For the heat shock protein 90 (anti HSP90 Santa Cruz Biotechnology – SC-59577) pull-down assay, HUVECs growing in 100 mm petri dishes were tripsinized washed with PBS and resuspended in ice cold low salt lysis buffer (1% Igepal, 50 mM Tris-HCl pH 8) supplemented with a cocktail of proteinase inhibitors. μMACSTM Protein A/G Separation kit was used for the immunoprecipitation assay. First, the samples were labelled with the antibody of interest (anti HSP90 – 2 μg of antibody per 2 mg of protein in 1 mL of cell lysate). The antibody of interest was captured by addition of protein G MicroBeadsTM (130-071-101 Miltenyi Biotec). Further processing of the samples was performed in accordance with the instructions provided by the manufacture company. Protein quantification was done with QuantiProTM BCA Assay Kit (Sigma; QPBCA). The obtained eluates from the μColums were loaded in a NuPAGE® Novex® 3-8% Tris-Acetate Gel and the electrophoresis was performed in a XCell SureLockTM system (≈1 h of running time, 150 V with NuPAGE® Tris-Acetate SDS Running Buffer). The transfer was done with Invitrolon™ PVDF membrane in an XCell II TM Blot Module (≈1 h 30V with NuPAGE® Transfer Buffer). To detect the interaction of Ago2 with HSP90 the membrane was blocked (30 min in PBS-0.1% Tween® 20 –Sigma;-5% low fat milk) and incubated with anti-Ago2 antibody (1:500 in a PBS-0.1% Tween® solution; Ago2 Abcam – ab32381) overnight at 4ºC. The membrane was then incubated with specific secondary antibody (anti-rabbit: GE Healthcare Life Sciences). The detection of Ago2 bands was performed by enhanced chemiofluorescence methodology [(ECF); GE Healthcare Life Sciences] and using a Biorad FX Molecular Imager System (Bio-Rad). Lane detection and band quantification was done with Image Lab software.

RT-PCR for gene expression profile of treated cells. The gene expression profile of specific targets of miR132 was evaluated in HUVECs transfected with NPs, with or without miRNA. Total RNA from experimental groups was isolated using TRIzol (Invitrogen) and a RNeasy Minikit (Qiagen, Valencia). cDNA was prepared from 1 mg total RNA using Taqman Reverse transcription reagents (Applied Biosystems, CA). Quantitative PCR (qPCR) was performed using Power SYBR Green PCR Master Mix and the detection using an ABI PRISM 7500 System (Applied Biosystems). Quantification of target genes was performed relative to the reference gene GAPDH: relative expression= 2[-(Ctsample-CtGADPH)]. The mean minimal cycle threshold values [164] were calculated from quadruplicate reactions. Primer sequences are published in supporting information (**Table 4**).

Table 4- Primers for qRT- PCR

Target gene	Sense primer sequence	Anti-sense primer sequence	Concentration (nM)
GAPDH [b]	AGCCACATCGCTCAGACACC	CAGCGCCAGCATCG	10
RASA1 [b]	TTCTTAGCCAGATGAATGTTG	CACCAATGTAGTATCTC	4

[a] PCR conditions: initial denaturation step at 94ºC for 5 min; 40 cycles of denaturation at 94ºC for 30 sec, annealing at 60ºC for 33 sec and extension at 72ºC for 30 sec. At the end was performed a final 7 minutes extension at 72ºC. After amplification, the melting curve profile or agarose gel electrophoresis was used to determine the specificity of PCR products. [b] GAPDH (Glyceraldehyde 3-phosphate dehydrogenase) and RASA1 (RAS p21 protein activator).

Survival and angiogenesis assays. After transfection, cells were washed 3 times with warm PBS and left in complete EGM2 medium overnight. Cells were incubated under low oxygen (0.1%), in serum deprived conditions for another 48 h. Survival was assessed using the ATP-based assay Cell Titer Glow (Promega) following manufacturer's instructions. An in vitro angiogenesis assay was conducted using IBIDI micro-angiogenesis slides (IBIDI) and Matrigel according to manufacturer instructions [214]. After 24 h, tube length and number of branching points was measured (blinded analysis) and compared between conditions.

***In vivo* studies.** The Experimental Animal Committee of University of Eastern Finland approved all procedures. Unilateral hindlimb ischemia (UHI) was induced by ligating the right femoral artery proximal to the bifurcation of the saphenous and popliteal arteries (by ligation of both femoral artery and vein proximal to the origin of the deep femoral branch) in C57BL/6J male mice (Jackson Laboratory, Bar Harbor, ME). Prior (Pre OP) and after UHI (Post OP) the leg which received the injury was examined using VeVo Doppler to determine the perfusion levels of the femoral artery. Animals were then treated with mouse endothelial cells (MS1 cell line) alone, or cells transfected with NP170-PFCE, cells transfected with NP170-PFCE-miR132 or cells transfected with SIPORT-miR132. The cells (5×10^6 cells per animal) were initially labelled with DiR and then suspended in a fibrin gel (50 mL) precursor solution and injected into the gastrocnemius muscle of the operated hindlimb.

Preparation of mouse endothelial cells. MILE SVEN 1 (MS1) endothelial cell line derived from mouse pancreatic islet was obtained from ATCC (CRL-2279). MS1 cells were cultured in Dulbecco's

Modified Eagle's Medium (DMEM) (Sigma Aldrich) supplemented with fetal bovine serum (5%, FBS) (Biosera) and penicillin-streptomycin solution (1%, Pen/Strep) (Sigma Aldrich). Prior to injection into the animal, the cells were incubated in medium (containing 2% FBS) with NP170-PFCE (500 mg/mL per 400,000 MS1 cells), NP170-PFCE-miR132 (500 mg/mL per 400,000 MS1 cells, 200 nM miRNA), or SIPORT-miR132 (200 nM of miRNA) for 4 h. After cell transfection, cells were washed 3 times with PBS, and then labelled with an IVIS probe for fluorescence detection using near-infrared lipophilic carbocyanine dye denoted by 1,1'-dioctadecyl-3,3,3',3'-tetramethylindotricarbocyanine iodide (DiR) (1.75 μg/mL dye in PBS per 5×10^6 cells, the incubation was done for 30 min at 370C, as recommended by the vendor (Caliper LifeSciences)). The cells were then washed with PBS, trypsinized, centrifuged. The pellet was re-suspended in a fibrin gel (50 mL); the solution was placed in a 1 mL diabetic syringe and kept on ice until needed for injection into the animals. For injection, 5 ×106 cells were prepared per syringe for injection in the mouse hindlimb.

The fibrin gels were made by crosslinking fibrinogen in the presence of thrombin (both from Sigma-Aldrich). The fibrinogen solution was prepared by dissolving human fibrinogen in Tris-buffered saline (TBS) (Sigma-Aldrich), pH 7.4 (20 mg/mL), and then sterilized by filtering through a 0.22 μm syringe filter (Acrodisc, Pall). Fresh thrombin solutions were prepared by dissolving human thrombin in TBS at pH 7.4 at a concentration of 50 U/mL. Fibrin gels (50 μL, unless otherwise stated) were prepared by mixing three different components: fibrinogen (10 mg/mL), CaCl2 (Merck, NJ, USA) (2.5 mM) and thrombin (2 U/mL).

***In Vivo* Imaging System (IVIS) analysis.** Animals were imaged under isofluorane anaesthesia, at days 1, 3, 5 and 7 post-surgery. IVIS was performed to image the transplanted cells using IVIS Lumina II hardware (Caliper LifeSciences). A laser with the values for far-red Cy5 imaging at a 640 nm excitation and 670 nm emission filter was used, after an exposure time of 0.5 seconds images were obtained. The imaging field was of 12.5 × 12.5 cm.

VeVo analysis. Ischemic gastrocnemius muscle perfusion was measured on day 0 (pre- and post-operative), day 3, 5 and day 7 after surgery. Perfusion data were acquired with a high-resolution imaging system (Vevo 770, VisualSonics Inc., Toronto, ON, Canada), using an ultrasound probe (RMV-704) in Power Doppler mode (power 100%, RF-cycle 5, gain 25, velocity medium, wall filter 15, scan speed 15, priority 100, intensity range maximum 53 and minimum 19). Video clips containing approximately 50 frames were captured and the vascularity index (normalized to the area of the muscle) in three evenly separated frames was quantified with VeVo 770 measurement software (VisualSonics). The results are represented as group means of ratios to intact values to reduce measurement dependent variation.

^{19}F/^{1}H in vivo MRI. MRI analysis was performed using a 9.4T horizontal bore (60 G/cm, inner bore diameter 120 mm) system (Varian), using Direct Drive console (VJ NMR) with a linear transmit and receiver, on animals 1, 3 5 and 7 days post-surgery. 19F MRI was performed to detect NP-labelled cells while 1H MRI was done for anatomy of the limbs. 19F MR images were acquired using a purpose built circular surface coil tunable to 19F. Mice were anesthetized by the use of isoflurane

(4%) in oxygen (100%) and placed in a purpose built cradle for horizontal positioning in the magnet bore. Maintenance anaesthesia was 1.5–2% isoflurane at 1 l min−1 oxygen flow. For 1H imaging, coronal GEMS images of the legs were taken at matrix size of 128 (later zero filled to 256), 30 averages, field of view 35 × 35 cm, 10 imaging planes of 1mm depth, TE/TR = 4/1.2 ms with a flip angle of 70 degrees. The 1H images were later isotropically zero-filled by a factor of two and filtered (modified third-order Butterworth filter) before Fourier transformation. For 19F imaging, coronal GEMS images of the legs cloned from the 1H images were taken at matrix size of 256, 60 averages, field of view 35 × 35 cm, 1 imaging plane of 10mm depth, TE/TR = 4/1.2 ms with a flip angle of 90 degrees. All images were Fourier transformed and overlaid. At all times a phantom, denoted P, was present to allow shimming and pulse calibration, and to aid orientation within the surface coil.

Post-mortem histological analysis. The animals were sacrificed 7 days post-surgery. The mice were perfused with PFA (1%) in citrate buffer through the abdominal aorta, the test muscle was excised and fixed with 4% PFA in 7.5% sucrose for 4 h. Sections (4 μm) were immunostained with rat anti-mouse CD31 antibody (dilution 1:25, MEC 13.3; BD Biosciences Pharmingen, San Diego, CA). As a secondary antibody, biotinylated rabbit anti-rat antibody (Vector Laboratories, Burlingame, CA) was used and detected using the avidin-biotin-horseradish peroxidise system (Vector Laboratories, CA, USA) with DAB as a chromogen (Zymed, San Francisko, California and Tyramide signal amplification system (TBA, Biotin System, PerkinElmer, Shelton, USA). Photographs of the stained sections were taken and processed using an Olympus AX70 microscope (Olympus Optical, Tokyo, Japan) and analySIS imaging software (Soft Imaging System GmbH, Muenster, Germany), respectively. Capillary density (capillary/muscle fibre ratios) was measured from three microscopic

fields of CD31 immunostained sections taken in a close proximity to the needle track at ×100 magnification in a blinded manner.

Acknowledgments. We thank Dr. Jeffrey Karp and Dr. Michael Goldberg for critical review of the manuscript. This work was supported by a Marie Curie-Reintegration Grant (FP7-People-2007-4-3-IRG; contract nº 230929), MIT-Portugal program, British Heart Foundation Programme Grant (RG/07/004/22659) and FCT (PTDC/CTM/099659/2008; and SFRH/BD/33466/2008, a fellowship to R.S.M.G.).

Chapter III annex:

In Vivo Oligonucleotides Delivery by a MRI-Detectable Nanomaterial

In Vivo Oligonucleotides Delivery by a MRI-Detectable Nanomaterial

Renata S.M. Gomes[1,2,3,4,], Ricardo Neves[1,2], Petra Korpisalo[4], Galina Dragneva[4], Lino Ferreira[1,2], Seppo Ylä-Herttuala[4]

1, CNC - Center for Neuroscience and Cell Biology, University of Coimbra, 3004-517 Coimbra, Portugal; 2, Biocant - Center of Innovation in Biotechnology, 3060-197 Cantanhede, Portugal; 3, Cardiovascular Biology & Medicine, Rayne institute, University College, London, UK; 4, A.I. Virtanen institute, Department of Biotechnology and Molecular Medicine, University of Eastern Finland, Finland.

Unpublished work. All procedures were performed in accordance to regulations for animal experimentation under the Finnish Academy of Sciences and the Helsinki Treaty.

3.A1. Abstract

Herein we report a methodology to transfect cells *in vivo* with oligonucleotides. Angiogenic oligonucleotides were attached to NPs and delivered within mouse limbs. A significant increase in capillary formation overtime was registered, the NPs were also successfully tracked via MRI and no signs of local inflammation, oedema or necrosis were seem, inferring little or no acidity produced in the limbs from the NPs PLGA degradation. We further report the therapeutic effect of cells transfected with miR132 and transplanted in a rabbit animal model to validate the results obtained in chapter 3 in a large animal model. Smooth muscle cells transfected with NPs carrying miRs and delivered within rabbits limbs, created an increase in angiogenesis again seen by a significant increase in capillary formation as well as notable perfusion illustrated by power doppler. MRI systems were sensitive enough to detect the NP labelled cells in these larger animals too. Here it is shown that methodologies for inductions of efficient angiogenesis without viral vectors are possible and practically feasible.

3.A2. Introduction

Limb ischemia often results from arterial occlusion and stenosis as a consequence of atherosclerosis. Endothelial dysfunction is an important factor in pathogenesis for plaque initiation and progression within limb ischemia [102, 215]. Common clinical practice to tackle limb ischemia involves surgical revascularization either by stent implantation, laiser revascularization or bypass surgery, however the success rates are still disappointing, leading to gangrene and amputation in a large majority of cases. It is speculated that successful treatment with the above therapies may eventually cause restenosis due to phenotypic redifferentiation of neovascular intimal smooth muscle cells [103].

Several approaches have been reported to treat ischemic limb including the use of endothelial progenitor cells [216], genetic engineered stem cells [217], and growth factors [218-220]. Yet the possibility to monitor the therapies by Magnetic Resonance Imaging (MRI) and to demonstrate their effect *in vivo* has not been demonstrated.

Here we report a theranostic platform to deliver angiogenic oligonucleotide. Biodegradable nanoparticles (NPs) containing perfluoro-1,5-crown ether (PFCE), a fluorine-based compound (NP170-PFCE), were initially loaded with an angiogenic oligonucleotide and its effect was evaluated in a ischemic mouse animal model. We further demonstrate the therapeutic effect of smooth muscle cells transfected with NPs carrying miR132 in a rabbit ischemic limb model. The results described in this chapter have been used to optimize the animal protocol that has been used in chapter III.

3.A3. Results and Discussion

3.A3.1. Angiogenic oligonucleotide-containing NPs administered at ischemic limbs increase neovascularization

To investigate whether NPs could also be used as a cell free vector for oligonucleotide delivery and also test for any possible toxicological effects of the biomaterial alone in the *in vivo* setting, we performed a small-scale animal trial. The NPs were monitored by MRI, which required the development of MRI sequences and the design of a new coil. A circular surface coil for higher sensitivity was modified and used on a 9.4T Varian MRI. The coil was adapted from a commercially available ^{1}H, re-tuned and capacitors for simultaneous $^{1}H/^{19}F$ imaging were added. All adaptations were done following principles from the developed volume birdcage coil for the 7T Varian MRI as described on the previous chapter (Chapter III). Healthy animals (C57Bl6 mice) received an injection of either NPs or NPs carrying an oligonucleotide, which was developed to induce angiogenesis when delivered using viral vectors (kindly provided by Dr Petra Korpisalo, University of Eastern Finland). Animals were sacrificed either at day 3 or day 7 and post mortem histology was performed followed by the MRI. Animals receiving only NPs overtime, shown no increase on the amount of capillaries per muscle fiber, as quantified and shown on the representative images (**Fig. 1 and 2**), however as shown by the MRI, the NPs were delivered and present in the limb muscle (**Fig. 3**). When NPs carrying the oligonucleotide were injected, a significant increase of the number of capillaries per muscle fiber was already noted at day 3 and further increased at day 7 (**Fig. 1 and 2**). Again MRI images demonstrate successful NP delivery and retention overtime. Other organs were also examined, namely the liver and kidneys so as to look for any NP toxicological *in vivo* effects. No modifications were observed (data not shown), therefore it is clear that the NPs by itself cannot cause any modifications of healthy tissue and can deliver biomolecules.

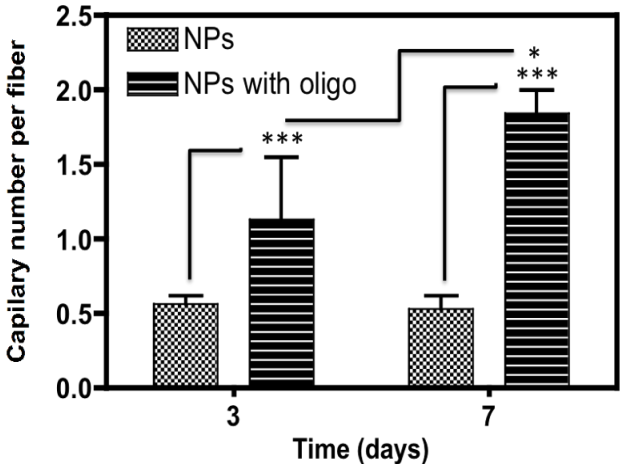

Figure 1- Quantification of number of capillaries per muscle fiber overtime. No significant increase in the number of capillaries overtime was observed when limbs were given NPs only. However when limbs received NPs carrying the oligonucleotidenucleotide (NPs with oligonucleotide) there was a significant increase in the number of capillaries per muscle fiber in comparison to NPs only (***p<0.0001), also there was significant increase overtime, from day 3 to day 7 (*p=0.0114).

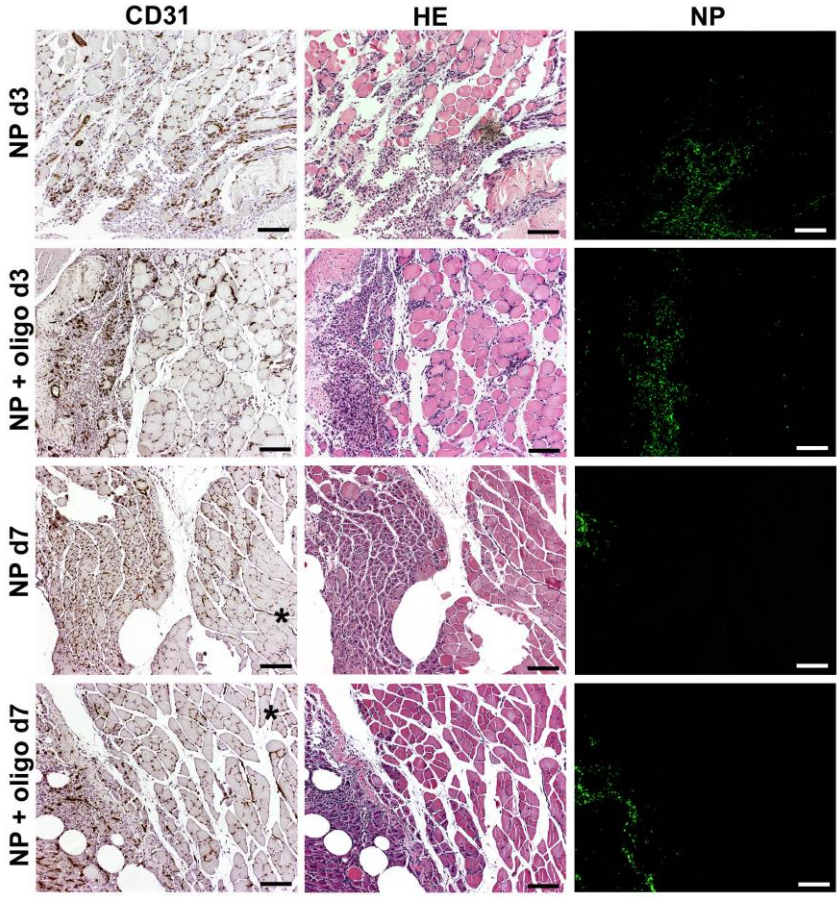

Figure 2- Histological and immunocytochemistry characterization of mouse limbs treated with NPs and oligonucleotide-containing NPs at different time points. Limbs were stained with hematoxylin and eosin and CD31 for neovascularization. NPs were monitored by their intrinsic fluorescence. Areas of increased CD31 staining co-localize with areas of NP presence. (Scale bar represents 50 μm).

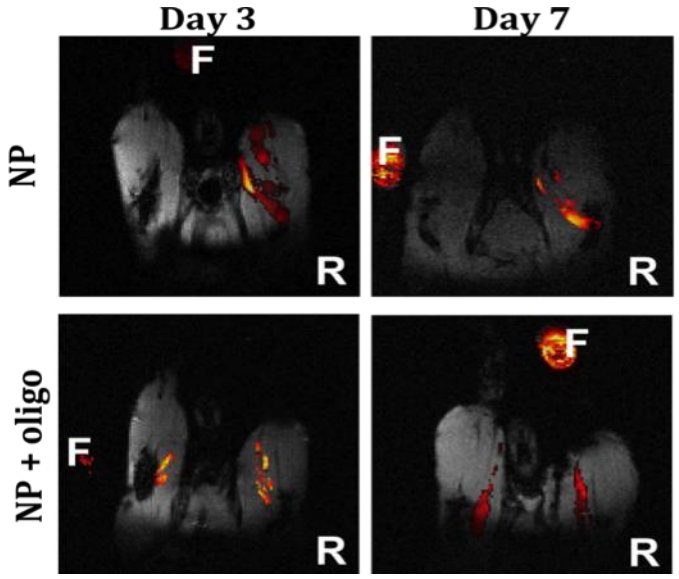

Figure 3- MRI images of limbs overtime. Representative MRI limb images overtime after receiving NPs only or NPs with oligonucleotide (NP + oligonucleotide). When delivering NPs only, one animal was kept with a non-injected leg to use as a calibration control for histological analysis, as well as for MRI null signal. However all other limb were injected with NPs. The MRI signal from the NPs is visible overtime in both cases, in the absence or presence of oligonucleotide.

3.A3.2. Smooth muscle cells transfected with miR132 increase the neovascularization of rabbit limbs

Next, the ability to label cells with the NPs and deliver SMCs *in vivo* was examined using rabbits. SMCs only (cells only), SMCs labeled with NPs (Cells +NPs) or SMCs labeled with miR132 (Cells + NP-miR) (in all cases 20×10^6 SMCs in fibrin gels) were delivered in the limb muscles of healthy rabbits where no limb injury was induced. The purpose of this study was to define a protocol for labelling SMCs and track them within medium sized animals and include VeVo measurements in addition to MRI and terminal histology. Also was important to increase the animal size to determine if our optimized protocols still allow MRI detection of the NPs in larger animals with more pre-clinical relevant dimensions. Cells alone or containing only NPs can proliferate overtime within the non-injured muscle at similar rates, indicative that NPs only do not induce any inhibition or enhancement of survival and proliferation. However cells which contained NPs carrying miR132 proliferated at a significantly higher rate when compared to cells only or cells + NP as shown by quantification of capillaries per muscle fiber (**Figure 4**) and in illustrative **Figure 5**.

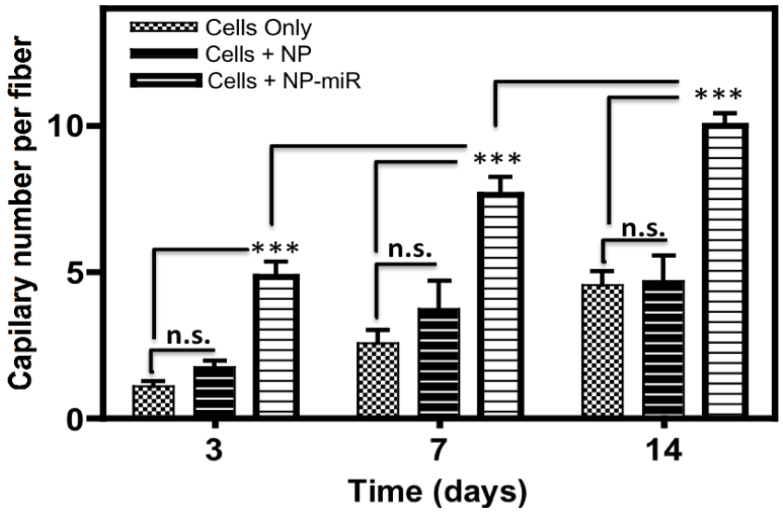

Figure 4- Quantification of number of capillaries per muscle fiber overtime. No significant increase in the number of capillaries was observed when limbs were given cells only or cells + NP. However when limbs received cells with NPs carrying miR132 (Cells + NP-miR) there was a significant increase in the number of capillaries per muscle fiber in comparison to controls (***$p<0.0001$), also there was significant increase overtime, from day 3 to 5 and again to day 7.

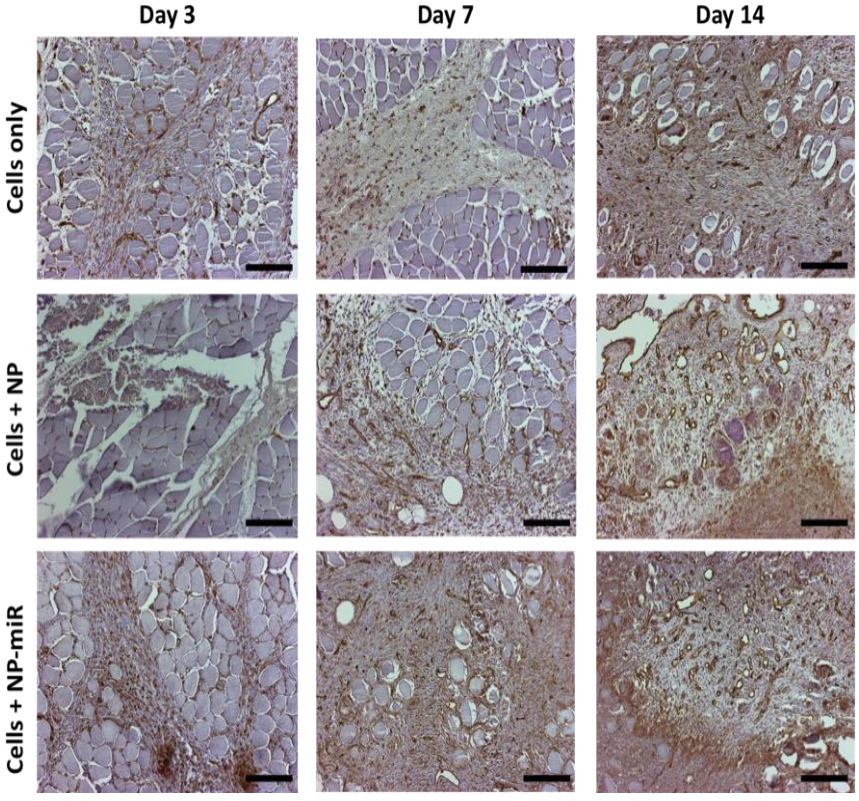

Figure 5- Representative images of limb staining. Limbs were stained for capillaries, with CD31 antibody, after receiving cells only or cells with NPs (Cells + NP) and cells with NPs carrying miR132 (Cells + NP-miR) (scale bar represents 50 μm).

Next, we determined whether ^{19}F imaging could be used to monitor the transplanted cells. As shown (**Figure 6**) with the purpose built coil for $^{19}F/^{1}H$ after further adaptations it could be detected from the cells transplanted in the limbs carrying miR or not. Unfortunately as the coil had to be re-tuned and extra capacitors added to increase sensitivity for the larger animals throughout the study, ^{19}F imaging for the rabbits was only available for day 14. It should be noted that the ^{19}F signal in animals treated with cells transfected with NP-miR132 is more dispersed. This might be due to *in vivo* cell division, as from the VeVo imaging (**Figure 7**) it is clear that the limbs of animals treated with cells containing NP-miR132 had improved blood perfusion. Furthermore, the number of capillaries per muscle fiber in the limbs of animals treated with cells containing NP-miR132 is higher than the ones treated with NPs without miR132.

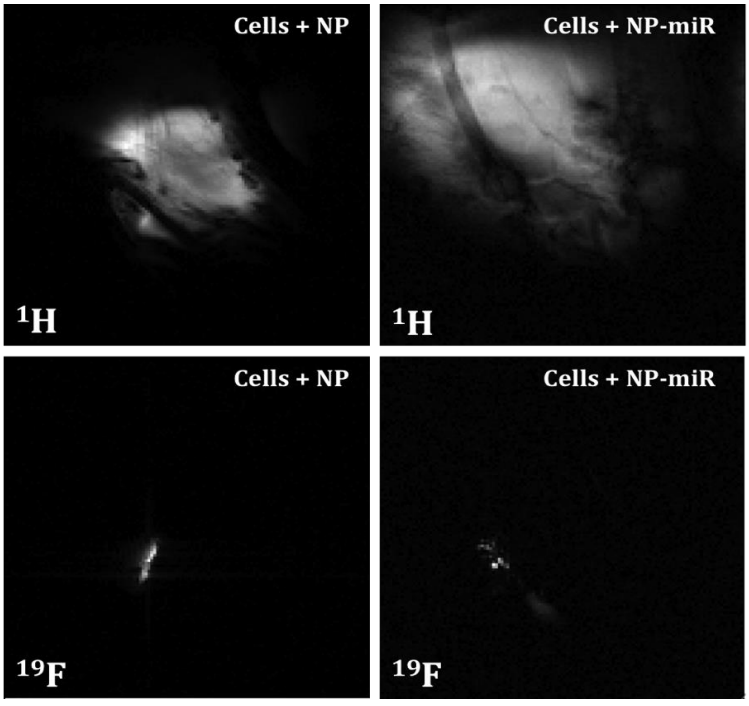

Figure 6- MRI images of limbs at day 14. Representative MRI limb images at day 14 after smooth muscle cell transplantation. Either cells containing NPs (Cells + NP) or cells containing NPs carrying miR 132 (Cells + NP-miR) were injected into healthy rabbit muscle. Where cells containing NP-miR were delivered a dilution of the ^{19}F signal is notable, inferring *in vivo* cell proliferation.

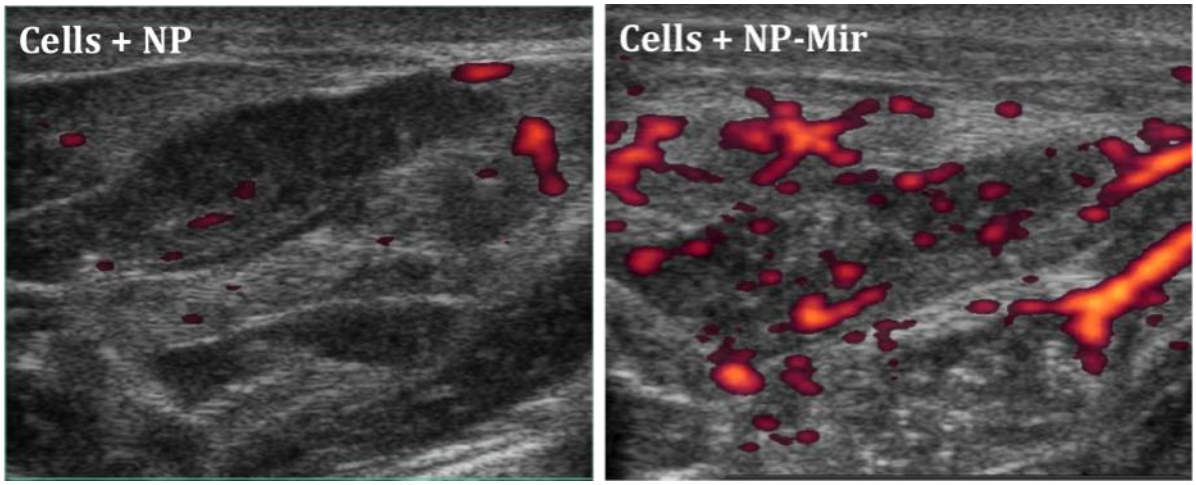

Figure 7- VeVo imaging of limbs at day 14. Representative VeVo imaging at day 14 after smooth muscle cell transplantation. Either cells containing NPs (Cells + NP) or cells containing NPs carrying miR 132 (Cells + NP-miR) were injected into healthy rabbit muscle. Where cells containing NP-miR were injected an increase in blood perfusion is clearly visible most probably due to *in vivo* cell proliferation and neovascularization.

3.A4. Conclusions

Our results show that NPs containing oligonucleotide neovascularization after administration in mice ischemic limbs. Animals treated with NPs carrying oligonucleotide show an increase in the number of capillaries overtime in comparison to its control. Furthermore, the newly developed circular surface coil to image via MRI the NPs has enough sensitivity to show NP tracking overtime. No signs of oedema or necrosis were observed in the animals, which indicate that NPs were not substantially toxic. This study was used as a form to establish protocols and set routines for larger animal trials. Furthermore it was interesting to see whether the oligonucleotide delivery via NPs was effective enough to compare with viral delivery. The group has a long-standing history of usage of viral vectors for cardiovascular gene therapy using angiogenic growth factor promotion [26, 30, 221-226] however interest is shifting towards the usage of non-viral vectors to promote angiogenesis.

Angiogenesis is a multi-factorial event and there is the need to deliver various angiogenic factors simultaneously, however regulations halt the use of various viral vectors simultaneously clinically, thus the deeper interest shifting towards using the NPs as delivery vectors. Whether the delivery via the NPs can match the efficiency of viral vectors is yet to be established and does not seem likely. However if significant levels of angiogenesis can be achieved and dual delivery permitted this might be enough reasoning to replace viral delivery in instance for promotion of neo-angiogenesis *in vivo*. Next we evaluated the therapeutic effect of smooth muscle cells transfected with NPs carrying miR132 in a rabbit ischemic model. It was clear that cells transfected with NPs carrying miR132 have a higher proliferation rate than cells transfected with NPs without miR132 or cells alone. In addition we were able to re-tune the sensitivity of a surface coil to detect ^{19}F signals from the transplanted cells in rabbit limbs, many orders of magnitude bigger than the mice limbs. VeVo measurements on power doppler mode were also possible to further permit studies on perfusion after implantation. All protocols and systems were well in place to allow full studies to be performed as it was with the *in vivo* study next done by us [227].

3.A5. Methods

***In vivo* studies.** Immunologically competent mice, C57BL/6J male mice (Jackson Laboratory, Bar Harbor, ME) or immunologically competent rabbits, New Zealand White male rabbits (Charles River), were used in the studies. Animals were kept in standard housing conditions.

Delivery of NPs containing oligonucleotides in C57BL/6J mice. NPs carrying an oligonucleotide (oligonucleotide) responsible for $VEGF_{165A}$ up-regulation [223] was delivered on normal legs, meaning no limb ischemia was performed in these animals. The conjugation between the oligonucleotide and

the NPs was performed in the same manner as miRs were conjugated to NPs, as described in Chapter III. Briefly, if cells were transplanted, 5×10^6 endothelial cells were injected per area, therefore for oligonucleotide delivery only with NPs, the amounts used were as if 5×10^6 cells were in use. For 5×10^6 endothelial cells, cells were labelled with 6.25 mg of NPs. Therefore, 6.25 mg were incubated with 93.75 μg of oligonucleotide, which results in approximately retention of 75 μg of oligonucleotide. The NPs were injected in a final volume of 50 μL of PBS per area. For this *in vivo* test, 2 groups were done, control group where NPs were injected (n=8, 4 terminated at each time point) and test group where NPs with oligonucleotide were delivered (n=8, 4 terminated at each time point). Animals were imaged under MRI at day 3 and 7 and terminated at both time points for histology as shown in the experimental diagram bellow.

Figure 1- Experimental *in vivo* design. Schedule for NP delivery, imaging and termination points in mice, which did not undergo limb ischemia surgery.

Delivery of smooth muscle cells transfected with NPs in New Zealand White rabbits. Rabbit smooth muscle cells obtained and isolated from rabbit aortas were cultured under and expanded within recommended conditions (DMEM media containing 10% serum and 1% (v/v) penicillin and streptomycin). Once enough cells were sub-cultured, cells were transfected with NPs only or NPs carrying miR132. NP-miR conjugation was performed as previously described (see chapter III). Three experimental groups have been performed: (i) SMCs alone were injected into rabbits (n=3), (ii) SMCs transfected with NPs only (n=3) or (iii) SMCs transfected with NPs carrying miR132

(n=3). Each injection was made of 20×10^6 SMCs in fibrin gels. Animals underwent, MRI, VeVo/Power Doppler at each time point as shown in Figure 2.

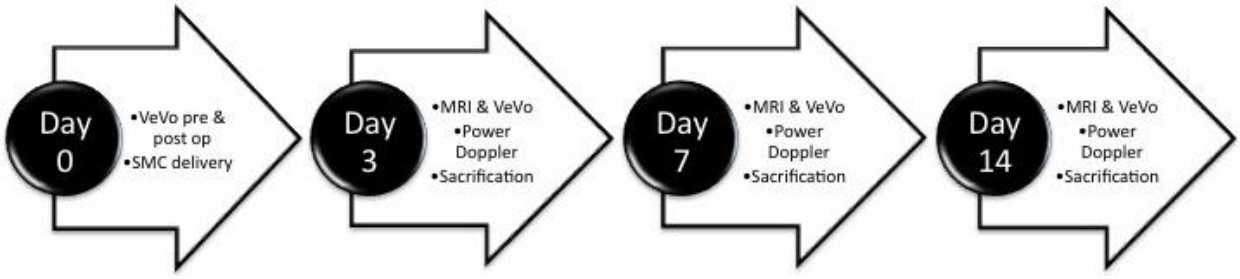

Figure 2- Experimental *in vivo* design. Schedule for SMC delivery, imaging and termination points in rabbits, which did not undergo limb ischemia surgery

Fibrin gel preparation. The fibrin gels were made by crosslinking fibrinogen in the presence of thrombin (both from Sigma-Aldrich). The fibrinogen solution was prepared by dissolving human fibrinogen in Tris-buffered saline (TBS) (Sigma-Aldrich), pH 7.4 (20 mg/mL), and then sterilized by filtering through a 0.22 μm syringe filter (Acrodisc, Pall). Fresh thrombin solutions were prepared by dissolving human thrombin in TBS at pH 7.4 at a concentration of 50 U/mL. Fibrin gels (50 μL for mice or 200 μL for rabbits) were prepared by mixing three different components: fibrinogen (10 mg/mL), $CaCl_2$ (Merck, NJ, USA) (2.5 mM) and thrombin (2 U/mL).

High-resolution ultrasound micro-imaging (VeVo). Muscle perfusion was measured where appropriate. Perfusion data was acquired with a high-resolution imaging system (Vevo 770, VisualSonics Inc.), using an ultrasound probe (RMV-704) in Power Doppler mode (power 100%, RF-cycle 5, gain 25, velocity medium, wall filter 15, scan speed 15, priority 100, intensity range maximum 53 and minimum 19). Video clips containing approximately 50 frames were captured and the vascularity index (normalized to the area of the muscle) in three evenly separated frames was

quantified with VeVo 770 measurement software (VisualSonics). The results are represented as group means of ratios to intact values to reduce measurement dependent variation.

^{19}F/^{1}H in vivo MRI. MRI was performed on the animals at the stated time points in each *in vivo* group. ^{19}F MRI was performed to detect the labelled cells with NPs and ^{1}H done for anatomy of the limbs, this was done using a purpose built circular surface coil tunable to ^{19}F. Anesthesia was induced using 4% isoflurane in 100% oxygen. Animals were placed in a purpose built cradle for subsequent horizontal positioning in the magnet bore. Maintenance anaesthesia was 1.5–2% isoflurane at 1 Lmin^{-1} oxygen flow. MRI was performed on a 9.4T horizontal bore (60 G/cm, inner bore diameter 120 mm) system (Varian), using Direct Drive console (VJ NMR) with a linear transmit and receiver. For ^{1}H imaging, coronal GEMS images of the legs were taken at matrix size of 125 (later zero filled to 256), 30 averages were taken, field of view was 35 × 35 cm, 10 imaging planes each of 1mm depth, TE/TR = 4/1.2 ms with a flip angle of 70 degrees resulting in a total experimental time of approximately 11 minutes. The ^{1}H images were later isotropically zero-filled by a factor of two and filtered (modified third-order Butterworth filter) before Fourier transformation. For ^{19}F imaging, coronal GEMS images of the legs cloned from the ^{1}H images were taken at matrix size of 256, 60 averages were taken, field of view was 35 × 35 cm, 1 imaging plane of 10 mm depth TE/TR = 4/1.2 ms with a flip angle of 90 degrees resulting in a total experimental time of approximately 37 min. All images were Fourier transformed and overlaid, green/red shows the labelled cells with NPs by the ^{19}F signals and grey denotes the anatomy by ^{1}H. At all times a phantom, denoted P, was present to allow shimming and pulse calibrations, furthermore aided orientation within the surface coil.

Post mortem histological analysis. Paraffin embedded sections (4 μm), immersion fixed with 4% PFA in 7.5% sucrose for 4 h, were used for immunohistochemical analysis. Sections were immunostained with rat anti-mouse CD31 antibody (dilution 1:25, Biosciences Pharmingen). As a secondary antibody, biotinylated rabbit anti-rat antibody (Vector Laboratories) was used. The avidin-biotin-horseradish peroxidise system (Vector Laboratories) with DAB as a chromogen (Zymed) and tyramide signal amplification system (TBA, Biotin System, PerkinElmer) for amplification of the signal was used. Photographs of the stained sections were taken and processed using an Olympus AX70 microscope (Olympus Optical) and analySIS imaging software (Soft Imaging System GmbH), respectively. It should be noted that CD31 for capillary staining was manually quantified in order to avoid inclusion of stained monocytes as a capillary (automated quantification, such as using ImageJ, in this case would not distinguish between CD31 staining from actual capillaries or other cells, e.g. monocytes). Capillary density (capillary/muscle fibre ratios) was measured from three microscopic fields of CD31 immunostained sections taken in a close proximity to the needle track at ×100 magnification in a blinded manner.

Statistical analysis. For analysis involving three or more groups, ANOVA was used, followed by a Student-Newman-Keuls post hoc test. For analysis of two groups, a paired *t*-test was used. Statistical analysis was performed using GraphPad Prism software (San Diego, CA, USA, http://www.graphpad.com/). Results were considered significant when $P \leq 0.05$.

Chapter IV:

Preconditioning of cardiosphere-derived cells under hypoxia or with prolyl-4-hydroxylase inhibitors

Preconditioning of cardiosphere-derived cells under hypoxia or with prolyl-4-hydroxylase inhibitors

Suat Cheng Tan[1,2*], Renata S.M. Gomes[1*], Kar Kheng Yeoh[3], Lucy Ambrose[1], Lisa. C. Heather[1], Christopher J. Schofield[3], Kay E. Davies[1], Kieran Clarke[1], and Carolyn A. Carr[1]

1, Department of Physiology, Anatomy & Genetics, University of Oxford, Sherrington Building, Parks Road, Oxford, OX1 3PT, UK. 2, School of Health Science, University Sains Malaysia, Health Campus, 16150 Kubang Kerian, Kelantan, Malaysia. 3, Department of Chemistry, University of Oxford, Chemistry Research Laboratory, Mansfield Road, Oxford, OX1 3TA, UK.

This chapter, optimizing *in vitro* cell culture procedures for stem cells (CDCs), constitutes parts of the paper in press at Molecular Biology Reports done with Dr Suat Cheng Tan.

4.1. Abstract

Myocardial infarction (MI) results in severe ischemia still causing high mortality rates [1]. The ischemia is downstream from occluded arteries causes cardiomyocytic necrosis and apoptosis within few hours. There is growing evidence that heart muscle has the ability to regenerate through the activation of resident cardiac stem cells or through recruitment of a stem cell population from other tissues [228]. Cardiosphere-derived cells (CDCs), isolated from heart explants, are a promising to restore myocardial plasticity and prevent further heart failure [229]. However, current protocols used to

expand CDCs require at least one month *in vitro* culture to obtain sufficient cells for transplantation. Here, CDC culture was optimized by preconditioning the cells under hypoxia (2% oxygen), which reflected the physiological oxygen level of the stem cell niche. The proliferation rate of cells from explants was 1.4-fold greater under hypoxia than under normoxia, generating 6×10^6 CDCs with higher expression of cardiac stem cell marker, c-Kit and pluripotency genes Oct-4, Nanog, Sox 2 and Klf4, within 21 days, a week faster than under normoxia. Hypoxic-preconditioning was mimicked by treatment with three HIF prolyl-4-hydroxylase inhibitors (PHDIs), dimethyloxaloylglycine (DMOG), ethyl 2-(2,3-dihyroxybenzamido) acetate (EDBA) and 2-(1-chloro-4-hydroxyisoquinoline-3-carboxamido) acetic acid) (BIC), which prevented degradation of the hypoxia inducible factors (HIFs) and activated the HIF-regulated genes, EPO, VEGF, CXCR-4 and TERT. Cell culture under hypoxia enhanced the therapeutic potential for MI and could be mimicked, in part, by treatment with PHDIs. In addition we show that we can label CDCs with PLGA NPs containing fluorine, both under normoxic or hypoxic conditions, without affecting their ability to differentiate *in vitro*. Furthermore, we can transplant labelled CDCs with NPs into *in vivo* models of rodent myocardial infarction, tracking them up to 13 days.

4.2. Introduction

Cardiac stem cells (CSCs) were first identified in the heart in 2003 [230], challenging the paradigm that the heart is a postmitotic organ [231, 232]. CSCs could be isolated based on a specific single cell marker such as c-Kit [74] or Sca-1 [86, 233]. In 2004, Messina *et al* developed a method to isolate CSCs from human and murine heart and expand them as cardiospheres [75]. The cardiospheres were expanded *in vitro* to obtain sufficient cardiosphere-derived cells (CDC) for transplantation [234]. The CDCs were clonogenic, expressed stem and endothelial progenitor cell markers, appeared to have the properties of adult cardiac stem cells and resulted in myocardial regeneration and functional improvement when injected into the infarcted rodent heart [75, 234, 235]. However, the culture protocol required at least one month to obtain sufficient CDCs for therapy. During this period, the infarcted heart will undergo the initial stages of scar formation and remodelling [236]. CDCs may be of better use if they could be administered as soon as possible after infarction.

Stem cells reside in complex microenvironments, which play an important role in signalling stem cell division, function and differentiation [237, 238]. Most *in vitro* tissue cultures are routinely maintained at atmospheric levels of 21% oxygen, whereas the average oxygen concentration at *in vivo* tissue level is about 2-9%, with considerable variation based on location [239-241]. Adult stem cell niches are hypoxic, with some oxygen levels as low as 1-2% [239]. *In vitro* cultivation of stem cells in a traditional incubator supplied by room air does not recapitulate the *in vivo* physiological condition and could result in a gradual loss of primitive stem cell characteristics [242]. Enhanced cell proliferation rates and reduced apoptosis have been reported for human and rat mesenchymal stem cells [243-245], neural stem cells [246-248], embryonic stem cells [249, 250] and adipose-derived stem cells [92, 251] when cultured under low oxygen concentrations (2% – 6% O2).

In understanding the dual control system of HIF system in the presence of oxygen, it is important to understand the differential sensitivity of prolyl and asparaginyl hydroxylation by hypoxia and its potential manipulation by PHD inhibitory (PHDI) agents. Here, the effects of three different PHDIs for HIF stabilization in CDC culture were compared: dimethyloxaloylglycine (DMOG) – a cell permeable, competitive inhibitor of the HIF cofactor, 2-oxoglutarate (2OG) [252]; ethyl 2-(2,3-dihyroxybenzamido) acetate (EDBA) – an aspirin metabolite that acts as an iron chelator to activate the HIF system via generic 2OG-oxygenase inhibition [253]; and 2-(1-chloro-4-hydroxyisoquinoline-3-carboxamido)acetic acid) (BIC, also known as FG2216) – a specific PHD inhibitor which has been used in clinical trials as a pro-angiogenic compound acting via the HIF-1α system [96].

In this work we investigated the effects of normoxia and hypoxic culture systems on CDCs. We further investigated the effect of a variety of chemicals, which have the ability to induce and maintain hypoxia, in order to maximize CDC stem properties during culture so these could be transplanted *in vivo*.

This novel study compared the effects of these three different inhibitors of PHD enzymes for HIF stabilization in CDC culture and investigated whether pharmacological inhibition of PHDs successfully mimicked the effects of hypoxic preconditioning. Also, the effects of these PHD inhibitors (PHDIs) on FIH reactivity were observed. Furthermore the ability to track cells labelled with NPs by magnetic resonance imaging (MRI) was also evaluated.

4.3. Results and Discussion

4.3.1. Optimizing in vitro cell culture procedures for stem cells (CDCs)

S*prague Dawley* neonatal rat heart (0.07 to 0.10 g) explanted on fibronectin coated dishes adhered well to the surface and generated a layer of thin, flat fibroblast-like cells after 1-2 days. Phase bright cells were observed growing from the explants and migrated over a fibroblast-like cell layer after 4 days. One neonatal rat heart generated approximately 1×10^6 explant derived cells (EDCs) after 7 days. The explants could be harvested up to 3 times with an interval of 1 week between each harvest.

Adult rat atrial explants were cultured under normoxia (21% O_2) or hypoxia (2% O_2) (**Fig. 1A**). After 3 to 6 days in both normoxic and hypoxic culture, fibroblast–like cells started to migrate away from the edge of the explants. Typically, under hypoxia, EDCs became confluent and were ready for harvesting within 10 days of plating, 5 days faster than normoxic EDCs. After 9 days in culture under hypoxia, $10.3 \pm 0.3 \times 10^5$ EDCs were produced from 0.1 g explants tissue, 1.4 fold more than those generated under normoxia ($7.3 \pm 1 \times 10^5$ EDC/0.1 g). These rates were maintained up to day 18, with hypoxic culture generating $22 \pm 1 \times 10^5$ EDCs/0.1 g while normoxic culture generated $18 \pm 1 \times 10^5$ EDCs/0.1 g (**Fig. 1B**). EDCs aggregated to form cardiospheres after 2 days in culture. Approximately 400 cardiospheres were obtained from each well after 4 days of incubation under normoxia or hypoxia (**Fig. 1C**), with hypoxic cardiospheres forming larger cell clusters (0.033 ± 0.004 mm^2) compared with those under normoxia (0.017 ± 0.002 mm^2) (**Fig. 1D**). Isolated cardiospheres were replated on fibronectin and formed cardiosphere-derived cells (CDCs) after 3-4 days of incubation. Hypoxic culture yielded higher cell numbers than normoxia at day 5 of each passage from P1 until P5 (**Fig. 1E**). On average, 5.2 ± 0.3-fold expansion was observed at each passage for hypoxic cells, whereas normoxic CDCs maintained a 3.0 ± 0.1-fold increase during each

passage. Approximately 6 × 10^6 P2 CDCs were obtained from hypoxic explants within 21 days, a week faster than the normoxic explants.

Adult atrial CDCs cultured under hypoxia expressed significantly higher HIF-1α mRNA (2.9 ± 0.6-fold), compared with normoxic CDCs (**Fig. 2A**). In line with this, HIF-1α protein levels were increased by 3.7 ± 0.5-fold in hypoxic CDCs, compared with normoxic CDCs (**Fig. 2A**). Activation of HIF-1α under hypoxia subsequently upregulated several important HIF-regulated genes including VEGF (3.5 ± 0.6-fold), EPO (3.3 ± 0.9-fold), CXCR4 (6.7 ± 1. 0) and TERT (2.7 ± 0.4-fold) (**Fig. 2A**). Elevated VEGF protein levels were confirmed.

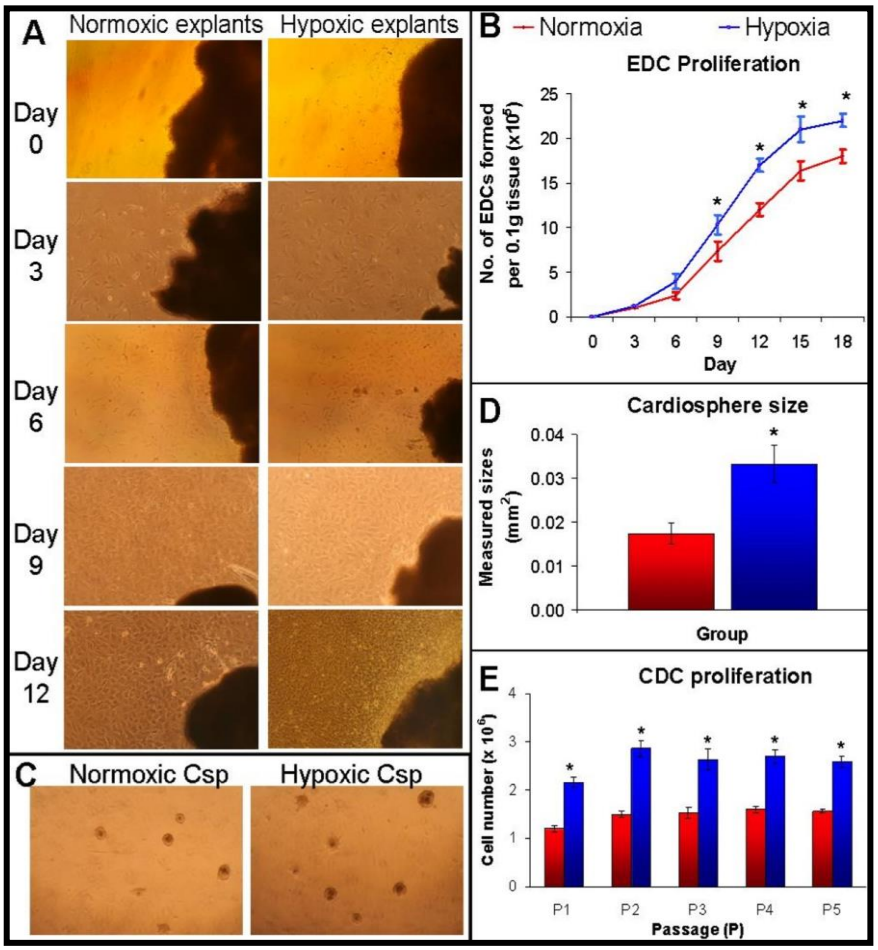

Figure 1- Hypoxic preconditioning of CDCs. (A) Adult rat atrial heart tissue was cultured under normoxia or hypoxia for 12 days. (B) EDCs generated under normoxia or hypoxia were harvested and cell numbers were counted. (C) Morphology of normoxic & hypoxic cardiospheres (Csp) were significantly different, with (D) hypoxic Csp 1.9-fold larger than the normoxic Csp. (E) Hypoxia also yielded higher cardiosphere-derived cell (CDC) numbers than normoxia at day 5 of each passage from P1 until P5 (* $p < 0.05$ vs. normoxia).

Under hypoxia, CDCs showed significantly increased mRNA expression for c-Kit (2.3 ± 0.1-fold) and the pluripotent markers, Oct-4 (2.9 ± 0.5-fold), Klf4 (3.1 ± 0.6-fold), Nanog (4.5 ± 1.1-fold) and Sox 2 (5.4 ± 1.5-fold), with reduced expression of mesenchymal markers CD90 and CD105 (32% and 65%, respectively). The mRNA expression of cardiac transcription factors (Nkx 2.5 and GATA 4) and the mature cardiomyocyte markers, Tnnt and MyHC was not significantly different after hypoxic culture (**Fig. 2A**).

Hypoxic CDCs were treated with either normal cell culture medium (negative control) or differentiation medium for 2 weeks. qRT-PCR showed that differentiation medium containing DMSO significantly increased Nkx 2.5 and Tnnt mRNA expression by 1.4 ± 0.1-fold and 2.0 ± 0.3-fold, respectively, compared with non-treated hypoxic CDCs, indicating that hypoxic CDCs began to differentiate when treated with cardiomyogenic stimuli (**Fig. 3A**). However, it was found that the levels of Nkx 2.5 and TnnT2 in DMSO-treated hypoxic CDCs were significantly lower by 33% and 45%, respectively, compared to DMSO-treated normoxic CDCs (**Fig. 3B**). Similar with qPCR data, immunostaining data also indicated that both normoxic and hypoxic CDCs showed positive staining for α-sarcomeric actin and TnnT2 after induction by DMSO, compared to non-treated CDCs (**Fig. 3C**). Furthermore, it was found that normoxic CDCs displayed a more obvious positive staining for α-sarcomeric actin and the structure of cardiomyocyte-like cells became organized (illustrated by TnnT2 staining, **Fig. 3C**), compared to hypoxic cells. Together, these findings indicate that cells cultured under hypoxia retained the ability to differentiate into cardiomyocytes, however, this ability was attenuated after hypoxia culture.

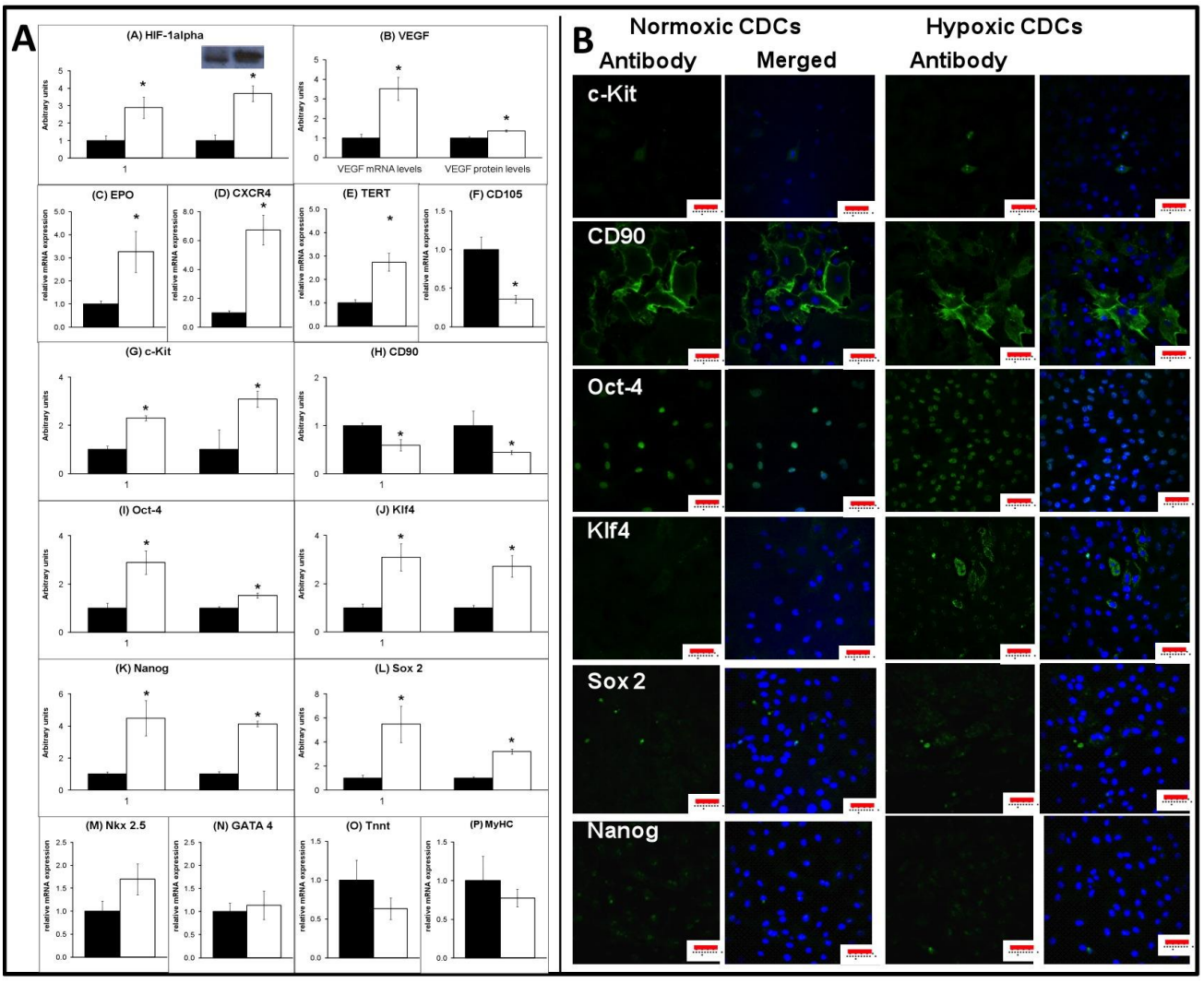

Figure 2. Relative mRNA and protein expression. (A) The relative mRNA of HIF-1α, (B) EPO, (C) VEGF, (D) CXCR 4, (E) TERT, (F) c-Kit, (G) CD90, (H) CD105, (I) Oct-4, (J) Klf-4, (K) Nanog, (L) Sox 2, (M) Nkx 2.5, (N) GATA 4, (O) Troponin T, TnnT2 and (P) myosin heavy chain, MyHC for normoxic P2 CDCs (represented by black boxes) and hypoxic P2 CDCs (represented by white boxes) (n = 3). * $p < 0.01$ vs. normoxic P2 CDCs. (B) Representative confocal images of the DMSO differentiation protocol for the corresponding gene products of A. Scale bars = 20 μm.

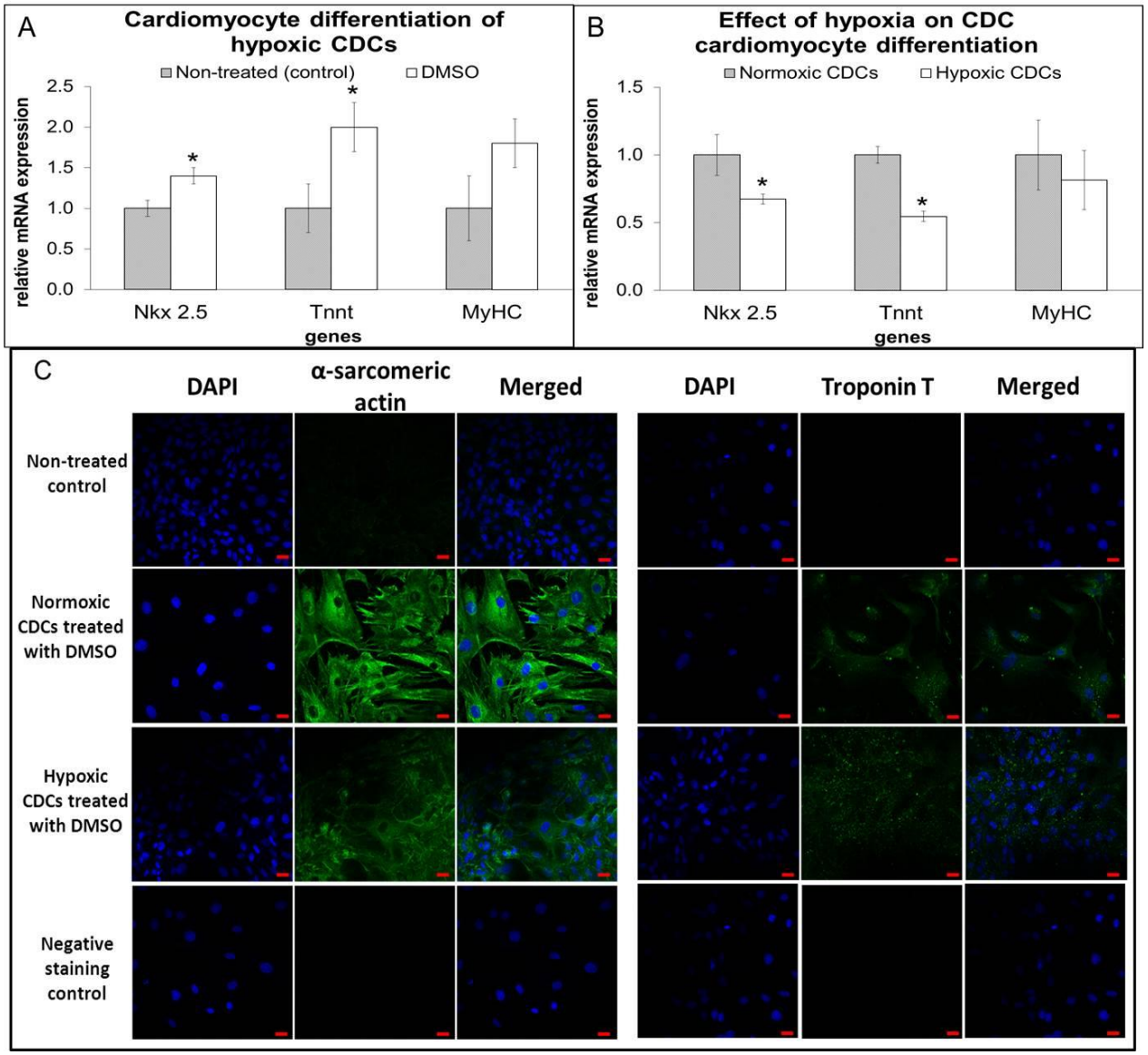

Figure 3. Cardiomyocyte differentiation of P2 CDCs. (A) The relative mRNA expression of Nkx 2.5, TnnT2 and MyHC for non-treated hypoxic CDCs (control) and hypoxic CDCs treated with DMSO for 2 weeks, normalized to non-treated hypoxic CDCs as control. * $p < 0.05$ vs. control. (B) The relative mRNA expression of Nkx 2.5, TnnT2 and MyHC for normoxic and hypoxic P2 CDC (n = 3) after treatment with DMSO for 2 weeks. mRNA expression of hypoxic cells was normalized to the geometric mean of GAPDH and Actb (housekeeping genes) and normoxic cells (calibrator). * $p < 0.05$ vs. normoxia. (C) Representative confocal images of the DMSO differentiation protocol. Scale bars = 20 μm.

Three PHDIs- DMOG, EDBA and BIC were used to mimic hypoxic preconditioning. The toxic effects of PHDIs across a gradient of PHDI drug concentrations chosen from the literature were assessed using the LDH assay over 4 days. An optimal, sub-lethal PHDI treatment for CDCs was chosen. Protein levels of HIF-1α and the HIF-regulated glucose transporter, GLUT-1 in P2 CDCs treated with DMOG, EDBA and BIC in gradient concentrations for 24 hours and 4 days were determined. It was found that HIF-1α activation by DMOG was time and concentration dependent, being maximal after 24 hours of 0.5 mM or 1 mM DMOG treatment but not significantly increased at the highest DMOG concentration (2 mM) or after prolonged treatment (4 days) (**Fig. 4 A(i)**). Similarly, GLUT-1 expression peaked after treatment with 1mM DMOG for 24 hours but decreased after prolonged treatment or at increased concentrations of DMOG (**Fig. 4 B(i)**). With EDBA, HIF-1α protein levels peaked after treatment with 0.5 mM for 24 hours (2.4 ± 0.3-fold), compared with non-treated control cells (**Fig. 4 A(ii)**). GLUT-1 protein expressions was significantly up-regulated in cells treated with 0.1 mM EDBA (3.3 ± 0.3-fold), 0.25 mM EDBA (3.4 ± 0.3-fold), and 0.5 mM EDBA (4.0 ± 0.3-fold), compared with the non-treated control cells (Figure 4 B(ii)). As anticipated, no HIF-1α and GLUT-1 protein expression was observed with EDBA treatment at high concentrations and after a prolonged culture period as this had been shown to be toxic to the cells (**Fig. 4 A and B (ii)**). BIC is a specific PHD inhibitor and thus significantly up-regulated both HIF-1α and GLUT-1 at low concentrations (30 μM). Also, due to the non-toxic nature of this drug, CDCs treated with BIC at higher concentrations for 4 days did not show decreased HIF-1α and GLUT-1, compared to non-treated cells (**Fig. 4 B(iii)**). Therefore, treatment for 24 hours with 1 mM DMOG, 0.5 mM EDBA or 30 μM BIC was applied in all the following experiments.

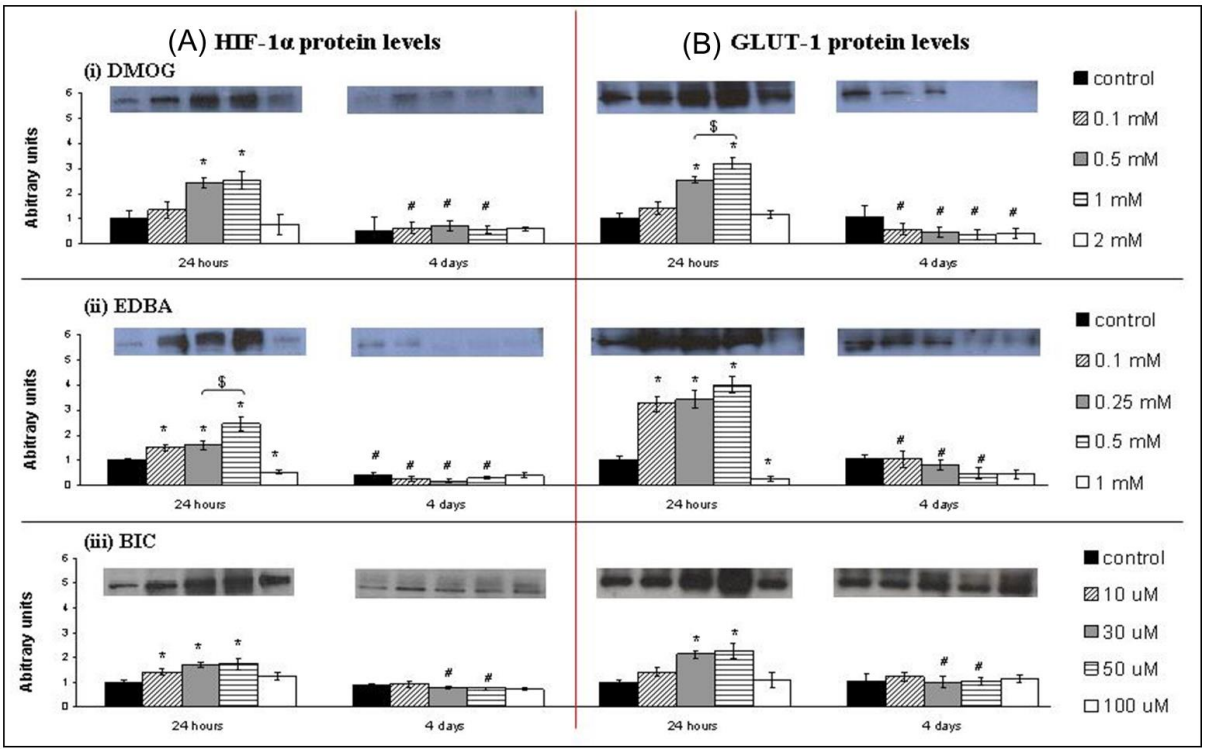

Image 4. Western blot analysis and quantification. Western blot analysis of (A) HIF-1α (left panel) and (B) GLUT-1 (right panel) protein levels in P2 CDCs treated with (i) DMOG, (ii) EDBA and (iii) BIC at a range of concentrations for 24 hours or 4 days (n = 3). Protein levels were expressed in arbitrary units relative to control cells at 24 hours. * $p < 0.05$ vs. control at 24 hours; # $p < 0.05$ vs. corresponding concentration at 24 hours; $ $p < 0.05$ between the two groups indicated.

Adult atrial CDCs were exposed to the three PHDIs for 6, 12, 24, 72 and 120 h and viable cell numbers were counted. PHDI-treatment did not result in a significant increase in CDC proliferation compared with non-treated control cells (**Fig. 5A**) and cell growth stopped after exposure to these PHDIs for 72 h. DMOG, EDBA and BIC treatment increased c-Kit mRNA expression by 1.59 ± 0.17-fold, 1.48 ± 0.16-fold and 1.60 ± 0.17-fold, respectively, compared with non-treated normoxic CDCs (**Fig. 5B**). However, the induction of c-Kit expression by these PHDIs was significantly lower than that induced by hypoxic culture (2.3 ± 0.1-fold, as

shown **Fig. 2A**). CD90 mRNA levels were significantly reduced after treatment with each PHDI, compared with normoxic cells, however only EDBA significantly reduced the expression of CD105 (**Fig. 5B**). Unlike culture under hypoxia, treatment with PHDIs did not significantly increase mRNA levels of Oct-4, Klf 4, Sox 2 and Nanog (data not shown).

DMOG and EDBA treatment significantly increased the mRNA levels of EPO, VEGF and CXCR 4, compared with normoxic CDCs, mimicking the hypoxic-preconditioned CDCs. BIC-treatment resulted in significantly higher EPO levels, compared both with normoxic controls and with DMOG-treated CDCs, but did not induce upregulation of VEGF mRNA (**Fig. 5B**). After induction of cardiomyogenic differentiation of PHDI-treated cells using DMSO, increased protein expression of sarcomeric actin and troponin T indicated that PHDI treatment did not impair the cardiomyocyte differentiation potential of CDCs (**Fig. 5C**).

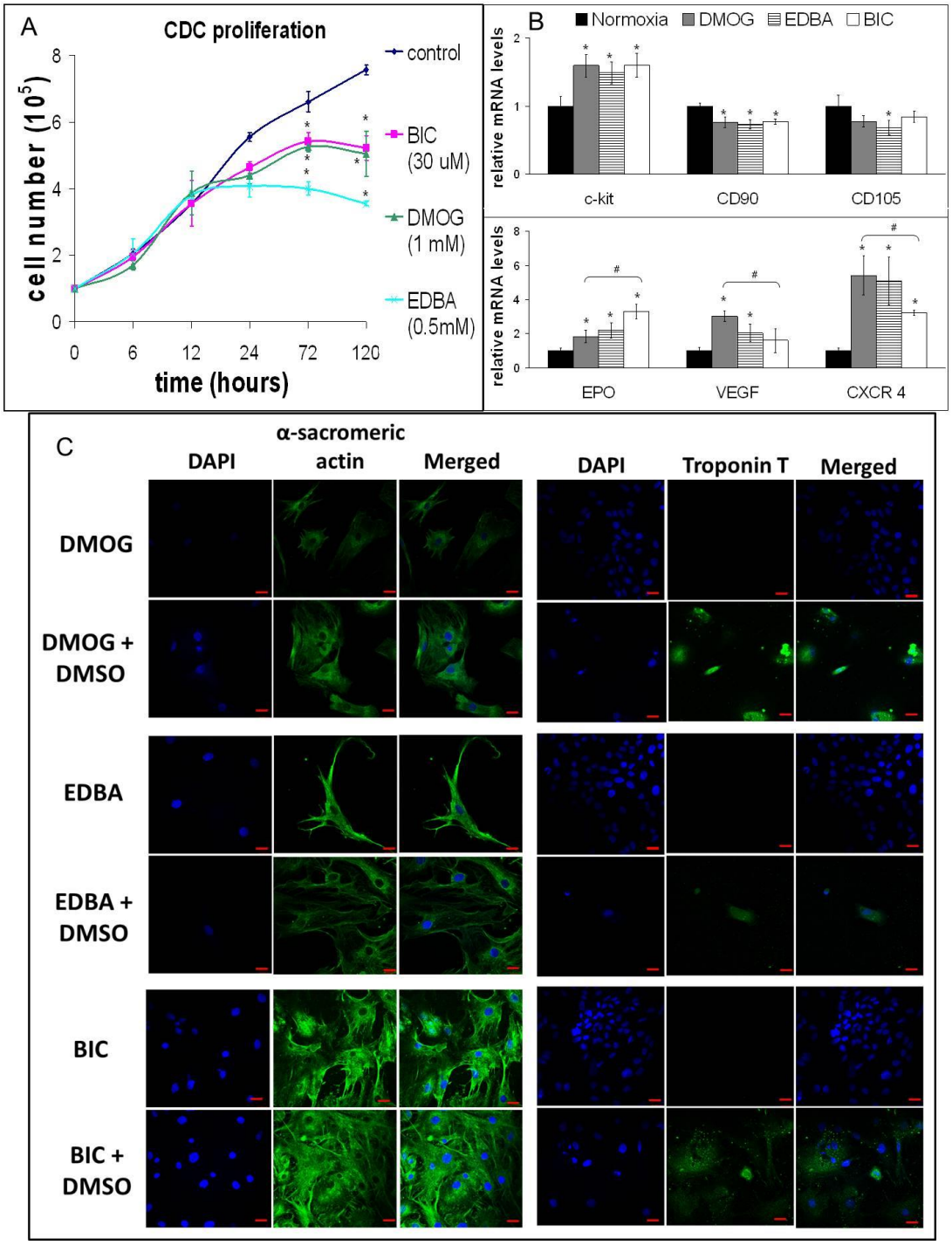

Figure 5. CDC proliferation, gene and protein expression after PHDI treatment and differentiation procedures. (A) PHDI-treated CDC proliferation over 120 h of treatment with 30 μM BIC, 1 mM DMOG and 0.5 mM EDBA (n = 4). All PHDIs significantly reduced cell numbers after prolonged treatment (over 72 h), compared with control. (B) Relative mRNA expression of c-Kit, CD90, CD105, EPO, VEGF and CXCR-4, in non-treated P2 CDCs (control) and CDCs treated with 1 mM DMOG, 0.5 mM EDBA and 30 μM BIC for 24 h (n = 4), normalized to the geometric mean of

GAPDH and Actb (housekeeping genes) and non-treated control cells (calibrator). * $p < 0.05$ vs. control. # $p < 0.05$ between two groups indicated. (C) Representative confocal images (of three independent experiments) of CDCs treated with DMSO, EDBA or BIC for 24 hours, followed by differentiation with DMSO for 2 weeks. An equal number of cells (8×10^5 per chamber) of each condition were trypsinized and seeded on 4-well chamber slides coated with fibronectin (10 μg/mL) and stained with DAPI and α-sarcomeric actin or troponin T. Scale bars = 20 μm.

4.3.2. Optimization of in vivo systems for tracking of CDCs in myocardial infarction models

NPs previously developed and used for limb ischemia models, were explored as a platform to label cells for in vivo tracking and miR delivery, however here NPs are only explored as a tracking platform for CDCs prepared under normoxic and hypoxic culture conditions. CDCs were labelled with NP-170-PFCE with 500 μg/mL for different time points. It was seen that CDCs within 4 h become close to 100% labelled and this does not affect their viability or proliferation (**Fig. 6 A.1 – A.3**). Furthermore the retention of NPs within CDCs was evaluated overtime, in order to establish their retention profile overtime, which can elucidate further issues in the in vivo settings. CDCs were labelled with NPs for 4 hours and then left within cell culture for up to 7 days, overtime up to 30% of the initial NPs was lost during proliferation. CDCs proliferated extensively, much more than the rate at which NPs were lost, this was because CDCs have a large cytoplasm and some cells were extremely overloaded with NPs, meaning that even after many doublings, the daughter cells were retaining a considerably large amount of NPs (**Fig. 6 B.1 – B.2**). When cell division was inhibited by using Mitomycin C, the amount of cells labelled with NPs was constant (**Fig. 6 B.1**).

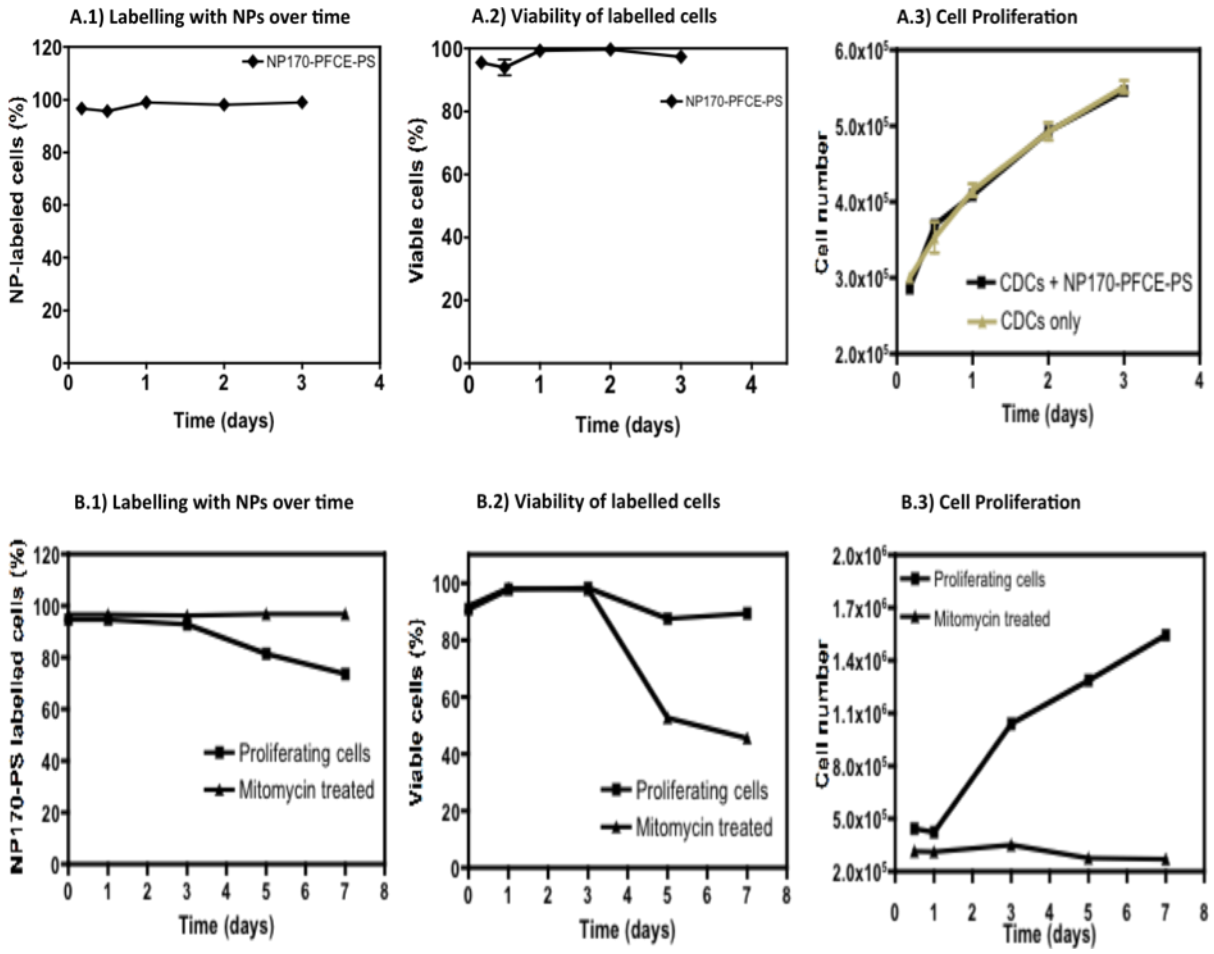

Figure 6- Quantitative assessment of NP uptake in CDCs (A.1 and B.1), viability (A.2 and B.2) and proliferation (A.3 and B.3) by FACS. Cells were incubated with fluorescently labelled NPs for 4 h. After incubation, cells were washed and characterized by FACS. Cell survival was quantified by the Mitotracker CMX-ROS assay, via FACS. Cells positive for Mitrotracker CMX-ROS have mitochondrial activity and thus were considered as live cells. In all plots, results are average ± SD, n=3.

CDCs either under normoxic or hypoxic culture conditions were able to internalise NPs. Even after 2 weeks of culture the NPs were still visible, to a lesser extent in hypoxia. However

under hypoxia CDCs proliferated even more, although they provide the daughter cells with NPs the individual cell NP load was smaller as shown (**Fig. 7**).

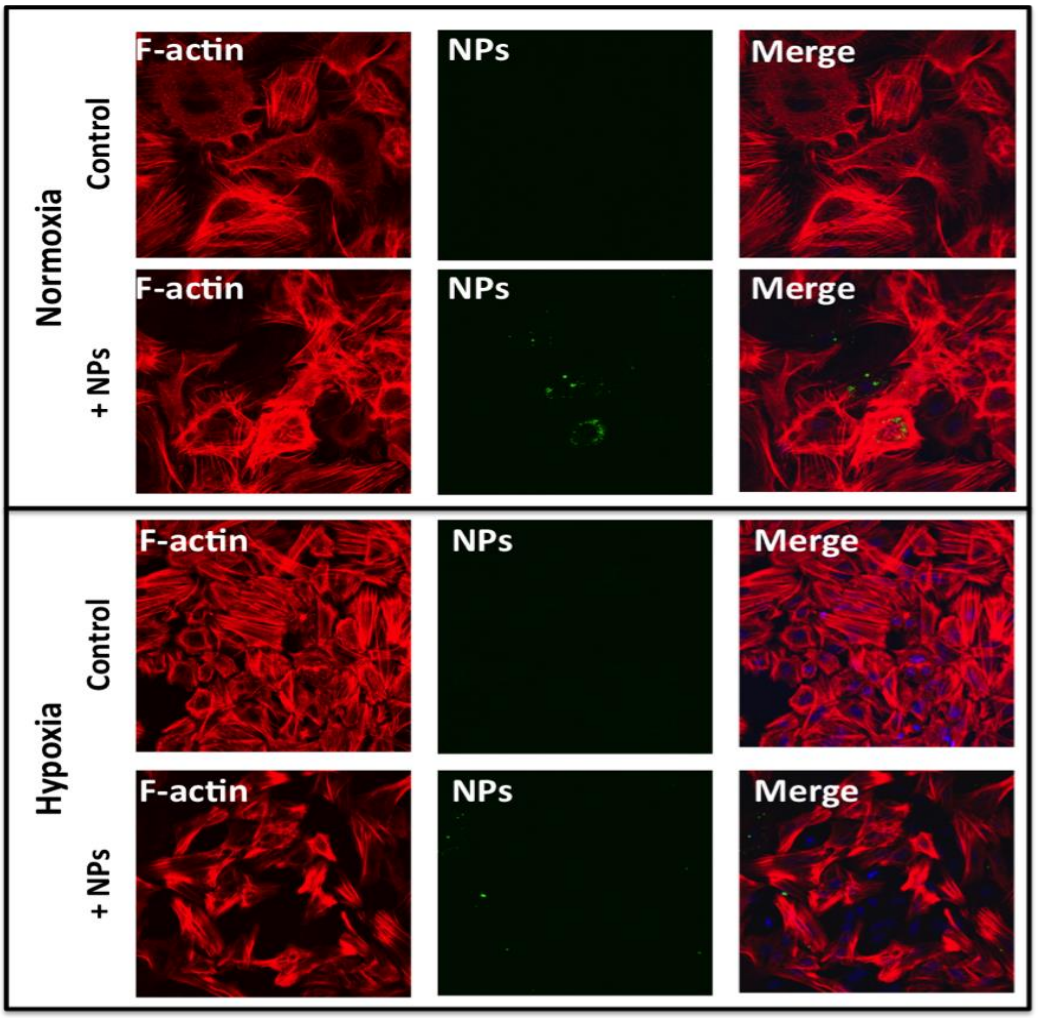

Figure 7. Confocal imaging of CDCs labelled with NP170-PFCE-PS (NPs) under normoxia and hypoxia. CDCs were labelled with NPs (green signal), and probed with rhodamine phalloidin dye for F-actin filament staining two weeks (14 days) after culture.

Next, we evaluate whether the presence of the biomaterial could impair or affect the differentiation of CDCs into cardiomyocyte like cells. CDCs labelled with NPs or not under hypoxia or normoxia were differentiated into cardiomyocyte-like cells following the protocols

described in Methods section. NPs do not affect the patterns of C-kit gene expression in CDCs. Under normoxia or hypoxia, CDCs treated with NPs have similar C-kit gene expression as untreated cells (**Fig. 8A**). Similarly, CDCs treated with NPs have similar expression of Nkx2.5 gene than untreated cells, both in normoxia or hypoxia conditions (**Fig. 8B**). Yet, the cells differentiate into cardiomyocyte-like cells since the expression of Nkx2.5 and TnnT2 genes is higher in differentiative conditions than in control conditions (**Fig. 8C**). In addition, cells express Troponin T at protein level (Fig. 9).

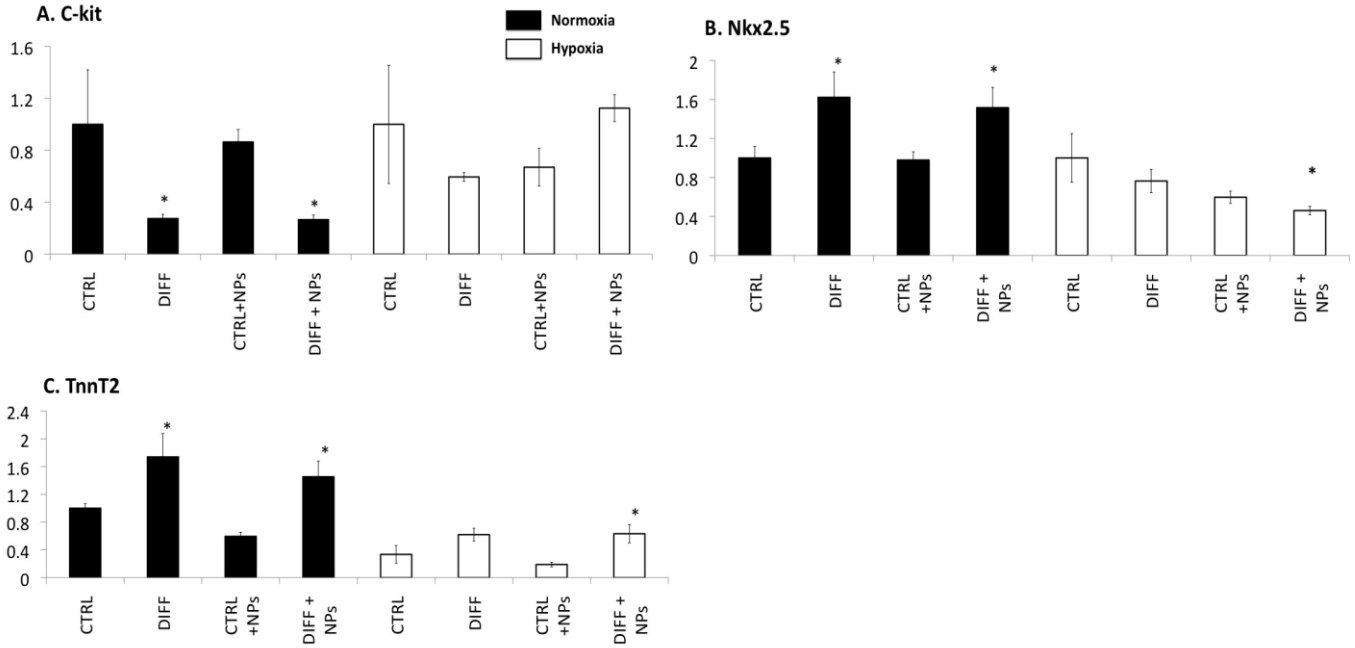

Figure 8. Gene expression on CDCs with or without NPs. The relative mRNA expression (normalised to Beta Actin and GAPDH genes) of C-kit (A), Nkx2.4 (B) and Troponin T, (TnnT2, C) for normoxic P2 CDCs (black boxes) and hypoxic P2 CDCs (white boxes). Prior differentiation (DIFF), some cells were labelled with nanoparticles (NPs) (n=3). * $p < 0.0.1$ (all plots show n=3 ±SD).

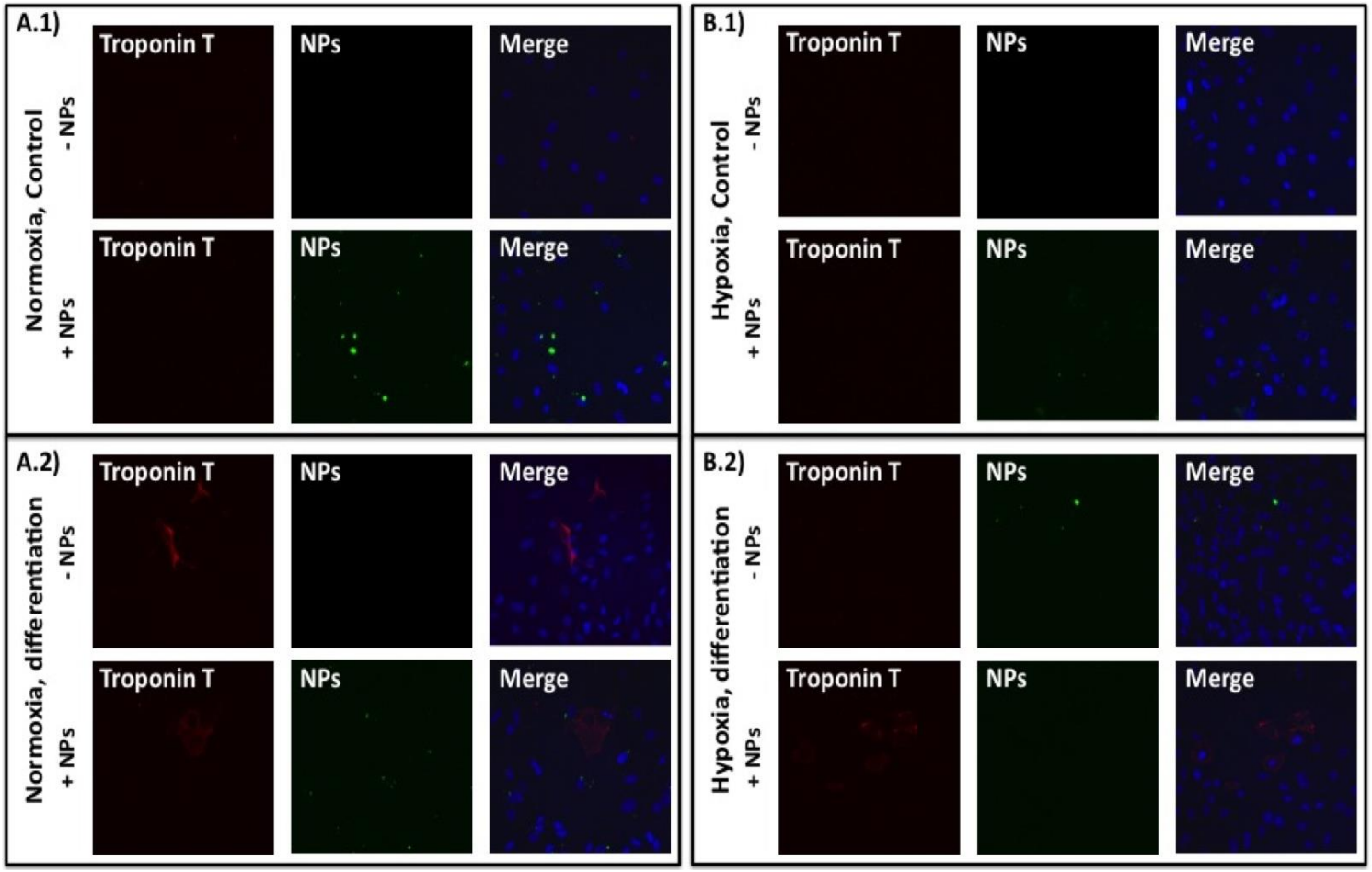

Figure 9- Expression of Troponin T, as assessed by confocal microscopy imaging, in cells differentiated in normoxic or hypoxic conditions in the presence of absence of NPs. Cells were cultured for 20 days under the differentiation protocols previously described.

Next, we investigated whether the NP-labelled cells could be successfully delivered into an *in vivo* model of myocardial infarction. As shown in **Figure 10**, CDCs were successfully labelled with NPs to the extent of attaining very clear images under the ^{19}F channel denoting for the labelled cells with the NPs.

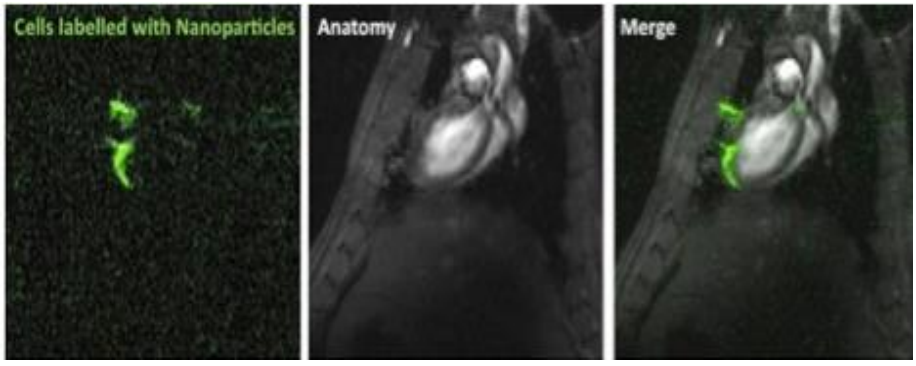

Figure 10- MRI imaging of delivered CDCs. CDCs (20×10^6) were labelled with NPs and delivered in the heart of a rodent model of myocardial infarction. Cardiac gated MRI images on ^{19}F channel show the presence of cells labelled with NPs.

After induction of myocardial infarction, CDCs labelled with NPs were injected into the infarcted area and it was possible to track the cells using ^{19}F MRI for up to 13 days as shown in **Figure 11**. At day 13 it was noted that the ^{19}F signal started to disperse. Here it is shown that suitable protocols and routines where developed so CDCs under normoxia or hypoxia could be labelled with NPs, delivered within in vivo models of cardiac infraction and monitor overtime using MRI.

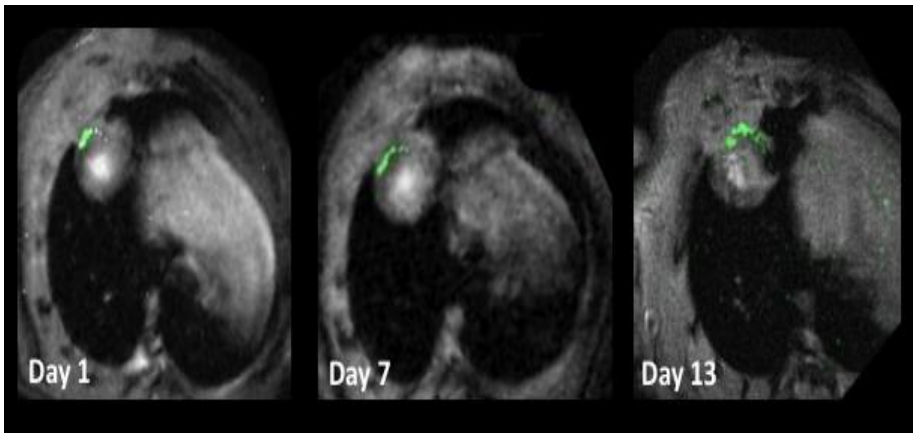

Figure 11- MRI imaging of delivered CDCs. CDCs (20×10^6) were labelled with NPs and delivered in the heart of a rodent model of myocardial infarction. Cardiac gated MRI images on ^{19}F channel show the presence of cells labelled with NPs up to day 13.

4.4. Conclusion

Stem cells reside in niches where they maintain their self-renewal capacity. In order to optimize the therapeutic potential of adult CDCs, cells were preconditioned with low oxygen culture or the prolyl hydroxylase inhibitors, DMOG, EDBA and BIC. Enhanced cell proliferation rates were found for hypoxic EDCs and CDCs under hypoxia, compared with normoxic cells. Further, hypoxic EDCs formed larger cardiospheres, compare with normoxic EDCs, which most likely resulted from rapid proliferation of cardiac stem cells in the core of the sphere [254]. Under hypoxia, cardiospheres showed a significant increase in the expression of vascular endothelial growth factor (VEGF), suggesting that hypoxic pre-treatment would improve the cardiosphere's ability to generate vascular networks [255].

Hypoxic preconditioning successfully increased the expression of c-Kit and reduced that of the mesenchymal markers CD90 and CD105 in the heterogeneous CDC population. In addition, proliferating hypoxic cells maintained expression of pluripotency factors Oct-4, Klf-4, Sox 2 and Nanog, with decreased expression of cardiac genes, in agreement with previous findings [243, 256-258]. Also, hypoxic-preconditioned CDCs showed increased expression of CXCR-4 (~3.2-fold), EPO (~3-fold) and VEGF (~1.5-fold), indicating preconditioning might stimulate stem cell homing and neovascularization in the infarcted myocardium. Implantation of the hypoxic CDCs into the infarcted mouse heart has been shown to result in greater cell engraftment and better functional recovery than treatment with conventionally cultured (normoxic) CDCs [259].

This was the first study using PHDIs to stabilize HIF in CDCs, mimicking the effects of hypoxic cell culture. Simulation of the hypoxic response using PHD inhibitors would remove the necessity for culture in hypoxic incubators, prior to in vivo application of stem cells, provided the beneficial effects of hypoxic culture could be recapitulated pharmacologically. The optimal PHDI treatment

for CDCs, with respect to their negative cytotoxicity effects and optimal potential to activate HIF-1α expression, was found to be 1 mM DMOG, 0.5 mM EDBA or 30 μM BIC for 24 hours. Cell proliferation was not affected by PHDI treatment at these doses. HIF is regulated by dual pathways involving oxygen-dependent prolyl and asparaginyl hydroxylation of its HIF-α subunits. BIC efficiently inhibited the PHD enzyme in CDC culture, but was not able to prevent the FIH enzyme from degrading HIF-α subunits, causing an incomplete activation of HIF.

PHDI-preconditioning using DMOG, EDBA and BIC partly mimicked the effects of hypoxic preconditioning as all three PHDIs significantly stabilized and activated HIF, and therefore induced metabolic changes and up-regulation of important cytokines such as CXCR-4. In addition, all three PHDIs significantly reduced the cardiac mesenchymal cell marker, CD90, and induced the expression of GLUT-1 protein. All PHDIs also were found to have no effect on CDC cardiomyocyte differentiation potential, in contrast to hypoxic CDCs, which showed attenuated cardiomyocyte differentiation after hypoxic preconditioning. Also, whilst DMOG and EDBA-treated CDCs had significantly increased c-Kit, EPO and VEGF mRNA expression, BIC treatment did not increase VEGF mRNA expression. The difference in PHDI effects on CDCs was probably due to the different affinity of the PHDIs to activate the HIF system.

Hypoxic treatment significantly increased the cell proliferation, shortening the time required to obtain adequate cell numbers for therapy, while both hypoxic and PHDI-preconditioning enhanced the therapeutic potential of CDCs by increasing the expression of CXCR-4, EPO and VEGF.

Being able to attain feasible cells numbers in real time is as important as the ability to non-invasively monitor these cells once transplanted *in vivo.* MRI is the most attractive imaging modality to track cells *in vivo* because it provides high-quality 3-dimensional functional and

anatomic information with high contrast [7]. Using this methodology is possible to track cells as they migrate within living tissues such as the heart. MRI combines the chemical sensitivity of nuclear magnetic resonance with high spatial and temporal resolution and therefore provides optimal technical characteristics to track stem cells at the myocardium. Beyond anatomical imaging, MRI has the ability to examine organ functionality and perfusion [164], detect a wide range of biologic information, including flow, motion, morphology and tissue composition.

However, cells need to be labelled with contrast agents before transplantation so that they can be imaged and distinguished from cells of resident tissues. Current labelling methods typically employ superparamagnetic iron oxide nanoparticles (SPIONs) to produce contrast effects in MRI proton images [3]. SPIONs are negative contrast MRI agents composed of an iron oxide core, responsible for the imaging contrast, and a dextran, carboxydextran or starch coating, which inhibits NP aggregation [4, 5]. Gadolinium containing NPs are positive contrast MRI agents, which have gadolinium oxide, Gd_2O_3, at its core, providing high-contrast enhancement in MRI [172]. These NPs are mainly used as a cardiovascular system contrast agent rather than a specific organ or cell marker; nevertheless they may be used for specific cell marking. All these NPs are usually introduced into cells by the use of transfection agents. Intracellular labelling with NPs may present several challenges, including the task of discriminating labelled cells from the image background. Often these methods require image interpretation of subtle contrast or relativity changes in regions believed to contain the cells. Quantification of cell numbers is challenging because several subject-dependent parameters must be determined.

NPs containing fluorine can be an alternative to SPIONs and NPs containing gadolinium since there is no fluorine in the human body, and therefore cells labelled with these NPs can be selectively imaged by ^{19}F MRI [11]. Importantly, the absolute number of labelled cells can be

estimated directly from the *in vivo* ^{19}F images [171] and its viability. Few studies have used fluorine-based nanomaterials to track stem cells, and in all these studies liposome containing fluorine were used. Unfortunately, these liposomes are susceptible to oxidation, aggregation, and have heterogeneous size [260]. As an alternative, poly(lactic-co-glycolic acid) (PLGA) NPs can be used to encapsulate fluorine. These NPs have not been used to label vascular cells, vascular progenitor cells or resident stem cells for cardiac remodelling. Here we show how fluorine-containing NPs can be used to label CDCs, without affecting their viability and proliferative capacity.

The detection threshold for NP-labeled cells is affected by a number of factors, including field strength, signal-to-noise ratio, pulse sequence and acquisition parameters, among others [173, 174]. The minimum detectable dose of cells has been reported to be 1×10^5 for a MRI with 1.5 T of field strength [175], but this number can be affected by differences in hardware, resolution of acquired images, cell type, and uptake of NPs by cells [174].

To the best of our knowledge, no example has been reported so far of the clinical use of NP-labeled stem cells in the myocardial infarction setting. However, there are already examples of the clinical translation of SPION-labeled cells in the context of other cell-based therapies. One study reports SPION labeling of dendritic cells in human patients as cancer vaccines [177]. This approach allowed the assessment of the accuracy of dendritic cell delivery and of inter and intra nodal cell migration patterns. The other reports the use of SPION-labeled neural stem cells for human brain regeneration [178]. Both studies seem to indicate the feasibility of using NP-labelled stem cells in humans.

The use of MRI allows one to accurately deliver the NP labeled stem cells to the infarcted area. This has been demonstrated for the catheter delivery of skeletal muscle-derived mesenchymal

progenitor cells (1×10^8) labeled with SPIONs to the anterior left ventricle myocardium in pigs [179]. The cells and the heart were imaged under a 1.5T MRI. A similar strategy has been adopted for the delivery of bone marrow aspirate (1 to 2×10^6 cells) at the periphery of the infarcted myocardium of a porcine model [180]. The use of MRI, labeled stem cells and catheters allow efficient and safe cell delivery into myocardial segments under direct and live imaging. The use of NP-labeled stem cells and MRI makes it possible to monitor cell survival after transplantation. Rat bone marrow mesenchymal stem cells labeled with SPIONs (1.25×10^5) can successfully be tracked for at least 16 weeks once injected into the myocardium under a 11.7 Tesla MRI [181]. Results showed that the hypointense signal attained from labeled cells on the myocardium decreased every time the animals were imaged (up to week 16), suggesting that the cells were lost or died over time. The loss of exogenous stem cells transplanted at the myocardium has been observed in other studies. The 1.5 T MRI signal of labelled swine mesenchymal stem cells with SPIONs (2.8×10^7 to 1.6×10^8 cells), delivered intra-myocardially into a swine myocardial infarction model, decreased over time [182]. The results suggest that the decrease was due to mesenchymal stem cell death.

The use of labeled cells allows researchers to examine the efficiency of stem cell delivery. For example, bone marrow-derived mesenchymal stem cells (6×10^7) labeled with iridium NPs and delivered intracoronary, intravenously or endocardially at the infarcted heart of pigs show that the intracoronary route was the most efficient. The labeled cells were retained within the myocardium for at least 14 days [183].

We have shown that we can label CDCs under either hypoxia or normoxia and transplant them in a model of rodent myocardial infarction, tracking them for at least 13 days. Unfortunately we were not able to directly quantify the number of cells via the ^{19}F signals, as our spectroscopy channels

were not in tune with the imaging channels. However the goal was to establish methodologies to allow rapid *in vitro* labelling of CDCs without affecting their viability, proliferation and ability to differentiate and transplant them into *in vivo* models, was achieved. Nonetheless, we were still left with two challenges; firstly we need to further develop the simultaneous imaging and spectroscopy sequences so as to using ^{19}F signals simultaneously for tracking and quantification of cell numbers; secondly we need to perfect systems to use ^{19}F to also measure oxygen levels in the imaged areas, as this can be indicative of cell/tissue death/regeneration. At the moment we are able to use the ^{19}F system to track the labelled cells with our NP construct and from cardiac gated imaging calculate left ventricle ejection fraction and correlate any improvement with the presence of the transplanted cells at the site, but not to directly show that they are still viable via *in situ* oxygen measurements.

4.5. Methods

Animals. Sprague Dawley rats were obtained from a commercial breeder (Harlan, Oxon, UK). Animals were kept under controlled conditions for temperature, humidity and light, with water and rat chow available ad libitum. Rats were anaesthetised with sodium pentobarbital (270 mg/kg body weight, IP; Euthatal, Merial, UK) to allow tissue removal. Body and heart weights were routinely recorded. All procedures performed had the necessary UK Home Office and local ethical approval.

Primary cell culture. Isolation and expansion of CDCs. Rat CDCs were cultured as previously described [234, 235]. Briefly adult (4 months) Sprague Dawley rat hearts were excised and heart weight was measured (n = 4). Adult heart atria were cut into two equal portions, which were minced into 1 mm explant tissue fragments in 0.05% trypsin-EDTA (Invitrogen). Digested tissue fragments were plated on fibronectin (Sigma) coated-petri dishes with 2 mL of complete explant medium (CEM) (Iscove's modified Dulbecco medium, IMDM supplemented with 20% foetal bovine serum, FBS) and allocated to two different incubators (Wolf Laboratories, UK) adjustable to different O_2 concentrations by infusion of nitrogen [261]. Normoxic cell culture was set at 21% O_2, whereas hypoxic cell culture was set at 2% O_2, both buffered with 5% CO_2. The O_2 concentration was monitored continuously using an oxygen sensor (Wolf Laboratories, UK). Supporting cells and phase bright cells (collectively known as explant-derived cells, EDC) grown out from the explants were harvested and re-suspended in poly-D-lysine-coated 24 well plates with cardiosphere growth medium, at a density of 3×10^4 cells per well. Cardiospheres were subsequently expanded in CEM on fibronectin-coated tissue culture flasks to generate cardiosphere-derived cells (CDCs), which were maintained in culture with CEM changed every 3 days and passaged every 5 days until passage 2 (P2). All experiments in this study used P2 CDCs at 70 to 80% confluence, unless otherwise stated.

Treatment of cells with PHDIs and cytotoxicity assay. A cytotoxity test across a gradient of PHDI concentrations was carried out to determine the optimal, sublethal PHDI treatment for CDCs. Three PHDIs: DMOG, EDBA and BIC were dissolved in CEM to give final concentrations ranging from 0.01 mM to 2 mM, based on concentrations used previously [262-264]. Cell death was

determined by measuring the concentration of lactate dehydrogenase [263] in cell culture medium using an ABX Pentra 400 Chemistry Analyzer.

Treatment of cells with PHDI at optimal concentrations. For subsequent PHDI experiments, CDCs were treated with 1 mM DMOG, 0.5 mM EDBA and BIC a 100μM for 24 h under normoxia (21% O2).

CDCs differentiation. CDCs were maintained under normoxia or hypoxia for 7 days before cardiomyocyte differentiation was induced using cardiomyocyte differentiation medium (CDM) (2% FBS ESQ (embroyonic stem cell-qualified) (Invitrogen), 1% insulin transferring selenium in IMDM: DMEM/F12; 1:1, Sigma, UK) supplemented with 1 μM dimethylsulfoxide (DMSO). The DMSO supplemented CDM was changed every two days for 6 days. Then, all cells were aspirated with PBS to remove the dead cells and 2 mL CDM supplemented with 50 μL of 1 μM ascorbic acid were added to the plate. The medium was changed every 2 days for the following 6 days before the cells were immunostained with antibodies against cardiac troponin T and α-sarcomeric actin. Protein and RNA were harvested from cell differentiated using CDM only. Negative control cells were treated with CEM for 5 days or 2 weeks, with medium changed every 2 days.

Primer design. Primer pairs were designed using Primer3 software based on interpretation of GenBank or Ensembl Genome Browser. Primer specificity was enhanced by designing a primer pair that flanked the exon-exon border of the gene of interest. Specific cardiac stem cell markers

(c-Kit), pluripotent stem cell markers (Oct-4, Sox 2, Klf-4, and Nanog), cardiac differentiation transcription factors (Nkx 2.5 and GATA 4), matured cardiomyocyte markers (Tnnt and MyHC) and mesenchymal stem cell markers (CD90 and CD105) were designed for CDC characterization. Specific hypoxia target genes such as hypoxia-induced factor-1 alpha (HIF-1α), vascular endothelial growth factor (VEGF), erythropoietin [265] and C-X-C chemokine receptor type 4 (CXCR-4), were designed to investigate the effects of hypoxia on CDC culture (**Table 1**).

Quantitative (real time) reverse transcriptase PCR (qRT-PCR). Total RNA was extracted from cultured cells using Trizol reagent (Sigma) according to the manufacturer's instructions, and treated with Turbo DNA-free (Ambion) to degrade any DNA present. Complementary DNA (cDNA) was synthesized from the RNA template using the AB high capacity transcriptase kit (Applied Biosystem). Real time PCR amplification was performed using the Applied Biosystems StepOnePlus Real-Time PCR System (AB International). After amplification, a melting curve was acquired by heating the product at 4°C/sec to 95°C, cooling it at 4°C/sec to 70°C, keeping it at 70°C for 20 secs, and then slowly heating it at 4°C/sec to 95°C to determine the specificity of PCR products. All qRT-PCR data were normalized to glyceraldehyde 3-phosphate dehydrogenase (GAPDH) and beta actin (Actb) as the reference genes, as previously described [266].

Table 1 – Primer list and details.

No.	Function	Primer	Gene name	Sense primer sequence	Anti-sense primer sequence
1	Markers for pluripotent stem cells	OCT-4 #	POU class 5 homeobox 1 (Pou5f1)	GAGGGATGTGGTTCGAGTGT	CCAGAGCAGTGACAGGAACA
2		Sox-2 #	SRY (sex determining region Y)-box 2	CACAACTCGGAGATCAGCAA	CTCCGGGAAGCGTGTACTTA
3		Klf-4 #	Kruppel-like factor 4	CCACAGACCTGGAAAGTGGT	GGAAGACGAGGATGAAGCTG
4		Nanog #	Homeobox protein NANOG	TACCTCAGCCTCCAGCAGAT	AGGCCGTTGCTAGTCTTCAA
5	Cardiac stem cell marker	c-Kit*	Stem cell factor cytokine receptor	AATCCGACAACCAAAGCAAC	TGACATCAGAGTTGGACACCA
6	Involved in stem cell homing to infarcted heart	CXCR-4	chemokine receptor type 4	GCTACCTTGCCATTGTCCAC	ACATCGGCGAAGATGATGTC
7	Early cardiac transcription markers	Nkx 2.5*	Homeobox protein NKX2-5	CATTTTATCCGCGAGCCTAC	GTCTGTCTCGGCTTTGTCCA
8		GATA 4	GATA binding protein 4	CAGTCCTGCACAGCCTACCT	CCGCAGTTGACACACTCTCT

No.	Function	Primer	Gene name	Sense primer sequence	Anti-sense primer sequence
9	Markers of mature cardiomyocyte	Tnnt 2	Troponin T type 2 (cardiac)	CGTATTCGCAATGAACGAGA	CTGTTCTCCTCCTCCTCACG
10		MyHC	Myosin heavy chain	TATGAGACGGACGCCATACA	CTCCAGAGAGGAGCACTTGG
11	Markers for mesenchymal cells or fibroblasts	CD90	Thy-1 cell surface antigen	CAGAATCCCACAAGCTCCAA	GCCAGGAAGTGTTTTGAACC
12		CD105	Endoglin	GGTACAGTGCATCGACATGG	GCTGGCCTAGCTCTATGGTG
13	Hypoxia induced transcription factor	HIF-1α	Hypoxia induced factor-1 alpha	GGTGGATATGTCTGGGTTGAG	TTCAACTGGTTTGAGGACAGA
14	Induce production of red blood cell	EPO	Erythropoietin	CCAGCCACCAGAGAGTCTTC	TGTGAGTGTTCGGAGTGGAG
15	Stimulate vasculogenesis and angiogenesis	VEGF-α*	vascular endothelial growth factor A	AATGATGAAGCCCTGGAGTG	ATGCTGCAGGAAGCTCATCT
16	Catalytic subunit of the enzyme telomerase	TERT #	telomerase reverse transcriptase	AGTGGTGAACTTCCCTGTGG	CAACCGCAAGACTGACAAGA

No.	Function	Primer	Gene name	Sense primer sequence	Anti-sense primer sequence
17	Housekeeping genes	GAPDH	glyceraldehyde-3-phosphate dehydrogenase	GGGTGTGAACCACGAGAAAT	ACTGTGGTCATGAGCCCTTC
18		Actb	Beta-actin	CTAAGGCCAACCGTGAAAAG	AACACAGCCTGGATGGCTAC
20	Encodes acidic ribosomal phosphoprotein. Used as housekeeping gene in telomere length measurement assay.	36β4	acidic ribosomal phosphoprotein	ACTGGTCTAGGACCCGAGAAG	TCAATGGTGCCTCTGGAGATT

* Exon sequences browsed using Ensembl Genome Browser; others were browsed using GenBank Genome Browser.

Primer sequences were kindly provided by Dr. Georgina M. Ellison

Western Blot analyses. A total of 50 μg of protein extracted from normoxic, hypoxic and PHDI-treated CDCs using lysis buffer containing protease inhibitors (Sigma), was subjected to immunoblot assay with anti-HIF-1α (1:2000, Novus), anti-HIF-2α (1:1000, Novus), anti-HIF-1α hydroxyl-Asn803 (1:4000, kindly provided by Ya-Min Tian, University of Oxford), anti-GLUT-1 (1:1000, Abcam) and anti-citrate synthase, CISY11-A (1:2000, Apha Diagnostic) as previously described [267]. Protein loading and transfer were confirmed by Ponceau S staining (Sigma), and protein levels were related to internal standards to ensure homogeneity between samples and gels. Bands were quantified using UN-SCAN-IT gel software (Silk Scientific, USA), and all samples were run in duplicate on separate gels to confirm results.

Immunocytochemistry. Conditioned CDCs were grown on Nunc Lab-Tek® 4-well chamber slides pre-coated with 10 μg/mL fibronectin and fixed with 4% (w/v) paraformaldehyde (Sigma, UK) for 10 minutes on ice. Fixed cells were blocked with 10% (v/v) donkey serum (Biosera, UK) in 0.1% (v/v) PBS-Tween for an hour at room temperature and then incubated with the anti-cardiac troponin I (cTnI) (1:100, Abcam) and anti-α-sacromeric actin (1:100, Abcam) primary antibodies diluted in PBS, overnight at 4^{o}C in a humidified chamber. Cells were then incubated with donkey anti-goat lgG-FITC (AF488) and the immunefluorescence detected using a confocal microscope (Zeiss Confocal LSM 700).

CDCs labelling with NP170 and viability overtime. CDCs (P2) were incubated for 4 h (unless stated differently, as in the time titration for optimal labelling, labelling times consisted of 4 h, 12 h, 1 day, 2 days and 3 days) in IMDM medium with 2% (v/v) FBS containing 500 μg/mL or no NPs. After 4 h, cells were washed with PBS three times. Cells were then incubated with mitotracker red CMX-ROS at 50 nM for 15 min at 37^{0}C in a CO_2 incubator.

Cells were later trypsinized with 0.2% (w/v) trypsin solution, centrifuged at 1300 rpm for 5 minutes, and fixed with 4% paraformaldehyde for 10 min at room temperature. After fixation they were re-washed and then re-suspended in 500 μL of PBS, ready for FACS analysis. The samples were run on FACS Calibur and analyzed on Cell Quest. 80,000 events were gated.

Differentiation of NP170 labelled cells. After incubation with NP170 (the control condition did not receive NP170), CDCs underwent differentiation under normoxic conditions only as described before.

Rodent model of myocardial infarction. The left anterior descending [268] coronary artery of female SD rats (200–250 g) was occluded using the method of Michael et al [269]. In brief, following anaesthesia, using 2% isoflurane in O_2, and thoracotamy, the pericardium was removed and a 5-0 prolene suture placed under the LAD, about 2 mm from the origin. The suture was tied, occluding the LAD, CDCs (10×10^6 cells in 50 μL of PBS) were injected over four sites in the peri-infarct region and the chest was closed.

Cardiac MRI for $^{19}F/^{1}H$ in purpose built coil and cradle. Animals were anaesthetized with 2.5% isoflurane in O_2 and positioned supine in a purpose built cradle, as shown in Figure 11, courtesy of Dr Daniel Stuckey, University of Oxford & Imperial College.

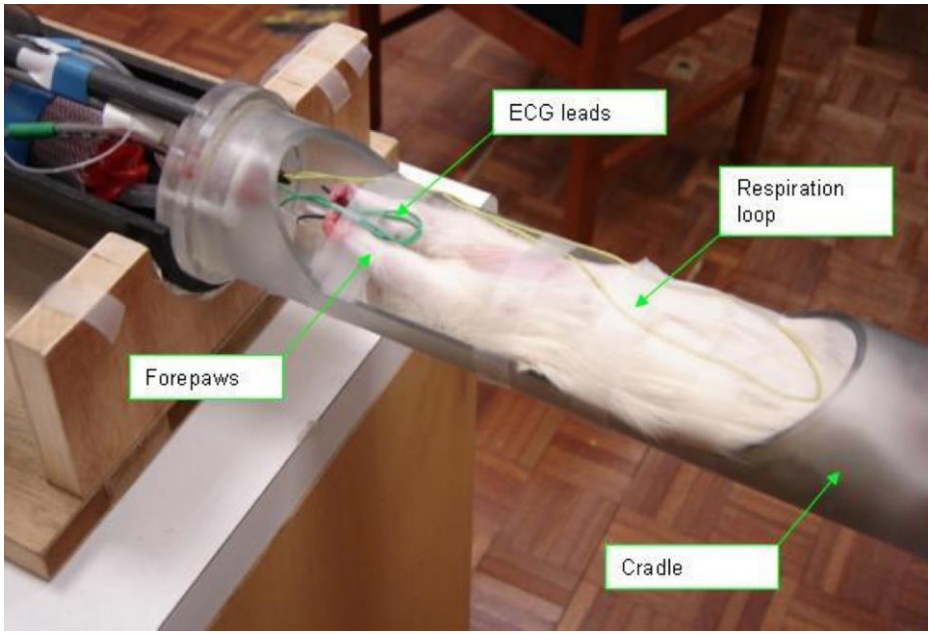

Figure 11- Purpose built cradle. Schematic drawing of the purpose built cradle, courtesy of Dr Daniel Stuckey.

ECG electrodes were inserted into the forepaws and a respiration loop was taped across the chest. The cradle was placed into a horizontal bore 7T MR system with a Varian console and 60 mm birdcage coil. ECG and respiration trigger levels were adjusted so acquisitions were triggered at the same point in the cardiac cycle. Scout images were acquired to determine the position of the heart. A long axis image (Figure 12) was planned from a stack of 6 axial images (Figure 12A-B show slice 1 and 6), and then another long axis image was acquired perpendicular to the first (Figure 12C). A true short axis image was planned from both long axis images (Figure 12D). The coil was tuned and matched between ^{19}F and ^{1}H and shim coils were used to homogenize the magnetic field across the heart. Contiguous 1.5 mm short axis, ECG and respiration gated cine images (field of view 40 mm^2, matrix size 256x256, echo time/repetition time (TE/TR) 1.43/4.6 ms, 17.5° pulse, 25-35 frames per cardiac cycle) were acquired to cover the entire left ventricle.

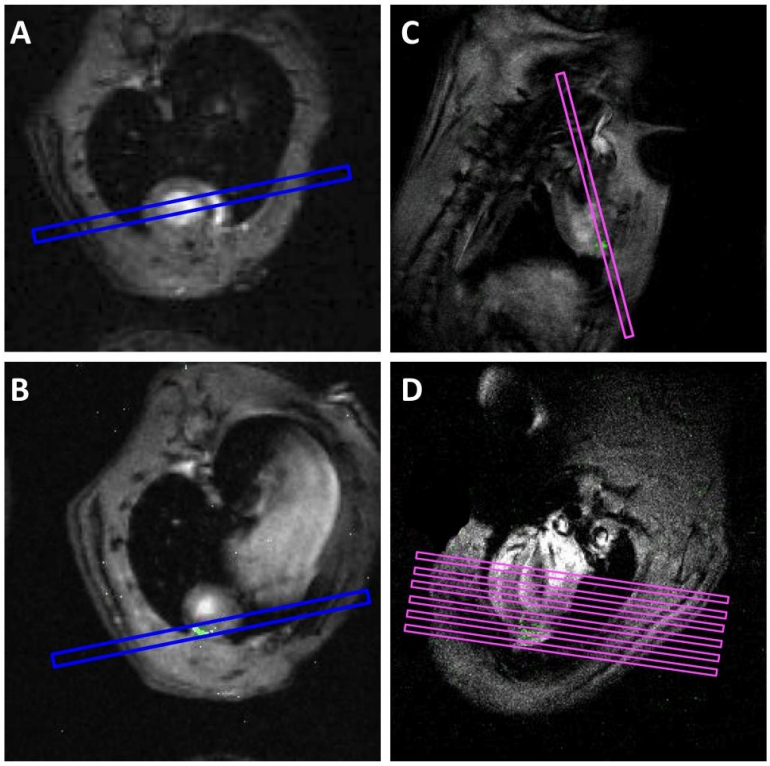

Figure 12- Axis planning. A long axis image was planned from a stack of 6 images (A-B, showing slice 1 and 6), and then another long axis image was acquired perpendicular to the first (C). A true short axis image was planned from both long axis images and imaged the entire left ventricle (D).

Statistical analysis. Data obtained were expressed as mean ± standard error of the mean [95]. All statistical analysis was performed using SPSS software. The statistical differences of measurement made in the same animals were analysed using a paired T-test, whereas multiple comparisons between groups were analysed using a one-way analysis of variance (ANOVA). Repeated Measures ANOVA was performed to compare curves. A Tukey post hoc test was used to analyze statistical difference between groups or curves. A value of $p < 0.05$ was considered statistically significant.

Chapter V

General Conclusions

5. General Conclusions

The development of tools to control cell activity is of utmost importance in Regenerative Medicine. For clinical efficacy, it is required that stem cells or their progenies survive and engraft into the host tissue. Traditional injection methods, widely used in animal models, often result in poor cell survival and low levels of cell integration into host tissue[270]. A significant number of cells die or are lost within hours after transplantation (typically >70 % in few days). Some methodologies have been proposed to augment cell survival including the exposure of donor cells to temperature shock, genetic modification to over-express growth factors, transduction of anti-apoptotic proteins, or preconditioning the cells with pharmacological agents and cytokines (reviewed in references [271, 272]). Despite these advances, the proposed methodologies have shown limited effectiveness [271]. In chapter III, the aim of the work was to develop fluorine-based NPs that could be used to track stem cells or their progenies by MRI and simultaneously deliver biomolecules, namely miRs, to enhance survival and angiogenic activity. The NPs had a fluorinated core to be monitored by MRI. NP170-PFCE, referred to as the NPs, were produced using a single emulsion protocol. These NPs had an effective diameter ranging from 170-218 nm and a negative zeta potential (-9 mV). Once coated with a cationic peptide, protamine sulphate (PS), NPs changed its zeta potential to positive (+7 mV). NP170-PFCE coated with PS also became suitable for biomolecule attachment. Furthermore these NPs were shown to be stable in cell culture media. The NP degradation was notably slow, bellow 20% over 21 days when exposed to both physiological and lysosomal pHs.

Our results show that NP170-PFCE NPs are a good vehicle for miR delivery. We determined that these NPs were able to carry 12μg of miR per mg of NP. We show that HUVECs internalize NP170-PFCE-PS and a significant part of the NPs remained within the early endosomes ($EEA1^+$ organelles, 45%, 24 h) and were not substantially trafficked to late endosomes/lysosomes ($Rab7^+$ organelles, 10%). This lead to the hypothesis that the

accumulation of miR in the endolysomal compartment facilitated the higher pro-survival and pro-angiogenic activities achieved for the delivery of miR132, miR424 and amiR92a by NP170-PFCE-PS not observed by siPORT (the commercial transfection reagent), which accumulated in the cytoplasm. Both miRs and amiRs have the potential to interact with Ago2. Furthermore, the number of Ago foci in the cells was null in the presence of NP170-PFCE-PS only, showing that Ago2 is activated only in the presence or delivery of miR.

A particular innovative aspect of the work of chapter III was to investigate if the accumulation of NPs containing miRs in the endolysosomal compartment could increase the efficacy of the delivered miR. This was the case because the machinery to process the miRNA is located in the membrane of the endolysosomes. Our work also raised hypothesis about the translocation of the miR from the endolysosomal compartment to the cytoplasm. HSP90 and HSP70 chaperones co-localize with miR and Ago2 foci, which suggests their involvement in the recognition and translocation of miR. NP170-PFCE (either by its geometry or protamine coating [198]) are recognized by HSP chaperones while miR is recognized by Ago2. In addition, the higher association with RISC after NP delivery under hypoxia may be related with the up-regulation of HSP chaperones [273], as proposed in the diagram bellow (**Figure 1**).

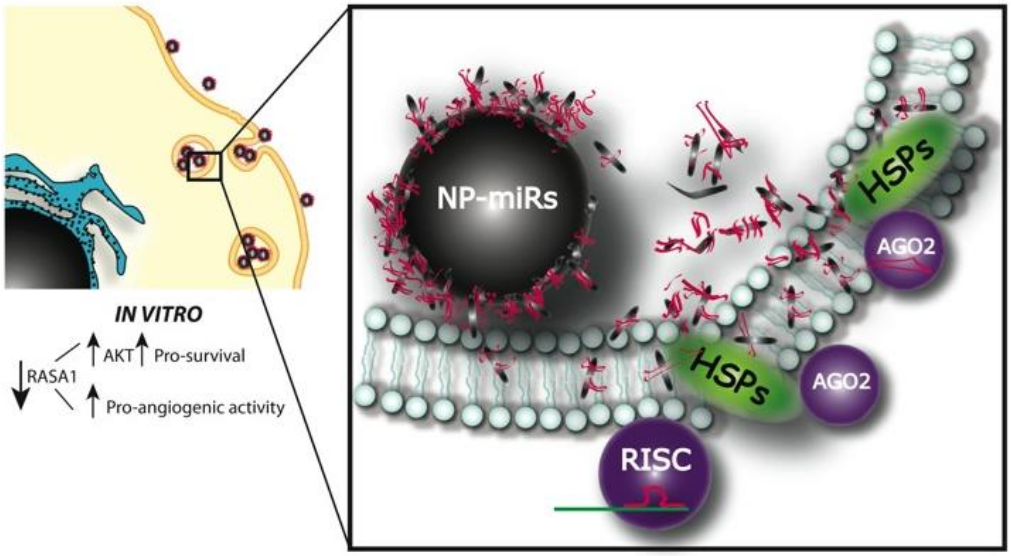

Figure 1. Schematic drawing of NP delivery of miR *in vitro*. miR delivery via NPs recruits higher levels of heat shock proteins (HSPs) which in turn transport miR from the endolysomal compartment to

the cytoplasm, allowing more effective RISC strand invasion for miR. This translates into a down regulation of RASA 1 gene expression which in turns enhance cell survival, via AKT pathway, and angiogenic activity.

Our results show that NPs can be tracked by MRI. MRI coils and imaging sequences have been developed to allow imaging cells labelled with NPs on fluorine and hydrogen frequencies. Unique volume cage coils were built suited for cardiac imaging. Manny validation studies were done at the *in vitro* level and it was clear that with these systems the NPs could be imaged as quickly as in 10 minutes producing high quality images.

Our NP170-PFCE NPs containing miR132 was very effective platform to track and manipulate *in vivo* transplanted cells. After optimisation in mice and rabbit models, we show that the delivery of angiogenic oligonucleotides attached to NPs, via local injection, increased capillary formation relatively to control. Furthermore we could track NPs via MRI over time *in vivo* and we saw no signs of oedema or necrosis, which led to believe that in situ acidity as a result from PLGA degradation, was not an issue. The pilot studies were indicative that we had methodologies for induction of efficient angiogenesis without using viral vectors. These results were validated in a full study in a limb ischemia mouse model where we hoped to ultimately create some regeneration or halt degradation of damaged limbs by the delivery of cells carrying NPs. We showed that the release of miR132 from the NPs increased by 3-fold the survival of ECs transplanted *in vivo* and 3.5-fold the blood perfusion in ischemic limbs relative to control.

Prior to this thesis, although some studies have reported the use of nanoparticles for the delivery of the miR, no study has used a theranostic approach. Therefore, a major contribution of this work was to develop a NP formulation with clinical relevance for *in vivo* cell tracking and miR delivery.

In chapter IV, we have applied our theranostic formulation in the context of cardiac stem cells transplantation. We optimised the expansion of CDCs *in vitro* so as to maximise its potential. It consisted in maintaining constant hypoxia either under hypoxic chambers or via the use of prolyl hydroxylase inhibitors (PHDI). Here it was clear that hypoxia enhances cell proliferation as well as increased retention of pluripotency gene and protein expression. Hypoxic preconditioning increased the expression of c-Kit and reduced mesenchymal markers CD90 and CD105 in the heterogeneous CDC population. In addition, proliferating hypoxic cells maintained expression of pluripotency factors Oct-4, Klf-4, Sox 2 and Nanog, with decreased expression of cardiac genes, in agreement with previous findings [243, 256-258]. Our results further indicate that preconditioning might stimulate stem cell homing and neovascularization in the infarcted myocardium. Hypoxic treatment significantly increased the cell proliferation, shortening the time required to obtain adequate cell numbers for therapy, while both hypoxic and PHDI-preconditioning enhanced the therapeutic potential of CDCs by increasing the expression of CXCR-4, EPO and VEGF. This was the first study using PHDIs to stabilize HIF in CDCs, mimicking the effects of hypoxic cell culture.

Being able to attain feasible cells numbers in real time is as important as the ability to non-invasively monitor these cells once transplanted *in vivo* via MRI. Using MRI it is possible to track cells as they migrate within living tissues such as the heart. However, cells need to be labelled with contrast agents, therefore we used our novel NP construct, NP170-PFCE. We have shown that we can label CDCs under either hypoxia or normoxia and transplant them in a model of rodent myocardial infarction, tracking them for at least 13 days. The labelling of these cells with the NPs did not alter its gene profiling or differentiation capability *in vitro*, therefore was a promising platform for tracking. However this study lacked on data for cell number quantification *in vivo* as our spectroscopy channels were not in tune with the imaging channels on the ^{19}F system that we had developed. Nevertheless our main goal was to establish

methodologies to allow rapid *in vitro* labelling of CDCs without affecting their viability, proliferation and ability to differentiate and transplant them into *in vivo* models. Yet we were still left with two challenges. First, to further develop the simultaneous imaging and spectroscopy sequences so as to using ^{19}F signals simultaneously for tracking and quantification of cell numbers. Second, to optimize our system in order to measure oxygen levels in the imaged areas, as this can be indicative of cell or tissue death and also regeneration.

At the moment we are able to the ^{19}F system to track the labelled cells with our NP construct and from cardiac gated imaging calculate left ventricle ejection fraction and correlate any improvement with the presence of the transplanted cells at the site. Furthermore we can label cells and deliver miRs using these NPs in limb ischemia models and salvage limbs as a consequence of increased cell survival due to intracellular delivery of miRs via NPs.

Chapter VI

Future Work

6. Future Work

6.1. Issues to address from previous work

Although we were able to establish a teranostic platform to deliver miR, creating ne-vascularization and simultaneously allow non-invasive tracking we were still left with two challenges at the imaging level.

The inability to measure oxygen levels in the imaged areas with ^{19}F MRI to determine *in vivo* oxygen levels indicative of regional death or regeneration, and also the incapacity to execute simultaneous imaging and spectroscopy for tracking and quantification of cells.

Modifications are under course to allow *in vivo* determination by modifying coils to do relaxometry targeting echo planar imaging for dynamic oxygen mapping which will allow partial oxygen (pO_2) measurements. The pO_2 value can be calculated by a pixel-by-pixel based method on the quantified ^{19}F R_1 and a priori calibrated ^{19}F R_1–pO_2 curve of hexafluorobenzene (HFB) or another fluorinated compound [274]. To address the issue of sequential imaging and *in vivo* spectroscopy, there is a need to re-design the cage coils to incorporate extra capacitors to increase sensitivity so MRS is performed straight after MRI. There is a need to re-design the electronics systems and the shell of the coils as well as to program and establish more sequences for the ^{19}F imaging.

Work in chapter IV was geared towards *in vivo* tracking of stem cell therapies in the infarcted myocardium where we previously performed trials however using iron oxide nanoparticles and CDCs not optimally cultured, meaning not under hypoxic conditions [78]. From this work, we show that our NP construct is ideal for tracking without affecting cell integrity and its differentiation abilities. Here we lack the experiments where we validate a miR which can

enhance the CDCs survival, to be carried by the NPs and deliver these cells *in vivo* for both tracking and enhancement of cell survival in the infarcted myocardium. In this manner we can perform a full animal study to determine the regional effects of combined stem cells therapy with miR delivery within the infarcted myocardium compared to the controls. In this study the newly developed coils to perform simultaneous ^{19}F MRI and MRS would be used.

6.2. Proposal of new ideas

The CDC therapy reported in here has tremendous potential for preventing heart failure following acute myocardial infarction (AMI), but limited availability of cells and the required numbers for transplant in the injured heart is problematic. Studies have shown that the therapeutic effect of CDCs is largely a paracrine effect, e.g, the cells secrete factors that exert an effect on the surviving heart cells [275]. Paracrine factors are contained in vesicles, exosomes, which are secreted by cells. Exosomes have angiogenic properties when delivered to sites of injury; exosomes from CD34+ cord blood derived cells were shown to have a regenerative effect [276]. Exosome secretion can be stimulated and genetically engineered to express peptide sequences in it outer membrane such as angiotensin receptor 1 peptide (AT1), which would bind to AT1 receptors, expressed in infarcted tissue. Our hypothesis is that the AT1 peptide expression facilitates site-specific homing of the exosomes *in vivo* to the injured heart [277]. Exosomes can be produced in xeno-free conditions to avoid immune complications. However, the current strategy for exosome delivery does not allow *in vivo* non-invasive tracking. Therefore, we are planning to use our NPs to track *in vivo* exosomes. The exosomes will also encapsulate NPs carrying angiogenic miR. The nanoparticles within the exosomes will be tracked in vivo using ^{19}F MRI. This strategy would allow a greater delivery of paracrine factors to the injured tissue that will stimulate rescue of remaining myocytes. I propose to develop a nanoparticle-exosomal complex (NpEx) targeting AT1 and other receptors expressed

in the damaged heart, to deliver miR. The NpEx complex will be tracked *in vivo* using ^{19}F MRI and the cardiac function monitored using *in vivo* cardiac gated ^{1}H MRI.

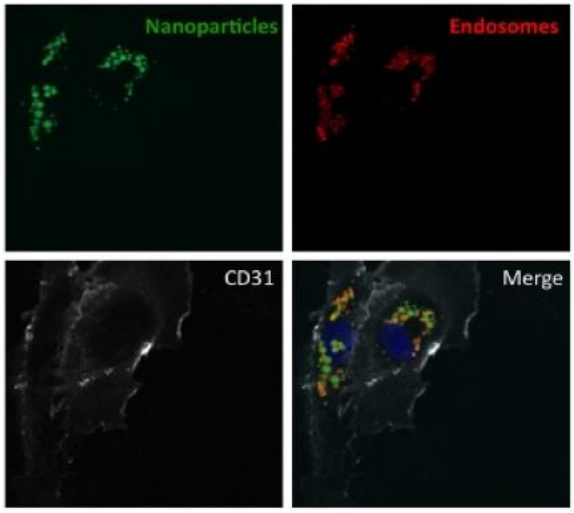

Figure 1 – Confocal images of labelled cells. Image shows ^{19}F NPs internalised by CD34+ differentiate cells into endothelial cells within endosomes shown in red.

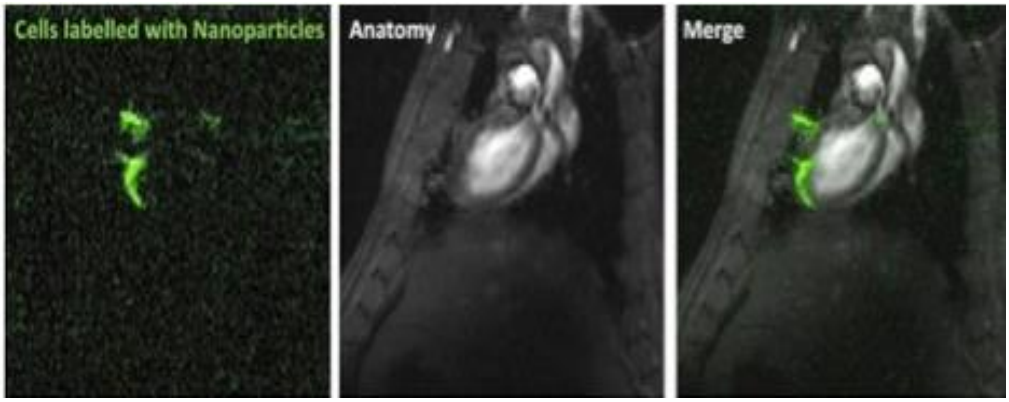

Figure 2- MRI imaging of delivered CDCs. CDCs (20×10^6) were labelled with NPs and delivered in the heart of a rodent model of myocardial infarction. Cardiac gated MRI images on ^{19}F channel show the presence of cells labelled with NPs.

I will address the following research question: **Can the function of the damaged heart be improved using nanoparticle-exosomal (NpEx) complexes?**

I will focus on the following objectives:

1. ***Design of lentiviral constructs for production of exosomal vesicles expressing AT1 peptide*** [277] **-** I will develop a lentiviral construct where the AT1 peptide would be inserted with a fluorescent reporter and a blasticidin resistance motif, which will allow proof of expression of the peptide and make the exosomes fluorescent. In addition other peptide sequences will be exploited and other lentiviral constructs will be made, to explore the most effective exosomal surface recognition system for homing to the damaged heart.

2. **Establishment of a CD34+ progenitor-derived cell line and cardiac stem cell lines infected with the lentiviral constructs -** Cord blood CD34+ progenitor and cardiac stem cells will be collected and infected with the lentivirus. Once infected, selection of the infected cells will be made via blasticidin exposure. The CD34+ cells will be guided towards an endothelial lineage where proliferation and manipulation will be straightforward. Exosomes from CD34+ derived cells will be attained from widely available umbilical cord blood; CD34+ cells are reported to be the sub-population, which holds the greatest regenerative potential for AMI [276]. Cardiac stem cells can be attained from primary culture; human cardiac stem cells extracted from aortic biopsies taken during bypass surgery are also available for manipulation.

3. **Labelling of established cell lines with novel fluorine nanoparticles carrying pro-angiogenic microRNA** Cells will be labelled with our fluorinated NP construct containing pro-angiogenic miRNA. Labelled exosomes (NpEx) will be collected and purified.

4. **Delivery of NpEx complexes to in vivo animal models of AMI (rodent and porcine models)** - Purified NpEx complexes will be delivered to the infarcted myocardium either via infusion or cardiac injection or both. The retention of the NpEx complexes will be recorded, and cardiac function measured, using in vivo cardiac gated MRI at various time points after delivery.

5. **Incorporation of further biochemical tools to verify and enhance results** - The effect of the NpEx complexes from CD34+ progenitor-derived cells and cardiac stem cells will be validated by verifying the expression of markers for neo-angiogenesis and regeneration both at protein and gene level. The signalling cascade by which the NpEx complex acts will be examined.

References

1. Roger, V. L.; Weston, S. A.; Redfield, M. M.; Hellermann-Homan, J. P.; Killian, J.; Yawn, B. P.; Jacobsen, S. J. Trends in heart failure incidence and survival in a community-based population. *JAMA : the journal of the American Medical Association* 2004, 292, 344-50.

2. Epstein, F. H. Cardiovascular disease epidemiology: a journey from the past into the future. *Circulation* 1996, 93, 1755-64.

3. Ferreira, L.; Karp, J. M.; Nobre, L.; Langer, R. New opportunities: the use of nanotechnologies to manipulate and track stem cells. *Cell Stem Cell* 2008, 3, 136-46.

4. Wang, Y. X.; Hussain, S. M.; Krestin, G. P. Superparamagnetic iron oxide contrast agents: physicochemical characteristics and applications in MR imaging. *European radiology* 2001, 11, 2319-31.

5. Reimer, P.; Balzer, T. Ferucarbotran (Resovist): a new clinically approved RES-specific contrast agent for contrast-enhanced MRI of the liver: properties, clinical development, and applications. *European radiology* 2003, 13, 1266-76.

6. Qiu, B.; Yang, X. Molecular MRI of hematopoietic stem-progenitor cells: in vivo monitoring of gene therapy and atherosclerosis. *Nat Clin Pract Cardiovasc Med* 2008, 5, 396-404.

7. Stroh, A.; Faber, C.; Neuberger, T.; Lorenz, P.; Sieland, K.; Jakob, P. M.; Webb, A.; Pilgrimm, H.; Schober, R.; Pohl, E. E.; Zimmer, C. In vivo detection limits of magnetically labeled embryonic stem cells in the rat brain using high-field (17.6 T) magnetic resonance imaging. *Neuroimage* 2005, 24, 635-45.

8. Allport, J. R.; Weissleder, R. In vivo imaging of gene and cell therapies. *Exp Hematol* 2001, 29, 1237-46.

9. Bulte, J. W. Hot spot MRI emerges from the background. *Nat Biotechnol* 2005, 23, 945-6.

10. Flogel, U.; Ding, Z.; Hardung, H.; Jander, S.; Reichmann, G.; Jacoby, C.; Schubert, R.; Schrader, J. In vivo monitoring of inflammation after cardiac and cerebral ischemia by fluorine magnetic resonance imaging. *Circulation* 2008, 118, 140-8.

11. Ahrens, E. T.; Flores, R.; Xu, H.; Morel, P. A. In vivo imaging platform for tracking immunotherapeutic cells. *Nat Biotechnol* 2005, 23, 983-7.

12. Noth, U.; Rodrigues, L. M.; Robinson, S. P.; Jork, A.; Zimmermann, U.; Newell, B.; Griffiths, J. R. In vivo determination of tumor oxygenation during growth and in response to carbogen breathing using 15C5-loaded alginate capsules as fluorine-19 magnetic resonance imaging oxygen sensors. *Int J Radiat Oncol Biol Phys* 2004, 60, 909-19.

13. Partlow, K. C.; Chen, J.; Brant, J. A.; Neubauer, A. M.; Meyerrose, T. E.; Creer, M. H.; Nolta, J. A.; Caruthers, S. D.; Lanza, G. M.; Wickline, S. A. 19F magnetic resonance imaging for stem/progenitor cell tracking with multiple unique perfluorocarbon nanobeacons. *Faseb J* 2007, 21, 1647-54.

14. Heidenreich, P. A.; Trogdon, J. G.; Khavjou, O. A.; Butler, J.; Dracup, K.; Ezekowitz, M. D.; Finkelstein, E. A.; Hong, Y.; Johnston, S. C.; Khera, A.; Lloyd-Jones, D.

M.; Nelson, S. A.; Nichol, G.; Orenstein, D.; Wilson, P. W.; Woo, Y. J. Forecasting the future of cardiovascular disease in the United States: a policy statement from the American Heart Association. *Circulation* 2011, 123, 933-44.

15. Stumpe, K. O. Antihypertensive therapy: new strategies beyond blood pressure control. *Journal of cardiovascular pharmacology* 1992, 20 Suppl 6, S1-4.

16. Unger, T.; Gohlke, P. Converting enzyme inhibitors in cardiovascular therapy: current status and future potential. *Cardiovascular research* 1994, 28, 146-58.

17. Scriabine, A. Beta-adrenoceptor blocking drugs in hypertension. *Annual review of pharmacology and toxicology* 1979, 19, 269-84.

18. Julius, S. Autonomic nervous system dysregulation in human hypertension. *The American journal of cardiology* 1991, 67, 3B-7B.

19. Frishman, W. H.; Landau, A.; Cretkovic, A. Combination drug therapy with calcium-channel blockers in the treatment of systemic hypertension. *Journal of clinical pharmacology* 1993, 33, 752-5.

20. Agabiti-Rosei, E.; Muiesan, M. L.; Rizzoni, D.; Romanelli, G.; Beschi, M.; Castellano, M. Regression of cardiovascular structural changes after long-term antihypertensive treatment with the calcium antagonist nitrendipine. *Journal of cardiovascular pharmacology* 1991, 18 Suppl 5, S5-9.

21. Calcium, calcium antagonism, and structural changes in hypertension. Satellite symposium to the 5th ESH meeting. Milan, June 7, 1991. *Journal of cardiovascular pharmacology* 1992, 19 Suppl 2, S1-62.

22. Pauletto, P.; Sartore, S.; Giuriato, L.; Scatena, M.; Tonello, M.; Scannapieco, G.; Pessina, A. C.; Dal Palu, C. Calcium antagonists and vascular smooth muscle cells in atherogenesis. *Journal of cardiovascular pharmacology* 1992, 19 Suppl 2, S8-16.

23. National Health System, U. K. Treating atherosclerosis http://www.nhs.uk/Conditions/Atherosclerosis/Pages/Treatment.aspx.

24. Beyar, R. High technology in medicine: lessons from cardiovascular innovations and future perspective. *Rambam Maimonides medical journal* 2013, 4, e0009.

25. Grines, C. L.; Watkins, M. W.; Mahmarian, J. J.; Iskandrian, A. E.; Rade, J. J.; Marrott, P.; Pratt, C.; Kleiman, N. A randomized, double-blind, placebo-controlled trial of Ad5FGF-4 gene therapy and its effect on myocardial perfusion in patients with stable angina. *J Am Coll Cardiol* 2003, 42, 1339-47.

26. Hedman, M.; Hartikainen, J.; Syvanne, M.; Stjernvall, J.; Hedman, A.; Kivela, A.; Vanninen, E.; Mussalo, H.; Kauppila, E.; Simula, S.; Narvanen, O.; Rantala, A.; Peuhkurinen, K.; Nieminen, M. S.; Laakso, M.; Yla-Herttuala, S. Safety and feasibility of catheter-based local intracoronary vascular endothelial growth factor gene transfer in the prevention of postangioplasty and in-stent restenosis and in the treatment of chronic myocardial ischemia: phase II results of the Kuopio Angiogenesis Trial (KAT). *Circulation* 2003, 107, 2677-83.

27. Kastrup, J.; Jorgensen, E.; Ruck, A.; Tagil, K.; Glogar, D.; Ruzyllo, W.; Botker, H. E.; Dudek, D.; Drvota, V.; Hesse, B.; Thuesen, L.; Blomberg, P.; Gyongyosi, M.; Sylven, C. Direct intramyocardial plasmid vascular endothelial growth factor-A165 gene therapy in

patients with stable severe angina pectoris A randomized double-blind placebo-controlled study: the Euroinject One trial. *J Am Coll Cardiol* 2005, 45, 982-8.

28. Kusumanto, Y. H.; van Weel, V.; Mulder, N. H.; Smit, A. J.; van den Dungen, J. J.; Hooymans, J. M.; Sluiter, W. J.; Tio, R. A.; Quax, P. H.; Gans, R. O.; Dullaart, R. P.; Hospers, G. A. Treatment with intramuscular vascular endothelial growth factor gene compared with placebo for patients with diabetes mellitus and critical limb ischemia: a double-blind randomized trial. *Hum Gene Ther* 2006, 17, 683-91.

29. Rajagopalan, S.; Mohler, E. R., 3rd; Lederman, R. J.; Mendelsohn, F. O.; Saucedo, J. F.; Goldman, C. K.; Blebea, J.; Macko, J.; Kessler, P. D.; Rasmussen, H. S.; Annex, B. H. Regional angiogenesis with vascular endothelial growth factor in peripheral arterial disease: a phase II randomized, double-blind, controlled study of adenoviral delivery of vascular endothelial growth factor 121 in patients with disabling intermittent claudication. *Circulation* 2003, 108, 1933-8.

30. Makinen, K.; Manninen, H.; Hedman, M.; Matsi, P.; Mussalo, H.; Alhava, E.; Yla-Herttuala, S. Increased vascularity detected by digital subtraction angiography after VEGF gene transfer to human lower limb artery: a randomized, placebo-controlled, double-blinded phase II study. *Mol Ther* 2002, 6, 127-33.

31. Albers, M.; Fratezi, A. C.; De Luccia, N. Assessment of quality of life of patients with severe ischemia as a result of infrainguinal arterial occlusive disease. *Journal of vascular surgery* 1992, 16, 54-9.

32. Gaengel, K.; Genove, G.; Armulik, A.; Betsholtz, C. Endothelial-mural cell signaling in vascular development and angiogenesis. *Arteriosclerosis, thrombosis, and vascular biology* 2009, 29, 630-8.

33. Carmeliet, P. Angiogenesis in life, disease and medicine. *Nature* 2005, 438, 932-6.

34. Coultas, L.; Chawengsaksophak, K.; Rossant, J. Endothelial cells and VEGF in vascular development. *Nature* 2005, 438, 937-45.

35. Presta, M.; Dell'Era, P.; Mitola, S.; Moroni, E.; Ronca, R.; Rusnati, M. Fibroblast growth factor/fibroblast growth factor receptor system in angiogenesis. *Cytokine & growth factor reviews* 2005, 16, 159-78.

36. Fagiani, E.; Christofori, G. Angiopoietins in angiogenesis. *Cancer Lett* 2013, 328, 18-26.

37. Bridges, E.; Oon, C. E.; Harris, A. Notch regulation of tumor angiogenesis. *Future Oncol* 2011, 7, 569-88.

38. Katoh, M.; Katoh, M. WNT signaling pathway and stem cell signaling network. *Clinical cancer research : an official journal of the American Association for Cancer Research* 2007, 13, 4042-5.

39. Katoh, M.; Nakagama, H. FGF Receptors: Cancer Biology and Therapeutics. *Medicinal research reviews* 2013.

40. Dewhirst, M. W.; Cao, Y.; Moeller, B. Cycling hypoxia and free radicals regulate angiogenesis and radiotherapy response. *Nature reviews. Cancer* 2008, 8, 425-37.

41. Clapp, C.; Thebault, S.; Jeziorski, M. C.; Martinez De La Escalera, G. Peptide hormone regulation of angiogenesis. *Physiological reviews* 2009, 89, 1177-215.

42. Murohara, T. Autologous adipose tissue as a new source of progenitor cells for therapeutic angiogenesis. *Journal of cardiology* 2009, 53, 155-63.

43. Lavergne, M.; Vanneaux, V.; Delmau, C.; Gluckman, E.; Rodde-Astier, I.; Larghero, J.; Uzan, G. Cord blood-circulating endothelial progenitors for treatment of vascular diseases. *Cell proliferation* 2011, 44 Suppl 1, 44-7.

44. Asahara, T.; Murohara, T.; Sullivan, A.; Silver, M.; van der Zee, R.; Li, T.; Witzenbichler, B.; Schatteman, G.; Isner, J. M. Isolation of putative progenitor endothelial cells for angiogenesis. *Science* 1997, 275, 964-7.

45. Ott, I.; Keller, U.; Knoedler, M.; Gotze, K. S.; Doss, K.; Fischer, P.; Urlbauer, K.; Debus, G.; von Bubnoff, N.; Rudelius, M.; Schomig, A.; Peschel, C.; Oostendorp, R. A. Endothelial-like cells expanded from CD34+ blood cells improve left ventricular function after experimental myocardial infarction. *FASEB J* 2005, 19, 992-4.

46. Arai, M.; Misao, Y.; Nagai, H.; Kawasaki, M.; Nagashima, K.; Suzuki, K.; Tsuchiya, K.; Otsuka, S.; Uno, Y.; Takemura, G.; Nishigaki, K.; Minatoguchi, S.; Fujiwara, H. Granulocyte colony-stimulating factor: a noninvasive regeneration therapy for treating atherosclerotic peripheral artery disease. *Circulation journal : official journal of the Japanese Circulation Society* 2006, 70, 1093-8.

47. Subramaniyam, V.; Waller, E. K.; Murrow, J. R.; Manatunga, A.; Lonial, S.; Kasirajan, K.; Sutcliffe, D.; Harris, W.; Taylor, W. R.; Alexander, R. W.; Quyyumi, A. A. Bone marrow mobilization with granulocyte macrophage colony-stimulating factor improves endothelial dysfunction and exercise capacity in patients with peripheral arterial disease. *American heart journal* 2009, 158, 53-60 e1.

48. van Royen, N.; Schirmer, S. H.; Atasever, B.; Behrens, C. Y.; Ubbink, D.; Buschmann, E. E.; Voskuil, M.; Bot, P.; Hoefer, I.; Schlingemann, R. O.; Biemond, B. J.; Tijssen, J. G.; Bode, C.; Schaper, W.; Oskam, J.; Legemate, D. A.; Piek, J. J.; Buschmann, I. START Trial: a pilot study on STimulation of ARTeriogenesis using subcutaneous application of granulocyte-macrophage colony-stimulating factor as a new treatment for peripheral vascular disease. *Circulation* 2005, 112, 1040-6.

49. Shantsila, E.; Watson, T.; Lip, G. Y. Endothelial progenitor cells in cardiovascular disorders. *J Am Coll Cardiol* 2007, 49, 741-52.

50. Duong Van Huyen, J. P.; Smadja, D. M.; Bruneval, P.; Gaussem, P.; Dal-Cortivo, L.; Julia, P.; Fiessinger, J. N.; Cavazzana-Calvo, M.; Aiach, M.; Emmerich, J. Bone marrow-derived mononuclear cell therapy induces distal angiogenesis after local injection in critical leg ischemia. *Modern pathology : an official journal of the United States and Canadian Academy of Pathology, Inc* 2008, 21, 837-46.

51. Higashi, Y.; Kimura, M.; Hara, K.; Noma, K.; Jitsuiki, D.; Nakagawa, K.; Oshima, T.; Chayama, K.; Sueda, T.; Goto, C.; Matsubara, H.; Murohara, T.; Yoshizumi, M. Autologous bone-marrow mononuclear cell implantation improves endothelium-dependent vasodilation in patients with limb ischemia. *Circulation* 2004, 109, 1215-8.

52. Ishida, A.; Ohya, Y.; Sakuda, H.; Ohshiro, K.; Higashiuesato, Y.; Nakaema, M.; Matsubara, S.; Yakabi, S.; Kakihana, A.; Ueda, M.; Miyagi, C.; Yamane, N.; Koja, K.; Komori, K.; Takishita, S. Autologous peripheral blood mononuclear cell implantation for

patients with peripheral arterial disease improves limb ischemia. *Circulation journal : official journal of the Japanese Circulation Society* 2005, 69, 1260-5.

53. Motukuru, V.; Suresh, K. R.; Vivekanand, V.; Raj, S.; Girija, K. R. Therapeutic angiogenesis in Buerger's disease (thromboangiitis obliterans) patients with critical limb ischemia by autologous transplantation of bone marrow mononuclear cells. *Journal of vascular surgery* 2008, 48, 53S-60S; discussion 60S.

54. Ruiz-Salmeron, R.; de la Cuesta-Diaz, A.; Constantino-Bermejo, M.; Perez-Camacho, I.; Marcos-Sanchez, F.; Hmadcha, A.; Soria, B. Angiographic demonstration of neoangiogenesis after intra-arterial infusion of autologous bone marrow mononuclear cells in diabetic patients with critical limb ischemia. *Cell Transplant* 2011, 20, 1629-39.

55. Van Tongeren, R. B.; Hamming, J. F.; Fibbe, W. E.; Van Weel, V.; Frerichs, S. J.; Stiggelbout, A. M.; Van Bockel, J. H.; Lindeman, J. H. Intramuscular or combined intramuscular/intra-arterial administration of bone marrow mononuclear cells: a clinical trial in patients with advanced limb ischemia. *The Journal of cardiovascular surgery* 2008, 49, 51-8.

56. Walter, D. H.; Krankenberg, H.; Balzer, J. O.; Kalka, C.; Baumgartner, I.; Schluter, M.; Tonn, T.; Seeger, F.; Dimmeler, S.; Lindhoff-Last, E.; Zeiher, A. M. Intraarterial administration of bone marrow mononuclear cells in patients with critical limb ischemia: a randomized-start, placebo-controlled pilot trial (PROVASA). *Circulation. Cardiovascular interventions* 2011, 4, 26-37.

57. Lara-Hernandez, R.; Lozano-Vilardell, P.; Blanes, P.; Torreguitart-Mirada, N.; Galmes, A.; Besalduch, J. Safety and efficacy of therapeutic angiogenesis as a novel treatment in patients with critical limb ischemia. *Annals of vascular surgery* 2010, 24, 287-94.

58. Leistner, D. M.; Fischer-Rasokat, U.; Honold, J.; Seeger, F. H.; Schachinger, V.; Lehmann, R.; Martin, H.; Burck, I.; Urbich, C.; Dimmeler, S.; Zeiher, A. M.; Assmus, B. Transplantation of progenitor cells and regeneration enhancement in acute myocardial infarction (TOPCARE-AMI): final 5-year results suggest long-term safety and efficacy. *Clinical research in cardiology : official journal of the German Cardiac Society* 2011, 100, 925-34.

59. Traverse, J. H.; Henry, T. D.; Vaughan, D. E.; Ellis, S. G.; Pepine, C. J.; Willerson, J. T.; Zhao, D. X.; Piller, L. B.; Penn, M. S.; Byrne, B. J.; Perin, E. C.; Gee, A. P.; Hatzopoulos, A. K.; McKenna, D. H.; Forder, J. R.; Taylor, D. A.; Cogle, C. R.; Olson, R. E.; Jorgenson, B. C.; Sayre, S. L.; Vojvodic, R. W.; Gordon, D. J.; Skarlatos, S. I.; Moye, L. A.; Simari, R. D. Rationale and design for TIME: A phase II, randomized, double-blind, placebo-controlled pilot trial evaluating the safety and effect of timing of administration of bone marrow mononuclear cells after acute myocardial infarction. *American heart journal* 2009, 158, 356-63.

60. Traverse, J. H.; Henry, T. D.; Ellis, S. G.; Pepine, C. J.; Willerson, J. T.; Zhao, D. X.; Forder, J. R.; Byrne, B. J.; Hatzopoulos, A. K.; Penn, M. S.; Perin, E. C.; Baran, K. W.; Chambers, J.; Lambert, C.; Raveendran, G.; Simon, D. I.; Vaughan, D. E.; Simpson, L. M.; Gee, A. P.; Taylor, D. A.; Cogle, C. R.; Thomas, J. D.; Silva, G. V.; Jorgenson, B. C.; Olson, R. E.; Bowman, S.; Francescon, J.; Geither, C.; Handberg, E.; Smith, D. X.; Baraniuk, S.; Piller, L. B.; Loghin, C.; Aguilar, D.; Richman, S.; Zierold, C.; Bettencourt, J.; Sayre, S. L.; Vojvodic, R. W.; Skarlatos, S. I.; Gordon, D. J.; Ebert, R. F.; Kwak, M.; Moye, L. A.; Simari, R. D. Effect of intracoronary delivery of autologous bone marrow mononuclear cells 2 to 3 weeks following acute myocardial infarction on left ventricular function: the LateTIME randomized trial. *JAMA : the journal of the American Medical Association* 2011, 306, 2110-9.

61. Jeevanantham, V.; Butler, M.; Saad, A.; Abdel-Latif, A.; Zuba-Surma, E. K.; Dawn, B. Adult bone marrow cell therapy improves survival and induces long-term improvement in cardiac parameters: a systematic review and meta-analysis. *Circulation* 2012, 126, 551-68.

62. Perin, E. C.; Willerson, J. T.; Pepine, C. J.; Henry, T. D.; Ellis, S. G.; Zhao, D. X.; Silva, G. V.; Lai, D.; Thomas, J. D.; Kronenberg, M. W.; Martin, A. D.; Anderson, R. D.; Traverse, J. H.; Penn, M. S.; Anwaruddin, S.; Hatzopoulos, A. K.; Gee, A. P.; Taylor, D. A.; Cogle, C. R.; Smith, D.; Westbrook, L.; Chen, J.; Handberg, E.; Olson, R. E.; Geither, C.; Bowman, S.; Francescon, J.; Baraniuk, S.; Piller, L. B.; Simpson, L. M.; Loghin, C.; Aguilar, D.; Richman, S.; Zierold, C.; Bettencourt, J.; Sayre, S. L.; Vojvodic, R. W.; Skarlatos, S. I.; Gordon, D. J.; Ebert, R. F.; Kwak, M.; Moye, L. A.; Simari, R. D. Effect of transendocardial delivery of autologous bone marrow mononuclear cells on functional capacity, left ventricular function, and perfusion in chronic heart failure: the FOCUS-CCTRN trial. *JAMA : the journal of the American Medical Association* 2012, 307, 1717-26.

63. Losordo, D. W.; Henry, T. D.; Davidson, C.; Sup Lee, J.; Costa, M. A.; Bass, T.; Mendelsohn, F.; Fortuin, F. D.; Pepine, C. J.; Traverse, J. H.; Amrani, D.; Ewenstein, B. M.; Riedel, N.; Story, K.; Barker, K.; Povsic, T. J.; Harrington, R. A.; Schatz, R. A. Intramyocardial, autologous CD34+ cell therapy for refractory angina. *Circ Res* 2011, 109, 428-36.

64. Kandala, J.; Upadhyay, G. A.; Pokushalov, E.; Wu, S.; Drachman, D. E.; Singh, J. P. Meta-analysis of stem cell therapy in chronic ischemic cardiomyopathy. *The American journal of cardiology* 2013, 112, 217-25.

65. Friedenstein, A. J.; Chailakhyan, R. K.; Latsinik, N. V.; Panasyuk, A. F.; Keiliss-Borok, I. V. Stromal cells responsible for transferring the microenvironment of the hemopoietic tissues. Cloning in vitro and retransplantation in vivo. *Transplantation* 1974, 17, 331-40.

66. Dominici, M.; Le Blanc, K.; Mueller, I.; Slaper-Cortenbach, I.; Marini, F.; Krause, D.; Deans, R.; Keating, A.; Prockop, D.; Horwitz, E. Minimal criteria for defining multipotent mesenchymal stromal cells. The International Society for Cellular Therapy position statement. *Cytotherapy* 2006, 8, 315-7.

67. Caplan, A. I. Why are MSCs therapeutic? New data: new insight. *The Journal of pathology* 2009, 217, 318-24.

68. Matthay, M. A.; Goolaerts, A.; Howard, J. P.; Lee, J. W. Mesenchymal stem cells for acute lung injury: preclinical evidence. *Critical care medicine* 2010, 38, S569-73.

69. Mei, S. H.; Haitsma, J. J.; Dos Santos, C. C.; Deng, Y.; Lai, P. F.; Slutsky, A. S.; Liles, W. C.; Stewart, D. J. Mesenchymal stem cells reduce inflammation while enhancing bacterial clearance and improving survival in sepsis. *American journal of respiratory and critical care medicine* 2010, 182, 1047-57.

70. Boyle, A. J.; McNiece, I. K.; Hare, J. M. Mesenchymal stem cell therapy for cardiac repair. *Methods Mol Biol* 2010, 660, 65-84.

71. Mohyeddin-Bonab, M.; Mohamad-Hassani, M. R.; Alimoghaddam, K.; Sanatkar, M.; Gasemi, M.; Mirkhani, H.; Radmehr, H.; Salehi, M.; Eslami, M.; Farhig-Parsa, A.; Emami-Razavi, H.; Alemohammad, M. G.; Solimani, A. A.; Ghavamzadeh, A.; Nikbin, B. Autologous in vitro expanded mesenchymal stem cell therapy for human old myocardial infarction. *Archives of Iranian medicine* 2007, 10, 467-73.

72. Yang, Z.; Zhang, F.; Ma, W.; Chen, B.; Zhou, F.; Xu, Z.; Zhang, Y.; Zhang, D.; Zhu, T.; Wang, L.; Wang, H.; Ding, Z.; Zhang, Y. A novel approach to transplanting bone marrow stem cells to repair human myocardial infarction: delivery via a noninfarct-relative artery. *Cardiovascular therapeutics* 2010, 28, 380-5.

73. Lalu, M. M.; McIntyre, L.; Pugliese, C.; Fergusson, D.; Winston, B. W.; Marshall, J. C.; Granton, J.; Stewart, D. J. Safety of cell therapy with mesenchymal stromal cells (SafeCell): a systematic review and meta-analysis of clinical trials. *PloS one* 2012, 7, e47559.

74. Beltrami, A. P.; Barlucchi, L.; Torella, D.; Baker, M.; Limana, F.; Chimenti, S.; Kasahara, H.; Rota, M.; Musso, E.; Urbanek, K.; Leri, A.; Kajstura, J.; Nadal-Ginard, B.; Anversa, P. Adult cardiac stem cells are multipotent and support myocardial regeneration. *Cell* 2003, 114, 763-76.

75. Messina, E.; De Angelis, L.; Frati, G.; Morrone, S.; Chimenti, S.; Fiordaliso, F.; Salio, M.; Battaglia, M.; Latronico, M. V.; Coletta, M.; Vivarelli, E.; Frati, L.; Cossu, G.; Giacomello, A. Isolation and expansion of adult cardiac stem cells from human and murine heart. *Circ Res* 2004, 95, 911-21.

76. Dawn, B.; Stein, A. B.; Urbanek, K.; Rota, M.; Whang, B.; Rastaldo, R.; Torella, D.; Tang, X. L.; Rezazadeh, A.; Kajstura, J.; Leri, A.; Hunt, G.; Varma, J.; Prabhu, S. D.; Anversa, P.; Bolli, R. Cardiac stem cells delivered intravascularly traverse the vessel barrier, regenerate infarcted myocardium, and improve cardiac function. *Proc Natl Acad Sci U S A* 2005, 102, 3766-71.

77. Anversa, P.; Nadal-Ginard, B. Myocyte renewal and ventricular remodelling. *Nature* 2002, 415, 240-3.

78. Carr, C. A.; Stuckey, D. J.; Tan, J. J.; Tan, S. C.; Gomes, R. S.; Camelliti, P.; Messina, E.; Giacomello, A.; Ellison, G. M.; Clarke, K. Cardiosphere-derived cells improve function in the infarcted rat heart for at least 16 weeks-an MRI study. *PloS one* 2011, 6, e25669.

79. Chugh, A. R.; Beache, G. M.; Loughran, J. H.; Mewton, N.; Elmore, J. B.; Kajstura, J.; Pappas, P.; Tatooles, A.; Stoddard, M. F.; Lima, J. A.; Slaughter, M. S.; Anversa, P.; Bolli, R. Administration of cardiac stem cells in patients with ischemic cardiomyopathy: the SCIPIO trial: surgical aspects and interim analysis of myocardial function and viability by magnetic resonance. *Circulation* 2012, 126, S54-64.

80. Makkar, R. R.; Smith, R. R.; Cheng, K.; Malliaras, K.; Thomson, L. E.; Berman, D.; Czer, L. S.; Marban, L.; Mendizabal, A.; Johnston, P. V.; Russell, S. D.; Schuleri, K. H.; Lardo, A. C.; Gerstenblith, G.; Marban, E. Intracoronary cardiosphere-derived cells for heart regeneration after myocardial infarction (CADUCEUS): a prospective, randomised phase 1 trial. *Lancet* 2012, 379, 895-904.

81. Tallini, Y. N.; Greene, K. S.; Craven, M.; Spealman, A.; Breitbach, M.; Smith, J.; Fisher, P. J.; Steffey, M.; Hesse, M.; Doran, R. M.; Woods, A.; Singh, B.; Yen, A.; Fleischmann, B. K.; Kotlikoff, M. I. c-kit expression identifies cardiovascular precursors in the neonatal heart. *Proc Natl Acad Sci U S A* 2009, 106, 1808-13.

82. Andersen, D. C.; Andersen, P.; Schneider, M.; Jensen, H. B.; Sheikh, S. P. Murine "cardiospheres" are not a source of stem cells with cardiomyogenic potential. *Stem Cells* 2009, 27, 1571-81.

83. Williams, A. R.; Hatzistergos, K. E.; Addicott, B.; McCall, F.; Carvalho, D.; Suncion, V.; Morales, A. R.; Da Silva, J.; Sussman, M. A.; Heldman, A. W.; Hare, J. M. Enhanced effect of combining human cardiac stem cells and bone marrow mesenchymal stem cells to reduce infarct size and to restore cardiac function after myocardial infarction. *Circulation* 2013, 127, 213-23.

84. Tan JJ, C. C., Stuckey DJ, Ellison GM, Messina E, Giacomello A, Clarke K. Isolation and Expansion of Cardiosphere-Derived Stem Cells. *Curr. Protoc. Stem Cell Biol.* 2011, 16:2C.3.1-2C.3.12.

85. Oh, H.; Chi, X.; Bradfute, S. B.; Mishina, Y.; Pocius, J.; Michael, L. H.; Behringer, R. R.; Schwartz, R. J.; Entman, M. L.; Schneider, M. D. Cardiac muscle plasticity in adult and embryo by heart-derived progenitor cells. *Ann N Y Acad Sci* 2004, 1015, 182-9.

86. Tang, Y. L.; Shen, L.; Qian, K.; Phillips, M. I. A novel two-step procedure to expand cardiac Sca-1+ cells clonally. *Biochem Biophys Res Commun* 2007, 359, 877-83.

87. Mohyeldin, A.; Garzon-Muvdi, T.; Quinones-Hinojosa, A. Oxygen in stem cell biology: a critical component of the stem cell niche. *Cell Stem Cell* 2010, 7, 150-61.

88. Holzwarth, C.; Vaegler, M.; Gieseke, F.; Pfister, S. M.; Handgretinger, R.; Kerst, G.; Muller, I. Low physiologic oxygen tensions reduce proliferation and differentiation of human multipotent mesenchymal stromal cells. *BMC cell biology* 2010, 11, 11.

89. Bae, D.; Mondragon-Teran, P.; Hernandez, D.; Ruban, L.; Mason, C.; Bhattacharya, S. S.; Veraitch, F. S. Hypoxia enhances the generation of retinal progenitor cells from human induced pluripotent and embryonic stem cells. *Stem Cells Dev* 2012, 21, 1344-55.

90. Yoshida, Y.; Takahashi, K.; Okita, K.; Ichisaka, T.; Yamanaka, S. Hypoxia enhances the generation of induced pluripotent stem cells. *Cell Stem Cell* 2009, 5, 237-41.

91. Eliasson, P.; Jonsson, J. I. The hematopoietic stem cell niche: low in oxygen but a nice place to be. *Journal of cellular physiology* 2010, 222, 17-22.

92. Lee, E. Y.; Xia, Y.; Kim, W. S.; Kim, M. H.; Kim, T. H.; Kim, K. J.; Park, B. S.; Sung, J. H. Hypoxia-enhanced wound-healing function of adipose-derived stem cells: increase in stem cell proliferation and up-regulation of VEGF and bFGF. *Wound repair and regeneration : official publication of the Wound Healing Society [and] the European Tissue Repair Society* 2009, 17, 540-7.

93. Kim, J. H.; Park, S. H.; Park, S. G.; Choi, J. S.; Xia, Y.; Sung, J. H. The pivotal role of reactive oxygen species generation in the hypoxia-induced stimulation of adipose-derived stem cells. *Stem Cells Dev* 2011, 20, 1753-61.

94. Khan, N. A.; Hemmelgarn, B.; Padwal, R.; Larochelle, P.; Mahon, J. L.; Lewanczuk, R. Z.; McAlister, F. A.; Rabkin, S. W.; Hill, M. D.; Feldman, R. D.; Schiffrin, E. L.; Campbell, N. R.; Logan, A. G.; Arnold, M.; Moe, G.; Campbell, T. S.; Milot, A.; Stone, J. A.; Jones, C.; Leiter, L. A.; Ogilvie, R. I.; Herman, R. J.; Hamet, P.; Fodor, G.; Carruthers, G.; Culleton, B.; Burns, K. D.; Ruzicka, M.; deChamplain, J.; Pylypchuk, G.; Gledhill, N.; Petrella, R.; Boulanger, J. M.; Trudeau, L.; Hegele, R. A.; Woo, V.; McFarlane, P.; Touyz, R. M.; Tobe, S. W. The 2007 Canadian Hypertension Education Program recommendations for the management of hypertension: part 2 - therapy. *The Canadian journal of cardiology* 2007, 23, 539-50.

95. Semenza, G. L.; Wang, G. L. A nuclear factor induced by hypoxia via de novo protein synthesis binds to the human erythropoietin gene enhancer at a site required for transcriptional activation. *Mol Cell Biol* 1992, 12, 5447-54.

96. Tian, Y. M.; Yeoh, K. K.; Lee, M. K.; Eriksson, T.; Kessler, B. M.; Kramer, H. B.; Edelmann, M. J.; Willam, C.; Pugh, C. W.; Schofield, C. J.; Ratcliffe, P. J. Differential sensitivity of HIF hydroxylation sites to hypoxia and hydroxylase inhibitors. *J Biol Chem*.

97. Asikainen, T. M.; Ahmad, A.; Schneider, B. K.; Ho, W. B.; Arend, M.; Brenner, M.; Gunzler, V.; White, C. W. Stimulation of HIF-1alpha, HIF-2alpha, and VEGF by prolyl 4-hydroxylase inhibition in human lung endothelial and epithelial cells. *Free Radic Biol Med* 2005, 38, 1002-13.

98. Lewin, M.; Carlesso, N.; Tung, C. H.; Tang, X. W.; Cory, D.; Scadden, D. T.; Weissleder, R. Tat peptide-derivatized magnetic nanoparticles allow in vivo tracking and recovery of progenitor cells. *Nat Biotechnol* 2000, 18, 410-4.

99. Lisy, K.; Peet, D. J. Turn me on: regulating HIF transcriptional activity. *Cell Death Differ* 2008, 15, 642-9.

100. Chowdhury, R.; Hardy, A.; Schofield, C. J. The human oxygen sensing machinery and its manipulation. *Chem Soc Rev* 2008, 37, 1308-19.

101. Ross, R. Atherosclerosis--an inflammatory disease. *The New England journal of medicine* 1999, 340, 115-26.

102. Endemann, D. H.; Schiffrin, E. L. Endothelial dysfunction. *Journal of the American Society of Nephrology : JASN* 2004, 15, 1983-92.

103. Nakagawa, M.; Naruko, T.; Ikura, Y.; Komatsu, R.; Iwasa, Y.; Kitabayashi, C.; Inoue, T.; Itoh, A.; Yoshiyama, M.; Ueda, M. A decline in platelet activation and inflammatory cell infiltration is associated with the phenotypic redifferentiation of neointimal smooth muscle cells after bare-metal stent implantation in acute coronary syndrome. *Journal of atherosclerosis and thrombosis* 2010, 17, 675-87.

104. Hassan, W.; Dong, Y.; Wang, W. Encapsulation and 3D culture of human adipose-derived stem cells in an in-situ crosslinked hybrid hydrogel composed of PEG-based hyperbranched copolymer and hyaluronic acid. *Stem cell research & therapy* 2013, 4, 32.

105. Nagahama, R.; Matoba, T.; Nakano, K.; Kim-Mitsuyama, S.; Sunagawa, K.; Egashira, K. Nanoparticle-mediated delivery of pioglitazone enhances therapeutic neovascularization in a murine model of hindlimb ischemia. *Arteriosclerosis, thrombosis, and vascular biology* 2012, 32, 2427-34.

106. Prokoph, S.; Chavakis, E.; Levental, K. R.; Zieris, A.; Freudenberg, U.; Dimmeler, S.; Werner, C. Sustained delivery of SDF-1alpha from heparin-based hydrogels to attract circulating pro-angiogenic cells. *Biomaterials* 2012, 33, 4792-800.

107. Elcin, Y. M.; Dixit, V.; Gitnick, G. Controlled release of endothelial cell growth factor from chitosan-albumin microspheres for localized angiogenesis: in vitro and in vivo studies. *Artificial cells, blood substitutes, and immobilization biotechnology* 1996, 24, 257-71.

108. Simon-Yarza, T.; Tamayo, E.; Benavides, C.; Lana, H.; Formiga, F. R.; Grama, C. N.; Ortiz-de-Solorzano, C.; Kumar, M. N.; Prosper, F.; Blanco-Prieto, M. J. Functional

benefits of PLGA particulates carrying VEGF and CoQ in an animal of myocardial ischemia. *Int J Pharm* 2013.

109. Chen, L.; He, Z.; Chen, B.; Yang, M.; Zhao, Y.; Sun, W.; Xiao, Z.; Zhang, J.; Dai, J. Loading of VEGF to the heparin cross-linked demineralized bone matrix improves vascularization of the scaffold. *J Mater Sci Mater Med* 2010, 21, 309-17.

110. Sheridan, M. H.; Shea, L. D.; Peters, M. C.; Mooney, D. J. Bioabsorbable polymer scaffolds for tissue engineering capable of sustained growth factor delivery. *J Control Release* 2000, 64, 91-102.

111. Chen, J.; Tian, H.; Dong, X.; Guo, Z.; Jiao, Z.; Li, F.; Kano, A.; Maruyama, A.; Chen, X. Effective Tumor Treatment by VEGF siRNA Complexed with Hydrophobic Poly(Amino Acid)-Modified Polyethylenimine. *Macromol Biosci* 2013.

112. Egilmez, N. K.; Jong, Y. S.; Sabel, M. S.; Jacob, J. S.; Mathiowitz, E.; Bankert, R. B. In situ tumor vaccination with interleukin-12-encapsulated biodegradable microspheres: induction of tumor regression and potent antitumor immunity. *Cancer Res* 2000, 60, 3832-7.

113. Mullerad, J.; Cohen, S.; Benharroch, D.; Apte, R. N. Local delivery of IL-1 alpha polymeric microspheres for the immunotherapy of an experimental fibrosarcoma. *Cancer investigation* 2003, 21, 720-8.

114. Sabel, M. S.; Skitzki, J.; Stoolman, L.; Egilmez, N. K.; Mathiowitz, E.; Bailey, N.; Chang, W. J.; Chang, A. E. Intratumoral IL-12 and TNF-alpha-loaded microspheres lead to regression of breast cancer and systemic antitumor immunity. *Annals of surgical oncology* 2004, 11, 147-56.

115. van de Weert, M.; Hennink, W. E.; Jiskoot, W. Protein instability in poly(lactic-co-glycolic acid) microparticles. *Pharm Res* 2000, 17, 1159-67.

116. Ekholm, M.; Hietanen, J.; Lindqvist, C.; Rautavuori, J.; Santavirta, S.; Suuronen, R. Histological study of tissue reactions to epsilon-caprolactone-lactide copolymer in paste form. *Biomaterials* 1999, 20, 1257-62.

117. Cleland, J. L.; Duenas, E. T.; Park, A.; Daugherty, A.; Kahn, J.; Kowalski, J.; Cuthbertson, A. Development of poly-(D,L-lactide--coglycolide) microsphere formulations containing recombinant human vascular endothelial growth factor to promote local angiogenesis. *J Control Release* 2001, 72, 13-24.

118. Kim, T. K.; Burgess, D. J. Pharmacokinetic characterization of 14C-vascular endothelial growth factor controlled release microspheres using a rat model. *The Journal of pharmacy and pharmacology* 2002, 54, 897-905.

119. Zhu, G.; Mallery, S. R.; Schwendeman, S. P. Stabilization of proteins encapsulated in injectable poly (lactide- co-glycolide). *Nat Biotechnol* 2000, 18, 52-7.

120. Ding, A. G.; Schwendeman, S. P. Acidic microclimate pH distribution in PLGA microspheres monitored by confocal laser scanning microscopy. *Pharm Res* 2008, 25, 2041-52.

121. Jiang, W.; Schwendeman, S. P. Stabilization and controlled release of bovine serum albumin encapsulated in poly(D, L-lactide) and poly(ethylene glycol) microsphere blends. *Pharm Res* 2001, 18, 878-85.

122. Lavelle, E. C.; Yeh, M. K.; Coombes, A. G.; Davis, S. S. The stability and immunogenicity of a protein antigen encapsulated in biodegradable microparticles based on blends of lactide polymers and polyethylene glycol. *Vaccine* 1999, 17, 512-29.

123. Hans, F. P.; Moser, M.; Bode, C.; Grundmann, S. MicroRNA regulation of angiogenesis and arteriogenesis. *Trends Cardiovasc Med* 2010, 20, 253-62.

124. Bartel, D. P. MicroRNAs: target recognition and regulatory functions. *Cell* 2009, 136, 215-33.

125. Treiber, T.; Treiber, N.; Meister, G. Regulation of microRNA biogenesis and function. *Thromb Haemost* 2012, 107, 605-10.

126. Yang, J. S.; Lai, E. C. Alternative miRNA biogenesis pathways and the interpretation of core miRNA pathway mutants. *Molecular cell* 2011, 43, 892-903.

127. Baek, D.; Villen, J.; Shin, C.; Camargo, F. D.; Gygi, S. P.; Bartel, D. P. The impact of microRNAs on protein output. *Nature* 2008, 455, 64-71.

128. Ebert, M. S.; Sharp, P. A. Roles for microRNAs in conferring robustness to biological processes. *Cell* 2012, 149, 515-24.

129. Osella, M.; Bosia, C.; Cora, D.; Caselle, M. The role of incoherent microRNA-mediated feedforward loops in noise buffering. *PLoS computational biology* 2011, 7, e1001101.

130. Suarez, Y.; Sessa, W. C. MicroRNAs as novel regulators of angiogenesis. *Circ Res* 2009, 104, 442-54.

131. Szklarczyk, D.; Franceschini, A.; Kuhn, M.; Simonovic, M.; Roth, A.; Minguez, P.; Doerks, T.; Stark, M.; Muller, J.; Bork, P.; Jensen, L. J.; von Mering, C. The STRING database in 2011: functional interaction networks of proteins, globally integrated and scored. *Nucleic acids research* 2011, 39, D561-8.

132. Poliseno, L.; Tuccoli, A.; Mariani, L.; Evangelista, M.; Citti, L.; Woods, K.; Mercatanti, A.; Hammond, S.; Rainaldi, G. MicroRNAs modulate the angiogenic properties of HUVECs. *Blood* 2006, 108, 3068-71.

133. Fish, J. E.; Santoro, M. M.; Morton, S. U.; Yu, S.; Yeh, R. F.; Wythe, J. D.; Ivey, K. N.; Bruneau, B. G.; Stainier, D. Y.; Srivastava, D. miR-126 regulates angiogenic signaling and vascular integrity. *Developmental cell* 2008, 15, 272-84.

134. Wang, S.; Aurora, A. B.; Johnson, B. A.; Qi, X.; McAnally, J.; Hill, J. A.; Richardson, J. A.; Bassel-Duby, R.; Olson, E. N. The endothelial-specific microRNA miR-126 governs vascular integrity and angiogenesis. *Developmental cell* 2008, 15, 261-71.

135. Png, K. J.; Halberg, N.; Yoshida, M.; Tavazoie, S. F. A microRNA regulon that mediates endothelial recruitment and metastasis by cancer cells. *Nature* 2012, 481, 190-4.

136. Bonauer, A.; Carmona, G.; Iwasaki, M.; Mione, M.; Koyanagi, M.; Fischer, A.; Burchfield, J.; Fox, H.; Doebele, C.; Ohtani, K.; Chavakis, E.; Potente, M.; Tjwa, M.; Urbich, C.; Zeiher, A. M.; Dimmeler, S. MicroRNA-92a controls angiogenesis and functional recovery of ischemic tissues in mice. *Science* 2009, 324, 1710-3.

137. Doebele, C.; Bonauer, A.; Fischer, A.; Scholz, A.; Reiss, Y.; Urbich, C.; Hofmann, W. K.; Zeiher, A. M.; Dimmeler, S. Members of the microRNA-17-92 cluster exhibit a cell-intrinsic antiangiogenic function in endothelial cells. *Blood* 2010, 115, 4944-50.

138. Fasanaro, P.; D'Alessandra, Y.; Di Stefano, V.; Melchionna, R.; Romani, S.; Pompilio, G.; Capogrossi, M. C.; Martelli, F. MicroRNA-210 modulates endothelial cell response to hypoxia and inhibits the receptor tyrosine kinase ligand Ephrin-A3. *The Journal of biological chemistry* 2008, 283, 15878-83.

139. Pulkkinen, K.; Malm, T.; Turunen, M.; Koistinaho, J.; Yla-Herttuala, S. Hypoxia induces microRNA miR-210 in vitro and in vivo ephrin-A3 and neuronal pentraxin 1 are potentially regulated by miR-210. *FEBS Lett* 2008, 582, 2397-401.

140. Wurdinger, T.; Tannous, B. A.; Saydam, O.; Skog, J.; Grau, S.; Soutschek, J.; Weissleder, R.; Breakefield, X. O.; Krichevsky, A. M. miR-296 regulates growth factor receptor overexpression in angiogenic endothelial cells. *Cancer cell* 2008, 14, 382-93.

141. Ghosh, G.; Subramanian, I. V.; Adhikari, N.; Zhang, X.; Joshi, H. P.; Basi, D.; Chandrashekhar, Y. S.; Hall, J. L.; Roy, S.; Zeng, Y.; Ramakrishnan, S. Hypoxia-induced microRNA-424 expression in human endothelial cells regulates HIF-alpha isoforms and promotes angiogenesis. *The Journal of clinical investigation* 2010, 120, 4141-54.

142. Anand, S.; Majeti, B. K.; Acevedo, L. M.; Murphy, E. A.; Mukthavaram, R.; Scheppke, L.; Huang, M.; Shields, D. J.; Lindquist, J. N.; Lapinski, P. E.; King, P. D.; Weis, S. M.; Cheresh, D. A. MicroRNA-132-mediated loss of p120RasGAP activates the endothelium to facilitate pathological angiogenesis. *Nature medicine* 2010, 16, 909-14.

143. Boucher, J. M.; Peterson, S. M.; Urs, S.; Zhang, C.; Liaw, L. The miR-143/145 cluster is a novel transcriptional target of Jagged-1/Notch signaling in vascular smooth muscle cells. *The Journal of biological chemistry* 2011, 286, 28312-21.

144. Dentelli, P.; Rosso, A.; Orso, F.; Olgasi, C.; Taverna, D.; Brizzi, M. F. microRNA-222 controls neovascularization by regulating signal transducer and activator of transcription 5A expression. *Arteriosclerosis, thrombosis, and vascular biology* 2010, 30, 1562-8.

145. Giacca, M. Virus-mediated gene transfer to induce therapeutic angiogenesis: where do we stand? *Int J Nanomedicine* 2007, 2, 527-40.

146. Vickers, K. C.; Remaley, A. T. Lipid-based carriers of microRNAs and intercellular communication. *Current opinion in lipidology* 2012, 23, 91-7.

147. Shi, M. A.; Shi, G. P. Intracellular delivery strategies for microRNAs and potential therapies for human cardiovascular diseases. *Science signaling* 2010, 3, pe40.

148. Kanwar, J. R.; Mahidhara, G.; Kanwar, R. K. Antiangiogenic therapy using nanotechnological-based delivery system. *Drug discovery today* 2011, 16, 188-202.

149. Foley, S.; Crowley, C.; Smaihi, M.; Bonfils, C.; Erlanger, B. F.; Seta, P.; Larroque, C. Cellular localisation of a water-soluble fullerene derivative. *Biochem Biophys Res Commun* 2002, 294, 116-9.

150. Martin, C. R.; Kohli, P. The emerging field of nanotube biotechnology. *Nature reviews. Drug discovery* 2003, 2, 29-37.

151. Rawat, M.; Singh, D.; Saraf, S.; Saraf, S. Nanocarriers: promising vehicle for bioactive drugs. *Biological & pharmaceutical bulletin* 2006, 29, 1790-8.

152. Hsieh, T. H.; Chen, J. J.; Chen, L. H.; Chiang, P. T.; Lee, H. Y. Time-course gait analysis of hemiparkinsonian rats following 6-hydroxydopamine lesion. *Behavioural brain research* 2011, 222, 1-9.

153. Rawat, M.; Singh, D.; Saraf, S.; Saraf, S. Development and in vitro evaluation of alginate gel-encapsulated, chitosan-coated ceramic nanocores for oral delivery of enzyme. *Drug development and industrial pharmacy* 2008, 34, 181-8.

154. Schneider, B. H.; Dickinson, E. L.; Vach, M. D.; Hoijer, J. V.; Howard, L. V. Highly sensitive optical chip immunoassays in human serum. *Biosensors & bioelectronics* 2000, 15, 13-22.

155. Sohn, Y. D.; Somasuntharam, I.; Che, P. L.; Jayswal, R.; Murthy, N.; Davis, M. E.; Yoon, Y. S. Induction of pluripotency in bone marrow mononuclear cells via polyketal nanoparticle-mediated delivery of mature microRNAs. *Biomaterials* 2013, 34, 4235-41.

156. Schade, A.; Delyagina, E.; Scharfenberg, D.; Skorska, A.; Lux, C.; David, R.; Steinhoff, G. Innovative Strategy for MicroRNA Delivery in Human Mesenchymal Stem Cells via Magnetic Nanoparticles. *International journal of molecular sciences* 2013, 14, 10710-26.

157. Thomas, M.; Lange-Grunweller, K.; Dayyoub, E.; Bakowsky, U.; Weirauch, U.; Aigner, A.; Hartmann, R. K.; Grunweller, A. PEI-complexed LNA antiseeds as miRNA inhibitors. *RNA biology* 2012, 9, 1088-98.

158. Chen, Y.; Zhu, X.; Zhang, X.; Liu, B.; Huang, L. Nanoparticles modified with tumor-targeting scFv deliver siRNA and miRNA for cancer therapy. *Mol Ther* 2010, 18, 1650-6.

159. Zhou, Y.; Zhang, L.; Zhao, W.; Wu, Y.; Zhu, C.; Yang, Y. Nanoparticle-mediated delivery of TGF-beta1 miRNA plasmid for preventing flexor tendon adhesion formation. *Biomaterials* 2013, 34, 8269-78.

160. Babar, I. A.; Cheng, C. J.; Booth, C. J.; Liang, X.; Weidhaas, J. B.; Saltzman, W. M.; Slack, F. J. Nanoparticle-based therapy in an in vivo microRNA-155 (miR-155)-dependent mouse model of lymphoma. *Proc Natl Acad Sci U S A* 2012, 109, E1695-704.

161. Tivnan, A.; Orr, W. S.; Gubala, V.; Nooney, R.; Williams, D. E.; McDonagh, C.; Prenter, S.; Harvey, H.; Domingo-Fernandez, R.; Bray, I. M.; Piskareva, O.; Ng, C. Y.; Lode, H. N.; Davidoff, A. M.; Stallings, R. L. Inhibition of neuroblastoma tumor growth by targeted delivery of microRNA-34a using anti-disialoganglioside GD2 coated nanoparticles. *PloS one* 2012, 7, e38129.

162. Su, J.; Baigude, H.; McCarroll, J.; Rana, T. M. Silencing microRNA by interfering nanoparticles in mice. *Nucleic acids research* 2011, 39, e38.

163. Frangioni, J. V.; Hajjar, R. J. In vivo tracking of stem cells for clinical trials in cardiovascular disease. *Circulation* 2004, 110, 3378-83.

164. Zhou, R.; Acton, P. D.; Ferrari, V. A. Imaging stem cells implanted in infarcted myocardium. *J Am Coll Cardiol* 2006, 48, 2094-106.

165. Arnold, J. M.; Liu, P.; Demers, C.; Dorian, P.; Giannetti, N.; Haddad, H.; Heckman, G. A.; Howlett, J. G.; Ignaszewski, A.; Johnstone, D. E.; Jong, P.; McKelvie, R. S.; Moe, G. W.; Parker, J. D.; Rao, V.; Ross, H. J.; Sequeira, E. J.; Svendsen, A. M.; Teo, K.; Tsuyuki, R. T.; White, M. Canadian Cardiovascular Society consensus conference recommendations on heart failure 2006: diagnosis and management. *The Canadian journal of cardiology* 2006, 22, 23-45.

166. Stuckey, D. J.; Carr, C. A.; Tyler, D. J.; Clarke, K. Cine-MRI versus two-dimensional echocardiography to measure in vivo left ventricular function in rat heart. *NMR in biomedicine* 2008, 21, 765-72.

167. Jenkins, C.; Moir, S.; Chan, J.; Rakhit, D.; Haluska, B.; Marwick, T. H. Left ventricular volume measurement with echocardiography: a comparison of left ventricular opacification, three-dimensional echocardiography, or both with magnetic resonance imaging. *European heart journal* 2009, 30, 98-106.

168. Partington, S. L.; Kwong, R. Y.; Dorbala, S. Multimodality imaging in the assessment of myocardial viability. *Heart failure reviews* 2011, 16, 381-95.

169. Kraitchman, D. L.; Wu, J. C.-M. *Stem cell labeling for delivery and tracking using noninvasive imaging*. CRC Press/Taylor & Francis: Boca Raton, 2012; p xxi, 451 p.

170. Ferreira, L. Nanoparticles as tools to study and control stem cells. *J Cell Biochem* 2009, 108, 746-52.

171. Srinivas, M.; Morel, P. A.; Ernst, L. A.; Laidlaw, D. H.; Ahrens, E. T. Fluorine-19 MRI for visualization and quantification of cell migration in a diabetes model. *Magn Reson Med* 2007, 58, 725-34.

172. Engstrom, M.; Klasson, A.; Pedersen, H.; Vahlberg, C.; Kall, P. O.; Uvdal, K. High proton relaxivity for gadolinium oxide nanoparticles. *MAGMA* 2006, 19, 180-6.

173. Bulte, J. W.; Douglas, T.; Witwer, B.; Zhang, S. C.; Lewis, B. K.; van Gelderen, P.; Zywicke, H.; Duncan, I. D.; Frank, J. A. Monitoring stem cell therapy in vivo using magnetodendrimers as a new class of cellular MR contrast agents. *Academic radiology* 2002, 9 Suppl 2, S332-5.

174. Liu, W.; Frank, J. A. Detection and quantification of magnetically labeled cells by cellular MRI. *European journal of radiology* 2009, 70, 258-64.

175. Hill, J. M.; Dick, A. J.; Raman, V. K.; Thompson, R. B.; Yu, Z. X.; Hinds, K. A.; Pessanha, B. S.; Guttman, M. A.; Varney, T. R.; Martin, B. J.; Dunbar, C. E.; McVeigh, E. R.; Lederman, R. J. Serial cardiac magnetic resonance imaging of injected mesenchymal stem cells. *Circulation* 2003, 108, 1009-14.

176. Walczak, P.; Kedziorek, D. A.; Gilad, A. A.; Lin, S.; Bulte, J. W. Instant MR labeling of stem cells using magnetoelectroporation. *Magn Reson Med* 2005, 54, 769-74.

177. de Vries, I. J.; Lesterhuis, W. J.; Barentsz, J. O.; Verdijk, P.; van Krieken, J. H.; Boerman, O. C.; Oyen, W. J.; Bonenkamp, J. J.; Boezeman, J. B.; Adema, G. J.; Bulte, J. W.; Scheenen, T. W.; Punt, C. J.; Heerschap, A.; Figdor, C. G. Magnetic resonance tracking of dendritic cells in melanoma patients for monitoring of cellular therapy. *Nat Biotechnol* 2005, 23, 1407-13.

178. Zhu, J.; Zhou, L.; XingWu, F. Tracking neural stem cells in patients with brain trauma. *The New England journal of medicine* 2006, 355, 2376-8.

179. Garot, J.; Unterseeh, T.; Teiger, E.; Champagne, S.; Chazaud, B.; Gherardi, R.; Hittinger, L.; Gueret, P.; Rahmouni, A. Magnetic resonance imaging of targeted catheter-based implantation of myogenic precursor cells into infarcted left ventricular myocardium. *J Am Coll Cardiol* 2003, 41, 1841-6.

180. Dick, A. J.; Guttman, M. A.; Raman, V. K.; Peters, D. C.; Pessanha, B. S.; Hill, J. M.; Smith, S.; Scott, G.; McVeigh, E. R.; Lederman, R. J. Magnetic resonance fluoroscopy allows targeted delivery of mesenchymal stem cells to infarct borders in Swine. *Circulation* 2003, 108, 2899-904.

181. Stuckey, D. J.; Carr, C. A.; Martin-Rendon, E.; Tyler, D. J.; Willmott, C.; Cassidy, P. J.; Hale, S. J.; Schneider, J. E.; Tatton, L.; Harding, S. E.; Radda, G. K.; Watt, S.; Clarke, K. Iron particles for noninvasive monitoring of bone marrow stromal cell engraftment into, and isolation of viable engrafted donor cells from, the heart. *Stem Cells* 2006, 24, 1968-75.

182. Kraitchman, D. L.; Heldman, A. W.; Atalar, E.; Amado, L. C.; Martin, B. J.; Pittenger, M. F.; Hare, J. M.; Bulte, J. W. In vivo magnetic resonance imaging of mesenchymal stem cells in myocardial infarction. *Circulation* 2003, 107, 2290-3.

183. Freyman, T.; Polin, G.; Osman, H.; Crary, J.; Lu, M.; Cheng, L.; Palasis, M.; Wilensky, R. L. A quantitative, randomized study evaluating three methods of mesenchymal stem cell delivery following myocardial infarction. *Eur Heart J* 2006, 27, 1114-22.

184. Abriata, L. A.; ML, M. S.; Tomatis, P. E. Sequence-function-stability relationships in proteins from datasets of functionally annotated variants: The case of TEM beta-lactamases. *FEBS Lett* 2012, 586, 3330-5.

185. Ahamed, M.; Karns, M.; Goodson, M.; Rowe, J.; Hussain, S. M.; Schlager, J. J.; Hong, Y. DNA damage response to different surface chemistry of silver nanoparticles in mammalian cells. *Toxicol Appl Pharmacol* 2008, 233, 404-10.

186. Ruiz-Cabello, J.; Walczak, P.; Kedziorek, D. A.; Chacko, V. P.; Schmieder, A. H.; Wickline, S. A.; Lanza, G. M.; Bulte, J. W. In vivo "hot spot" MR imaging of neural stem cells using fluorinated nanoparticles. *Magn Reson Med* 2008, 60, 1506-11.

187. Breunig, M.; Lungwitz, U.; Liebl, R.; Fontanari, C.; Klar, J.; Kurtz, A.; Blunk, T.; Goepferich, A. Gene delivery with low molecular weight linear polyethylenimines. *The journal of gene medicine* 2005, 7, 1287-98.

188. Kim, H. D.; Kim, K. S.; Ki, S. C.; Choi, Y. S. Electron Microprobe Analysis and Tissue Reaction around Titanium Alloy Spinal Implants. *Asian spine journal* 2007, 1, 1-7.

189. Zaky, A.; Elbakry, A.; Ehmer, A.; Breunig, M.; Goepferich, A. The mechanism of protein release from triglyceride microspheres. *Journal of controlled release : official journal of the Controlled Release Society* 2010, 147, 202-10.

190. Ki, S. C.; Kim, B. H.; Ryu, J. H.; Yoon, D. H.; Chung, Y. Y. Total hip arthroplasty using two-incision technique. *Clinics in orthopedic surgery* 2011, 3, 268-73.

191. Drotleff, S.; Lungwitz, U.; Breunig, M.; Dennis, A.; Blunk, T.; Tessmar, J.; Gopferich, A. Biomimetic polymers in pharmaceutical and biomedical sciences. *European*

journal of pharmaceutics and biopharmaceutics : official journal of Arbeitsgemeinschaft fur Pharmazeutische Verfahrenstechnik e.V 2004, 58, 385-407.

192. Bartel, D. P. MicroRNAs: genomics, biogenesis, mechanism, and function. *Cell* 2004, 116, 281-97.

193. Kota, J.; Chivukula, R. R.; O'Donnell, K. A.; Wentzel, E. A.; Montgomery, C. L.; Hwang, H. W.; Chang, T. C.; Vivekanandan, P.; Torbenson, M.; Clark, K. R.; Mendell, J. R.; Mendell, J. T. Therapeutic microRNA delivery suppresses tumorigenesis in a murine liver cancer model. *Cell* 2009, 137, 1005-17.

194. Panyam, J.; Sahoo, S. K.; Prabha, S.; Bargar, T.; Labhasetwar, V. Fluorescence and electron microscopy probes for cellular and tissue uptake of poly(D,L-lactide-co-glycolide) nanoparticles. *International journal of pharmaceutics* 2003, 262, 1-11.

195. Bauhuber, S.; Liebl, R.; Tomasetti, L.; Rachel, R.; Goepferich, A.; Breunig, M. A library of strictly linear poly(ethylene glycol)-poly(ethylene imine) diblock copolymers to perform structure-function relationship of non-viral gene carriers. *Journal of controlled release : official journal of the Controlled Release Society* 2012.

196. Paik, K. H.; Park, Y. H.; Ryoo, B. Y.; Yang, S. H.; Lee, J. C.; Kim, C. H.; Ki, S. S.; Kim, J. M.; Park, M. J.; Ahn, H. J.; Choi, W.; Chung, J. H. Prognostic value of immunohistochemical staining of p53, bcl-2, and Ki-67 in small cell lung cancer. *Journal of Korean medical science* 2006, 21, 35-9.

197. Pollinger, K.; Hennig, R.; Breunig, M.; Tessmar, J.; Ohlmann, A.; Tamm, E. R.; Witzgall, R.; Goepferich, A. Kidney Podocytes as Specific Targets for cyclo(RGDfC)-Modified Nanoparticles. *Small* 2012.

198. Lungwitz, U.; Breunig, M.; Liebl, R.; Blunk, T.; Goepferich, A. Methoxy poly(ethylene glycol)--low molecular weight linear polyethylenimine-derived copolymers enable polyplex shielding. *European journal of pharmaceutics and biopharmaceutics : official journal of Arbeitsgemeinschaft fur Pharmazeutische Verfahrenstechnik e.V* 2008, 69, 134-48.

199. Elbakry, A.; Zaky, A.; Liebl, R.; Rachel, R.; Goepferich, A.; Breunig, M. Layer-by-layer assembled gold nanoparticles for siRNA delivery. *Nano Lett* 2009, 9, 2059-64.

200. Morbach, C.; Breunig, M.; Weidemann, F.; Topp, M.; Ritter, C.; Schneider, P.; Einsele, H.; Stork, S.; Angermann, C. E. [52 year-old patient with severe heart failure due to multiple myeloma]. *Der Internist* 2009, 50, 225-9.

201. Silversides, C. K.; Salehian, O.; Oechslin, E.; Schwerzmann, M.; Vonder Muhll, I.; Khairy, P.; Horlick, E.; Landzberg, M.; Meijboom, F.; Warnes, C.; Therrien, J. Canadian Cardiovascular Society 2009 Consensus Conference on the management of adults with congenital heart disease: complex congenital cardiac lesions. *The Canadian journal of cardiology* 2010, 26, e98-117.

202. Hild, W. A.; Breunig, M.; Goepferich, A. Quantum dots - nano-sized probes for the exploration of cellular and intracellular targeting. *European journal of pharmaceutics and biopharmaceutics : official journal of Arbeitsgemeinschaft fur Pharmazeutische Verfahrenstechnik e.V* 2008, 68, 153-68.

203. Ki, S.; Sugihara, F.; Kasahara, K.; Tochio, H.; Okada-Marubayashi, A.; Tomita, S.; Morita, M.; Ikeguchi, M.; Shirakawa, M.; Kokubo, T. A novel magnetic resonance-based method to measure gene expression in living cells. *Nucleic acids research* 2006, 34, e51.

204. Arbab, A. S.; Yocum, G. T.; Kalish, H.; Jordan, E. K.; Anderson, S. A.; Khakoo, A. Y.; Read, E. J.; Frank, J. A. Efficient magnetic cell labeling with protamine sulfate complexed to ferumoxides for cellular MRI. *Blood* 2004, 104, 1217-23.

205. Velic, A.; Gabriels, G.; Hirsch, J. R.; Schroter, R.; Edemir, B.; Paasche, S.; Schlatter, E. Acute rejection after rat renal transplantation leads to downregulation of NA+ and water channels in the collecting duct. *American journal of transplantation : official journal of the American Society of Transplantation and the American Society of Transplant Surgeons* 2005, 5, 1276-85.

206. Nkansah, M. K.; Tzeng, S. Y.; Holdt, A. M.; Lavik, E. B. Poly(lactic-co-glycolic acid) nanospheres and microspheres for short- and long-term delivery of bioactive ciliary neurotrophic factor. *Biotechnology and bioengineering* 2008, 100, 1010-9.

207. Cairns, J. A.; Connolly, S.; McMurtry, S.; Stephenson, M.; Talajic, M. Canadian Cardiovascular Society atrial fibrillation guidelines 2010: prevention of stroke and systemic thromboembolism in atrial fibrillation and flutter. *The Canadian journal of cardiology* 2011, 27, 74-90.

208. Breunig, M.; Lungwitz, U.; Liebl, R.; Goepferich, A. Fluorescence resonance energy transfer: evaluation of the intracellular stability of polyplexes. *European journal of pharmaceutics and biopharmaceutics : official journal of Arbeitsgemeinschaft fur Pharmazeutische Verfahrenstechnik e.V* 2006, 63, 156-65.

209. Lungwitz, U.; Breunig, M.; Blunk, T.; Gopferich, A. Polyethylenimine-based non-viral gene delivery systems. *European journal of pharmaceutics and biopharmaceutics : official journal of Arbeitsgemeinschaft fur Pharmazeutische Verfahrenstechnik e.V* 2005, 60, 247-66.

210. Kim, Y. W.; Ki, S. H.; Lee, J. R.; Lee, S. J.; Kim, C. W.; Kim, S. C.; Kim, S. G. Liquiritigenin, an aglycone of liquiritin in Glycyrrhizae radix, prevents acute liver injuries in rats induced by acetaminophen with or without buthionine sulfoximine. *Chemico-biological interactions* 2006, 161, 125-38.

211. Breunig, M.; Brummer, M.; Potthoff, P.; Klamert, A. [The Bavarian Health Survey]. *Gesundheitswesen* 1998, 60 Suppl 2, S101-3.

212. Brigham, T. A.; Finfrock, S. R.; Breunig, M. K.; Bushell, D. The use of programmed materials in the analysis of academic contingencies. *Journal of applied behavior analysis* 1972, 5, 177-82.

213. Horisawa, E.; Kubota, K.; Tuboi, I.; Sato, K.; Yamamoto, H.; Takeuchi, H.; Kawashima, Y. Size-dependency of DL-lactide/glycolide copolymer particulates for intra-articular delivery system on phagocytosis in rat synovium. *Pharm Res* 2002, 19, 132-9.

214. Johnstone, D. E.; Abdulla, A.; Arnold, J. M.; Bernstein, V.; Bourassa, M.; Brophy, J.; Davies, R.; Gardner, M.; Hoeschen, R.; Mickleborough, L.; et al. Diagnosis and management of heart failure. Canadian Cardiovascular Society. *The Canadian journal of cardiology* 1994, 10, 613-31, 635-54.

215. Ross, R. Atherosclerosis is an inflammatory disease. *American heart journal* 1999, 138, S419-20.

216. Silva, E. A.; Kim, E. S.; Kong, H. J.; Mooney, D. J. Material-based deployment enhances efficacy of endothelial progenitor cells. *Proc Natl Acad Sci U S A* 2008, 105, 14347-52.

217. Yang, F.; Cho, S. W.; Son, S. M.; Bogatyrev, S. R.; Singh, D.; Green, J. J.; Mei, Y.; Park, S.; Bhang, S. H.; Kim, B. S.; Langer, R.; Anderson, D. G. Genetic engineering of human stem cells for enhanced angiogenesis using biodegradable polymeric nanoparticles. *Proc Natl Acad Sci U S A* 2010, 107, 3317-22.

218. Bhang, S. H.; Cho, S. W.; Lim, J. M.; Kang, J. M.; Lee, T. J.; Yang, H. S.; Song, Y. S.; Park, M. H.; Kim, H. S.; Yoo, K. J.; Jang, Y.; Langer, R.; Anderson, D. G.; Kim, B. S. Locally delivered growth factor enhances the angiogenic efficacy of adipose-derived stromal cells transplanted to ischemic limbs. *Stem Cells* 2009, 27, 1976-86.

219. Hopkins, S. P.; Bulgrin, J. P.; Sims, R. L.; Bowman, B.; Donovan, D. L.; Schmidt, S. P. Controlled delivery of vascular endothelial growth factor promotes neovascularization and maintains limb function in a rabbit model of ischemia. *Journal of vascular surgery* 1998, 27, 886-94; discussion 895.

220. Sun, Q.; Chen, R. R.; Shen, Y.; Mooney, D. J.; Rajagopalan, S.; Grossman, P. M. Sustained vascular endothelial growth factor delivery enhances angiogenesis and perfusion in ischemic hind limb. *Pharm Res* 2005, 22, 1110-6.

221. Yla-Herttuala, S. Cardiovascular gene therapy with vascular endothelial growth factors. *Gene* 2013, 525, 217-9.

222. Dragneva, G.; Korpisalo, P.; Yla-Herttuala, S. Promoting blood vessel growth in ischemic diseases: challenges in translating preclinical potential into clinical success. *Disease models & mechanisms* 2013, 6, 312-22.

223. Korpisalo, P.; Hytonen, J. P.; Laitinen, J. T.; Laidinen, S.; Parviainen, H.; Karvinen, H.; Siponen, J.; Marjomaki, V.; Vajanto, I.; Rissanen, T. T.; Yla-Herttuala, S. Capillary enlargement, not sprouting angiogenesis, determines beneficial therapeutic effects and side effects of angiogenic gene therapy. *Eur Heart J* 2011, 32, 1664-72.

224. Lahteenvuo, J. E.; Lahteenvuo, M. T.; Kivela, A.; Rosenlew, C.; Falkevall, A.; Klar, J.; Heikura, T.; Rissanen, T. T.; Vahakangas, E.; Korpisalo, P.; Enholm, B.; Carmeliet, P.; Alitalo, K.; Eriksson, U.; Yla-Herttuala, S. Vascular endothelial growth factor-B induces myocardium-specific angiogenesis and arteriogenesis via vascular endothelial growth factor receptor-1- and neuropilin receptor-1-dependent mechanisms. *Circulation* 2009, 119, 845-56.

225. Muona, K.; Makinen, K.; Hedman, M.; Manninen, H.; Yla-Herttuala, S. 10-year safety follow-up in patients with local VEGF gene transfer to ischemic lower limb. *Gene Ther* 2012, 19, 392-5.

226. Yla-Herttuala, S.; Alitalo, K. Gene transfer as a tool to induce therapeutic vascular growth. *Nature medicine* 2003, 9, 694-701.

227. Gomes, R. S.; das Neves, R. P.; Cochlin, L.; Lima, A.; Carvalho, R.; Korpisalo, P.; Dragneva, G.; Turunen, M.; Liimatainen, T.; Clarke, K.; Yla-Herttuala, S.; Carr, C.; Ferreira, L. Efficient pro-survival/angiogenic miRNA delivery by an MRI-detectable nanomaterial. *ACS Nano* 2013, 7, 3362-72.

228. Pepine, C. J. New concepts in the pathophysiology of acute myocardial infarction. *The American journal of cardiology* 1989, 64, 2B-8B.

229. Carr, C. A.; Stuckey, D. J.; Tan, J. J.; Tan, S. C.; Gomes, R. S.; Camelliti, P.; Messina, E.; Giacomello, A.; Ellison, G. M.; Clarke, K. Cardiosphere-derived cells improve function in the infarcted rat heart for at least 16 weeks--an MRI study. *PloS one* 2011, 6, e25669.

230. Hierlihy, A. M.; Seale, P.; Lobe, C. G.; Rudnicki, M. A.; Megeney, L. A. The post-natal heart contains a myocardial stem cell population. *FEBS Lett* 2002, 530, 239-43.

231. Soonpaa, M. H.; Field, L. J. Survey of studies examining mammalian cardiomyocyte DNA synthesis. *Circ Res* 1998, 83, 15-26.

232. Anversa, P.; Sussman, M. A.; Bolli, R. Molecular genetic advances in cardiovascular medicine: focus on the myocyte. *Circulation* 2004, 109, 2832-8.

233. Oh, H.; Bradfute, S. B.; Gallardo, T. D.; Nakamura, T.; Gaussin, V.; Mishina, Y.; Pocius, J.; Michael, L. H.; Behringer, R. R.; Garry, D. J.; Entman, M. L.; Schneider, M. D. Cardiac progenitor cells from adult myocardium: homing, differentiation, and fusion after infarction. *Proc Natl Acad Sci U S A* 2003, 100, 12313-8.

234. Smith, R. R.; Barile, L.; Cho, H. C.; Leppo, M. K.; Hare, J. M.; Messina, E.; Giacomello, A.; Abraham, M. R.; Marban, E. Regenerative potential of cardiosphere-derived cells expanded from percutaneous endomyocardial biopsy specimens. *Circulation* 2007, 115, 896-908.

235. Carolyn A. Carr, D. J. S., Jun Jie Tan, Suat Cheng Tan, Renata S. M. Gomes, Patrizia; Camelliti, E. M., Alessandro Giacomello, Georgina M. Ellison, Kieran Clarke. Cardiosphere-Derived Cells Improve Function in the Infarcted Rat Heart for at Least 16 Weeks – an MRI Study. *PLoSOne* 2011, 6.

236. French, B. A.; Kramer, C. M. Mechanisms of Post-Infarct Left Ventricular Remodeling. *Drug Discov Today Dis Mech* 2007, 4, 185-196.

237. Li, L.; Xie, T. Stem cell niche: structure and function. *Annu Rev Cell Dev Biol* 2005, 21, 605-31.

238. Scadden, D. T. The stem-cell niche as an entity of action. *Nature* 2006, 441, 1075-9.

239. Csete, M. Oxygen in the cultivation of stem cells. *Ann N Y Acad Sci* 2005, 1049, 1-8.

240. Simon, M. C.; Keith, B. The role of oxygen availability in embryonic development and stem cell function. *Nat Rev Mol Cell Biol* 2008, 9, 285-96.

241. Rodesch, F.; Simon, P.; Donner, C.; Jauniaux, E. Oxygen measurements in endometrial and trophoblastic tissues during early pregnancy. *Obstet Gynecol* 1992, 80, 283-5.

242. Bruder, S. P.; Jaiswal, N.; Haynesworth, S. E. Growth kinetics, self-renewal, and the osteogenic potential of purified human mesenchymal stem cells during extensive subcultivation and following cryopreservation. *J Cell Biochem* 1997, 64, 278-94.

243. Grayson, W. L.; Zhao, F.; Bunnell, B.; Ma, T. Hypoxia enhances proliferation and tissue formation of human mesenchymal stem cells. *Biochem Biophys Res Commun* 2007, 358, 948-53.

244. Lennon, D. P.; Edmison, J. M.; Caplan, A. I. Cultivation of rat marrow-derived mesenchymal stem cells in reduced oxygen tension: effects on in vitro and in vivo osteochondrogenesis. *J Cell Physiol* 2001, 187, 345-55.

245. Ju, S. Y.; Cho, K. A.; Cho, S. J.; Jung, Y. J.; Woo, S. Y.; Seoh, J. Y.; Han, H. S.; Ryu, K. H. Effect of hypoxic treatment on bone marrow cells that are able to migrate to the injured liver. *Cell Biol Int* 2009, 33, 31-5.

246. Studer, L.; Csete, M.; Lee, S. H.; Kabbani, N.; Walikonis, J.; Wold, B.; McKay, R. Enhanced proliferation, survival, and dopaminergic differentiation of CNS precursors in lowered oxygen. *J Neurosci* 2000, 20, 7377-83.

247. Zhao, T.; Huang, X.; Zhu, L. L.; Xiong, L.; Zhang, K.; Wu, L. Y.; Liu, B.; Wu, K. W.; Fan, M. [Effect of low glucose and/or hypoxia on the proliferation and metabolism of neural stem cells]. *Zhongguo Ying Yong Sheng Li Xue Za Zhi* 26, 412-5.

248. Chen, X.; Tian, Y.; Yao, L.; Zhang, J.; Liu, Y. Hypoxia stimulates proliferation of rat neural stem cells with influence on the expression of cyclin D1 and c-Jun N-terminal protein kinase signaling pathway in vitro. *Neuroscience* 165, 705-14.

249. Ingraham, C. A.; Park, G. C.; Makarenkova, H. P.; Crossin, K. L. Matrix metalloproteinase (MMP)-9 induced by Wnt signaling increases the proliferation and migration of embryonic neural stem cells at low O2 levels. *The Journal of biological chemistry*.

250. Theus, M. H.; Wei, L.; Cui, L.; Francis, K.; Hu, X.; Keogh, C.; Yu, S. P. In vitro hypoxic preconditioning of embryonic stem cells as a strategy of promoting cell survival and functional benefits after transplantation into the ischemic rat brain. *Exp Neurol* 2008, 210, 656-70.

251. Rehman, J.; Traktuev, D.; Li, J.; Merfeld-Clauss, S.; Temm-Grove, C. J.; Bovenkerk, J. E.; Pell, C. L.; Johnstone, B. H.; Considine, R. V.; March, K. L. Secretion of angiogenic and antiapoptotic factors by human adipose stromal cells. *Circulation* 2004, 109, 1292-8.

252. Cummins, E. P.; Seeballuck, F.; Keely, S. J.; Mangan, N. E.; Callanan, J. J.; Fallon, P. G.; Taylor, C. T. The hydroxylase inhibitor dimethyloxalylglycine is protective in a murine model of colitis. *Gastroenterology* 2008, 134, 156-65.

253. Forest, L.; Glade, N.; Demongeot, J. Lienard systems and potential-Hamiltonian decomposition: applications in biology. *C R Biol* 2007, 330, 97-106.

254. Guzeloglu-Kayisli, O.; Kayisli, U. A.; Amankulor, N. M.; Voorhees, J. R.; Gokce, O.; DiLuna, M. L.; Laurans, M. S.; Luleci, G.; Gunel, M. Krev1 interaction trapped-1/cerebral cavernous malformation-1 protein expression during early angiogenesis. *J Neurosurg* 2004, 100, 481-7.

255. Pugh, C. W.; Ratcliffe, P. J. Regulation of angiogenesis by hypoxia: role of the HIF system. *Nat Med* 2003, 9, 677-84.

256. Forristal, C. E.; Wright, K. L.; Hanley, N. A.; Oreffo, R. O.; Houghton, F. D. Hypoxia inducible factors regulate pluripotency and proliferation in human embryonic stem cells cultured at reduced oxygen tensions. *Reproduction* 139, 85-97.

257. Covello, K. L.; Kehler, J.; Yu, H.; Gordan, J. D.; Arsham, A. M.; Hu, C. J.; Labosky, P. A.; Simon, M. C.; Keith, B. HIF-2alpha regulates Oct-4: effects of hypoxia on stem cell function, embryonic development, and tumor growth. *Genes Dev* 2006, 20, 557-70.

258. Ji, L.; Liu, Y. X.; Yang, C.; Yue, W.; Shi, S. S.; Bai, C. X.; Xi, J. F.; Nan, X.; Pei, X. T. Self-renewal and pluripotency is maintained in human embryonic stem cells by co-culture with human fetal liver stromal cells expressing hypoxia inducible factor 1alpha. *J Cell Physiol* 2009, 221, 54-66.

259. Li, T. S.; Cheng, K.; Malliaras, K.; Matsushita, N.; Sun, B.; Marban, L.; Zhang, Y.; Marban, E. Expansion of human cardiac stem cells in physiological oxygen improves cell production efficiency and potency for myocardial repair. *Cardiovascular research* 89, 157-65.

260. Yu, Y. B. Fluorocarbon nanoparticles as multifunctional drug delivery vehicles. *J Drug Target* 2006, 14, 663-9.

261. Arbab, A. S.; Bashaw, L. A.; Miller, B. R.; Jordan, E. K.; Lewis, B. K.; Kalish, H.; Frank, J. A. Characterization of biophysical and metabolic properties of cells labeled with superparamagnetic iron oxide nanoparticles and transfection agent for cellular MR imaging. *Radiology* 2003, 229, 838-46.

262. Groenman, F. A.; Rutter, M.; Wang, J.; Caniggia, I.; Tibboel, D.; Post, M. Effect of chemical stabilizers of hypoxia-inducible factors on early lung development. *Am J Physiol Lung Cell Mol Physiol* 2007, 293, L557-67.

263. Lienard, B. M.; Conejo-Garcia, A.; Stolze, I.; Loenarz, C.; Oldham, N. J.; Ratcliffe, P. J.; Schofield, C. J. Evaluation of aspirin metabolites as inhibitors of hypoxia-inducible factor hydroxylases. *Chem Commun (Camb)* 2008, 6393-5.

264. Hsieh, M. M.; Linde, N. S.; Wynter, A.; Metzger, M.; Wong, C.; Langsetmo, I.; Lin, A.; Smith, R.; Rodgers, G. P.; Donahue, R. E.; Klaus, S. J.; Tisdale, J. F. HIF prolyl hydroxylase inhibition results in endogenous erythropoietin induction, erythrocytosis, and modest fetal hemoglobin expression in rhesus macaques. *Blood* 2007, 110, 2140-7.

265. Guascito, M. R.; Chirizzi, D.; Malitesta, C.; Mazzotta, E.; Siciliano, M.; Siciliano, T.; Tepore, A.; Turco, A. Low-potential sensitive H2O2 detection based on composite micro tubular Te adsorbed on platinum electrode. *Biosensors & bioelectronics* 2011, 26, 3562-9.

266. Tan, S. C.; Carr, C. A.; Yeoh, K. K.; Schofield, C. J.; Davies, K. E.; Clarke, K. Identification of valid housekeeping genes for quantitative RT-PCR analysis of cardiosphere-derived cells preconditioned under hypoxia or with prolyl-4-hydroxylase inhibitors. *Mol Biol Rep*.

267. Heather, L. C.; Cole, M. A.; Lygate, C. A.; Evans, R. D.; Stuckey, D. J.; Murray, A. J.; Neubauer, S.; Clarke, K. Fatty acid transporter levels and palmitate oxidation rate correlate with ejection fraction in the infarcted rat heart. *Cardiovascular research* 2006, 72, 430-7.

268. Hataishi, R.; Rodrigues, A. C.; Neilan, T. G.; Morgan, J. G.; Buys, E.; Shiva, S.; Tambouret, R.; Jassal, D. S.; Raher, M. J.; Furutani, E.; Ichinose, F.; Gladwin, M. T.; Rosenzweig, A.; Zapol, W. M.; Picard, M. H.; Bloch, K. D.; Scherrer-Crosbie, M. Inhaled

nitric oxide decreases infarction size and improves left ventricular function in a murine model of myocardial ischemia-reperfusion injury. *American journal of physiology. Heart and circulatory physiology* 2006, 291, H379-84.

269. Michael, L. H.; Entman, M. L.; Hartley, C. J.; Youker, K. A.; Zhu, J.; Hall, S. R.; Hawkins, H. K.; Berens, K.; Ballantyne, C. M. Myocardial ischemia and reperfusion: a murine model. *The American journal of physiology* 1995, 269, H2147-54.

270. Scudellari, M. The Delivery Dilemma. *Nature Reports Stem Cells* 2009.

271. Haider, H.; Ashraf, M. Strategies to promote donor cell survival: combining preconditioning approach with stem cell transplantation. *J Mol Cell Cardiol* 2008, 45, 554-66.

272. Robey, T. E.; Saiget, M. K.; Reinecke, H.; Murry, C. E. Systems approaches to preventing transplanted cell death in cardiac repair. *J Mol Cell Cardiol* 2008, 45, 567-81.

273. Breunig, M.; Bauer, S.; Goepferich, A. Polymers and nanoparticles: intelligent tools for intracellular targeting? *European journal of pharmaceutics and biopharmaceutics : official journal of Arbeitsgemeinschaft fur Pharmazeutische Verfahrenstechnik e.V* 2008, 68, 112-28.

274. Chen, J.; Lanza, G. M.; Wickline, S. A. Quantitative magnetic resonance fluorine imaging: today and tomorrow. *Wiley interdisciplinary reviews. Nanomedicine and nanobiotechnology* 2010, 2, 431-40.

275. Sahoo, S.; Klychko, E.; Thorne, T.; Misener, S.; Schultz, K. M.; Millay, M.; Ito, A.; Liu, T.; Kamide, C.; Agrawal, H.; Perlman, H.; Qin, G.; Kishore, R.; Losordo, D. W. Exosomes from human CD34(+) stem cells mediate their proangiogenic paracrine activity. *Circ Res* 2011, 109, 724-8.

276. Hosoda, T.; Zheng, H.; Cabral-da-Silva, M.; Sanada, F.; Ide-Iwata, N.; Ogorek, B.; Ferreira-Martins, J.; Arranto, C.; D'Amario, D.; del Monte, F.; Urbanek, K.; D'Alessandro, D. A.; Michler, R. E.; Anversa, P.; Rota, M.; Kajstura, J.; Leri, A. Human cardiac stem cell differentiation is regulated by a mircrine mechanism. *Circulation* 2011, 123, 1287-96.

277. Dvir, T.; Bauer, M.; Schroeder, A.; Tsui, J. H.; Anderson, D. G.; Langer, R.; Liao, R.; Kohane, D. S. Nanoparticles targeting the infarcted heart. *Nano Lett* 2011, 11, 4411-4.